

## PDF hosted at the Radboud Repository of the Radboud University Nijmegen

The following full text is a publisher's version.

For additional information about this publication click this link.

<http://hdl.handle.net/2066/19235>

Please be advised that this information was generated on 2017-12-05 and may be subject to change.

MR IMAGING AND MR SPECTROSCOPY  
TO GUIDE TREATMENT SELECTION FOR PATIENTS WITH  
TUMOURS IN THE BRAIN AND HEAD-NECK REGION



MR IMAGING AND MR SPECTROSCOPY  
TO GUIDE TREATMENT SELECTION FOR PATIENTS WITH  
TUMOURS IN THE BRAIN AND HEAD-NECK REGION

Een wetenschappelijke proeve  
op het gebied van de Medische Wetenschappen

Proefschrift ter verkrijging van de graad van doctor aan de Katholieke Universiteit Nijmegen, op gezag van de Rector Magnificus Prof. Dr. C.W.P.M. Blom, volgens besluit van het College van Decanen in het openbaar te verdedigen op woensdag 19 februari 2003 des namiddags om 1:30 uur door

Mark Jacobus Petrus Rijkema  
geboren op 22 februari 1972 te Zutphen.

Promotores: Prof. Dr. A. Heerschap  
Prof. Dr. A. van der Kogel

Manuscriptcommissie: Prof. Dr. W.J.G. Oyen  
Prof. Dr. C.W. Hilbers  
Prof. Dr. G.W.A.M. Padberg

ISBN: 90-9016565-7

Cover design: Annita van Betuw

Printed by: Print Partners Ipskamp Enschede, The Netherlands

All MRI and MRS studies were carried out at the Department of Radiology,  
University Medical Centre Nijmegen, The Netherlands.

Financial support by Schering Nederland BV for publication of this thesis is  
gratefully acknowledged.

# MR IMAGING AND MR SPECTROSCOPY

## TO GUIDE TREATMENT SELECTION FOR PATIENTS WITH

### TUMOURS IN THE BRAIN AND HEAD-NECK REGION

Abbreviations and symbols	7
1 Introduction	9
1.1 Biological aspects of tumours	10
1.2 Tumour treatment	11
1.3 Head and neck tumours	12
1.4 Meningiomas	12
1.5 Oligodendrogliomas	13
1.6 Rationale and outline of this thesis	13
2 Magnetic Resonance	21
2.1 A brief historical overview	
2.1.1 Magnetism	22
2.1.2 Nuclear Magnetic Resonance	22
2.1.3 Magnetic Resonance Imaging	22
2.2 Basic concepts of Magnetic Resonance	
2.2.1 Spin, precession, and resonance	23
2.2.2 Relaxation	25
2.2.3 Principle of imaging	27
2.2.4 Magnetic Resonance Spectroscopy	27
2.3 Magnetic Resonance applications	
2.3.1 Blood oxygen level dependent MRI	29
2.3.2 Dynamic contrast enhanced MRI	30
2.3.3 Physiological pharmacokinetic models	31
2.3.4 <sup>31</sup> P and <sup>1</sup> H Magnetic Resonance Spectroscopy	32

3	Functional imaging of laryngeal cancer	41
	3.1 Introduction	42
	3.2 Functional MR imaging	42
	3.2.1 Vascularity	43
	3.2.2 Oxygenation	44
	3.3 MRI Methods	45
	3.3.1 Dynamic contrast enhanced MRI	45
	3.3.2 Blood oxygen level dependent MRI	50
	3.4 Laryngeal cancer: application of functional MRI approaches	51
	3.5 Conclusion	54
4	Method for quantitative mapping of dynamic MRI contrast agent uptake in human tumours	59
5	Effects of breathing a hyperoxic hypercapnic gas mixture on blood oxygenation and vascularity of head and neck tumours as measured by MRI	75
6	Effect of breathing a hyperoxic hypercapnic gas mixture on the oxygenation of meningiomas	91
7	Characterisation of oligodendrogliomas using short echo time <sup>1</sup> H MR Spectroscopic Imaging	105
8	Summary	119
9	Nederlandse samenvatting	123
	Dankwoord	127
	Curriculum vitae	129
	List of publications	131

## ABBREVIATIONS AND SYMBOLS

$\gamma$	gyromagnetic ratio
$\Delta T$	time delay of tissue enhancement relative to the AIF
$\nu$	precession frequency
$^1\text{H MRS}$	hydrogen (proton) MRS
$^{31}\text{P MRS}$	phosphorus MRS
AIF	arterial input function
ARCON	Accelerated Radiotherapy with Carbogen and Nicotinamide
ATP	adenosine triphosphate
a.u.	arbitrary units
$B_0$	static (main) magnetic field
BIRP	$B_1$ independent rotation phase-cycled
BOLD	blood oxygen level dependent
Cho	choline containing compounds
Cr	creatine plus phosphocreatine
$C_p$	arterial plasma concentration of Gd
$C_t$	tissue concentration of Gd
DCE-MRI	dynamic contrast enhanced MRI
DNA	deoxyribonucleic acid
E	extraction fraction
EES	extravascular extracellular space
F	tumour blood flow
FID	free induction decay
FLOOD	flow and oxygenation dependent
fMRI	functional MRI
FoV	field of view
Gd-DTPA	Gadolinium-DTPA (DiethyleneTriaminePentaAceticacid), dimegluminegadopentetaat
Glx	glutamine plus glutamate
Ino	myo-inositol
$k_{ep}$	rate constant between EES and blood plasma
$K^{trans}$	volume transfer constant
Lac	lactate
MRI	Magnetic Resonance Imaging
MRS	Magnetic Resonance Spectroscopy
MRSI	Magnetic Resonance Spectroscopic Imaging
NAA	N-acetylaspartate plus N-acetylaspartylglutamate
NMR	Nuclear Magnetic Resonance
P	vascular permeability



PCr	phosphocreatine
PDE	phosphodiester
P <sub>i</sub>	inorganic phosphate
PME	phosphomonoester
pO <sub>2</sub>	partial oxygen pressure
ppm	parts per million
RF	radio frequency
S	vascular surface area
SNR	signal-to-noise ratio
STEAM	stimulated echo acquisition mode
SVS	single voxel spectroscopy
T1	longitudinal relaxation time
T2	transverse relaxation time
T2*	apparent transverse relaxation time
TE	echo time
TR	repetition time
v <sub>e</sub>	volume of EES per unit volume of tissue

# 1

## INTRODUCTION

Mark Rijpkema

## 1.1 BIOLOGICAL ASPECTS OF TUMOURS

The most fundamental properties of tumours are relatively autonomous growth and, for malignant tumours, invasion and metastasis. The rate of growth of a tumour has important clinical consequences, as it will determine for example the time from initiation to clinical symptoms, or how long after treatment the tumour will recur if the treatment is unsuccessful. Tumours usually begin as small aggregates of tumour cells, which exchange nutrients and waste products with their surroundings by simple diffusion (1,2). However, an increase in tumour size beyond ~1 mm requires the induction of vasculature, a process called angiogenesis (3-5). This restriction in size is caused by lack of nutrients and oxygen supply by diffusion. For example, in tissues the oxygen diffusion limit corresponds to a distance of 100-200  $\mu\text{m}$  between the capillary and the cells (6,7).

Tumour vessels often display an abnormal architecture, characterised by collapsing or poorly differentiated, fragile and leaky vessels, which are frequently unable to meet the rapid growth of tumour cells (8-10). This may result in local hypoxia and necrosis. Two forms of hypoxia have been identified in tumours: diffusion limited or 'chronic' hypoxia and perfusion limited or 'acute' hypoxia. Cells that are located relatively far away from a blood vessel may become chronically hypoxic because of the limited diffusion distance of oxygen (6). The second form of hypoxia is induced by transiently closing of blood vessels, resulting in local fluctuations of blood flow and oxygen supply (11,12). The combination of an inadequate vascular network and fluctuating tumour blood flow may lead to a combination of chronic and acute hypoxia in tumour cells.

Tissue oxygenation is the result of oxygen supply and the respiration rate of the cells. Oxygen consumption rates of tumours are in general intermediate between those of normal tissues with low metabolic rates and normal tissues with relatively high metabolic rates (10,13). Besides glucose oxidation, tumours may also feature aerobic glycolysis; the breakdown of glucose to lactic acid in the presence of oxygen (14). A third mechanism of glucose turnover is the anaerobic glycolysis. Lactic acid production has long been considered a specific biochemical marker of malignancies, and although nowadays this specificity has been disproved, the increased capacity for glycolysis still remains a characteristic of tumours (2). In general, the metabolic profile of tumours differs from that of normal tissue as a result of many physiological and chemical factors, for example differences in rate of proliferation, availability of nutrients, accumulation of waste products, and pH.

## 1.2 TUMOUR TREATMENT

The three main modalities for the treatment of tumours are surgery, radiation therapy, and chemotherapy, either used as a single treatment or in a combined regimen. The earliest discussions of the surgical treatment of tumours are found in the Edwin Smith papyrus from the Egyptian Middle Kingdom (circa 1600 BC), and surgery still forms the mainstay of treatment in many solid tumours (15). Radiation therapy was applied for the treatment of malignant tumours not long after the discovery of x-rays by Wilhelm Roentgen in 1895 (16,17). However, it was also soon recognised that radiation produced adverse effects in normal tissues. Only in the 1950s technological developments enabled large-scale application of radiotherapy. The introduction of chemotherapy in the fifth and sixth decades of the twentieth century has resulted in the development of therapeutic interventions for patients with several types of advanced solid tumours (18,19). Research in cancer drug discovery and development has provided approximately sixty approved products for the treatment of malignancies nowadays (20).

Radiotherapy is based on the interaction of ionising radiation with molecules in biological tissue. The absorption of radiation in tissues leads to the excitation and ionisation of atoms. This may result in breakage of chemical bonds and the formation of free radicals. The high reactivity of free radicals leads to a chain of reactions that can damage proteins, deoxynucleic acids, phospholipids and other macromolecules and thereby disrupt cellular functions and integrity. The most critical target for cell killing is the DNA of the cell (21). The extent of cellular damage following radiation exposure is dependent on several factors, including cellular repair of lesions, the stage of the cell proliferation cycle, and the radiobiological susceptibility of cells. The latter depends strongly on the presence or absence of various chemical compounds. In particular the presence of oxygen is believed to prolong the lifetime of free radicals of cellular  $H_2O$  and to enhance permanent damage to the target molecules (22). Thus, a high level of oxygen in tumour tissue increases the sensitivity of a tumour to radiotherapy (23). Measurement of pretreatment oxygenation status has been shown to be predictive of radiation response in both head and neck tumours and tumours of the uterine cervix (24,25).

As well-oxygenated cells are more radiosensitive than hypoxic cells, increasing tumour oxygen levels may improve the efficacy of radiotherapy. This may be achieved by breathing high oxygen content gases like carbogen; a gas mixture consisting of 95%  $O_2$  and 5%  $CO_2$ . In response to breathing different hyperoxic hypercapnic gas mixtures a reduction in the hypoxic fraction was found in hypoxic tumours (26). This was also shown in hypoxic marker studies, in which carbogen breathing reduced chronic hypoxia in laryngeal tumours (27). Improvement of tumour oxygenation and radiation response under hyperoxic conditions has been shown in several human tumours (28-30).

### 1.3 HEAD AND NECK TUMOURS

Head and neck carcinomas are malignant tumours that may arise on all lining membranes of the upper aerodigestive tract. Most of these tumours are squamous cell carcinomas. In the Western world, head and neck cancers account for 3-10% of all new cancers each year (31,32). In many developing countries head and neck cancer is more common, and it is among the leading causes of cancer mortality worldwide (31). The ratio for occurrence in males versus females is about 4:1. Greatest risk factor in head and neck carcinogenesis is tobacco use (33). Alcohol produces a modest independent risk (34), and the effects of alcohol and tobacco seem to be synergistic (35,36).

Presenting symptoms, patterns of disease spread, and survival rates all vary by site of the primary tumour within the head-neck region. The main treatment options are surgery and radiation therapy (37,38). Especially in the case of laryngeal tumours, strategies are being developed to spare the functionality of the organ involved. These include sophisticated radiation methods, and combinations of radiotherapeutic, chemotherapeutic, and surgical methods (30,39,40). As tumours in the head-neck region may have variable blood flow and contain large hypoxic regions, radiosensitivity may be improved by increasing the tumour oxygen level (27,41). Head and neck tumours have shown an improved response to accelerated radiotherapy in combination with carbogen breathing and administration of nicotinamide (ARCON). This may be caused by improved tumour oxygenation, possibly intermediated by vascular effects. ARCON yielded actuarial 3 year local control rates of 80% for advanced larynx tumours, which is higher than any other report in the literature for this category of patients (30). Comparable results were obtained for other squamous cell carcinomas in the head-neck region (30).

### 1.4 MENINGIOMAS

Meningiomas are tumours arising from meningotheial cells that form the external membranous covering of the brain. Although meningiomas are not strictly brain tumours they are usually classified as such, because they arise within the intracranial cavity and present with neurologic symptoms and signs (42). Meningiomas comprise about 15-20% of all intracranial tumours (42,43). The majority of these tumours is benign, 1-2% are malignant, and about 5-7% are atypical meningiomas (44). Several histologic variants exist, but only a few have prognostic importance. Meningiomas are considerably more frequent in women than in men, with a female to male ratio of about 2:1 (44,45).

Meningiomas occur primarily at the base of the skull and over the cerebral convexities. Symptoms and signs include increased intracranial pressure, cranial

nerve palsy, and epilepsy (46). When treatment is necessary, surgery is the primary therapeutical option. However, meningiomas tend to recur, especially if total resection is impossible. Among tumours that are completely resected, 20% recur within 10 years (47), and more than 80% recur after partial resection (48). For this reason additional treatment options for meningiomas are considered. Recently, there has been an increased interest in stereotactic radiosurgery and radiotherapy for the treatment of meningiomas (49,50). Although in general there is a fair response to radiotherapy, sometimes higher doses of radiation are needed to improve control rates. However, radiation dose levels are limited to avoid radiation damage to the normal central nervous system, complicating optimal radiation treatment for meningiomas (43).

## 1.5 OLIGODENDROGLIOMAS

The most common primary brain tumours are gliomas, which include both astrocytic and oligodendroglial tumours (45). Oligodendrogliomas arise from oligodendrocytes or their precursors and they are usually located in the cortex and white matter of the cerebral hemispheres. Oligodendroglial tumours occur in patients of all ages, with a peak incidence between 25 and 50 years, accounting for approximately 10% of all intracranial tumours in this age group (42,46). In the WHO tumour grading system oligodendrogliomas are divided into two categories, low grade and high grade, which is of both prognostic and therapeutic relevance (45).

The presenting symptoms of patients with oligodendrogliomas are due to the raised intracranial pressure and to local or general brain dysfunction. Surgical resection is the primary mode of treatment in symptomatic patients and those with progressive disease. Because oligodendrogliomas generally show an infiltrative growth pattern, surgical cure remains unlikely (46). Until recently, the identification of oligodendrogliomas among glial tumours did not have therapeutical consequences. However, in 1988 it was recognised that malignant oligodendrogliomas are sensitive to chemotherapy (51). A regimen of procarbazine, lomustine, and vincristine resulted in a marked shrinkage of tumours, as shown by neuroimaging. Subsequent studies established the beneficial effect of chemotherapy of both high and low grade oligodendrogliomas and mixed oligoastrocytomas (52-54). Because of this unique chemosensitivity of oligodendrogliomas compared to other brain tumours, differential diagnosis of these tumours has become increasingly important.

## 1.6 RATIONALE AND OUTLINE OF THIS THESIS

A powerful technique to investigate anatomy, physiology, and metabolism in humans is Magnetic Resonance (MR). MR imaging and MR spectroscopy allow us

to study patients with tumours in a noninvasive way. The identification of a tumoural mass and the assessment of its size and vascularisation can be achieved with MR imaging, while MR spectroscopy can provide additional metabolic information for tumour classification, differential diagnosis, prognosis, and follow-up. In the context of tumour therapy for example, it is important to know how efficiently blood is providing oxygen, nutrients, and drugs to tumour tissue. Identification and characterisation of tumours may thus assist in prediction of treatment response and selection of the best therapeutical option. For this purpose, MR techniques have been used to investigate tumour physiology and metabolism in patients with tumours in the head-neck region, patients with oligodendrogliomas, and patients with meningiomas. These studies are described in this thesis.

The general principles of MR imaging and MR spectroscopy and their main applications as used in this thesis are summarised in chapter 2. The role of MR imaging to study the physiology of squamous cell carcinomas of the larynx is discussed in chapter 3. Tumour blood oxygenation and vascularisation are assessed to characterise these tumours and the potential clinical applications of the MR imaging techniques used are investigated.

One of the central MR methods for the assessment of human tumours is dynamic contrast enhanced MRI. Its diagnostic value has been shown in for example breast tumours, cervix tumours, and prostate carcinoma, both in tumour detection, identification, staging, and monitoring tumour treatment response. In chapter 4 a method is presented for the quantification of the dynamic MR contrast agent uptake. Using a pharmacokinetic model, this dynamic contrast enhanced MRI data can be interpreted in physiological terms like vascular permeability, blood flow, and blood volume. The MRI method and the data analysis are implemented in a clinical protocol and tested for reproducibility.

Besides tumour blood flow also tumour oxygenation is an important factor determining the outcome of cancer therapy, especially radiotherapy. Because carbogen breathing is a promising radiosensitiser for tumours in the head-neck region, tumour blood oxygenation and vascularisation were studied by MRI to map the physiological characteristics of these tumours and their response to hyperoxygenation. This may clarify the good response of head and neck tumours to ARCON therapy, and may allow prediction of treatment outcome for individual tumours. This study is presented in chapter 5.

A similar MRI study investigating the effects of hyperoxygenation is described in chapter 6 for meningiomas. The radiosensitivity of meningiomas may be improved by increasing tumour oxygen levels, which may be achieved by breathing a high oxygen content gas, similar to tumours in the head-neck region. The effects of breathing a hyperoxic hypercapnic gas mixture are investigated by several MRI

techniques, to assess changes in tumour oxygenation and vascular function. This MRI protocol may allow optimisation of radiation schemes for patients with meningiomas.

In chapter 7 an MR spectroscopy study is described characterising brain tumours, in particular oligodendrogliomas. In general brain tumours are pathologically diagnosed by analysis of tumour tissue obtained invasively by biopsy. Both MR imaging and MR spectroscopy can be applied to characterise brain tumours in a noninvasive way and have been used extensively for this purpose. As oligodendroglial tumours cannot be distinguished easily from other brain tumours based on clinical presentation and MR imaging alone, MR spectroscopy may provide helpful additional information on the metabolic profile of these tumours. In this way, oligodendrogliomas are characterised to enable specific identification of these tumours, which may guide the treatment selection for these patients.



## REFERENCES

1. Folkman J. Tumor angiogenesis: therapeutic implications. *New Engl J Med* 285:1182-1186, 1971.
2. Vaupel PW. Blood flow, oxygenation, tissue pH distribution, and bioenergetic status of tumors. Ernst Schering Research Foundation, Berlin, Germany, 1994.
3. Folkman J. What is the evidence that tumors are angiogenesis dependent? *J Natl Cancer Inst* 82:4-6, 1989.
4. Fidler IJ, Ellis LM. The implications of angiogenesis to the biology and therapy of cancer metastasis. *Cell* 79:185, 1994.
5. Folkman J. Angiogenesis in cancer, vascular, rheumatoid and other disease. *Nature Med* 1:27, 1995.
6. Thomlinson RH, Gray LH. The histological structure of some human lung cancers and the possible implications for radiotherapy. *Br J Cancer* 9:539-549, 1955.
7. Gasparini G. The rationale and future potential of angiogenesis inhibitors in neoplasia. *Drugs* 58(1):17-38, 1999.
8. Jain RK. Transport of molecules across tumor vasculature. *Cancer Metastasis Rev* 6:559-593, 1987.
9. Jain RK. Determinants of tumor blood flow: a review. *Cancer Res* 48:1641-1658, 1988.
10. Vaupel P, Kallinowski F, Okunieff P. Blood flow, oxygen and nutrient supply, and metabolic microenvironment of human tumors: a review. *Cancer Res* 49:6449-6465, 1989.
11. Brown JM. Evidence for acutely hypoxic cells in mouse tumours, and a possible mechanism of reoxygenation. *Br J Radiol* 52:650-656, 1979.
12. Chaplin DJ, Olive PL, Durand RE. Intermittent blood flow in a murine tumour: radiobiological effects. *Cancer Res* 47:597-601, 1987.
13. Vaupel P, Kallinowski F, Okunieff P. Blood flow, oxygen consumption, and tissue oxygenation of human tumors. *Adv Exp Med Biol* 277:895-905, 1990.
14. Warburg O. On the origin of cancer cells. *Science* 123:309, 1956.
15. DeVita VT, Hellman S, Rosenberg SA (Eds.). *Cancer. Principles and practice of oncology*. Lippincott Williams and Wilkins, Philadelphia, USA, 6th edition, 253-264, 2001.
16. Coutard H. Roentgentherapy of epitheliomas of the tonsillar region, hypopharynx and larynx from 1920 to 1926. *AJR Am J Roentgenol* 28:313-332, 1932.
17. Paterson RP. The radical x-ray treatment of carcinomata. *Br J Radiol* 9:671-679, 1936.
18. Li MC, Hertz R, Spencer DB. Effect of methotrexate therapy upon choriocarcinoma and chorioadenoma *Proc Soc Exp Biol Med* 93:361, 1956.

19. DeVita VT, Hellman S, Rosenberg SA (Eds.). *Cancer. Principles and practice of oncology*. Lippincott Williams and Wilkins, Philadelphia, USA, 6th edition, 289-306, 2001.
20. Kaufman D, Chabner BA. Clinical strategies for cancer treatment: the role of drugs. In: Chabner BA, Longo DL (Eds.), *Cancer chemotherapy and biotherapy*, Lippincott-Raven, New York, USA, 1, 1996.
21. Dizdaroglu M. Measurement of radiation-induced damage in DNA at the molecular level. *Int J Radiat Biol* 61:175-179, 1992.
22. Littbrand B, Revesz L. The effect of oxygen on cellular survival and recovery after radiation *Br J Radiol* 42:914-917, 1969.
23. Gray LH, Conger AD, Ebert M, et al. The concentration of oxygen dissolved in tissues at the time of irradiation as a factor in radiotherapy. *Br J Radiol* 26:638-648, 1953.
24. Nordsmark M, Overgaard M, Overgaard J. Pretreatment oxygenation predicts radiation response in advanced squamous cell carcinoma of the head and neck. *Radiother Oncol* 41:31-39, 1996.
25. Hockel M, Schlenger K, Aral B, et al. Association between tumour hypoxia and malignant progression in advanced cancer of the uterine cervix. *Cancer Res* 56:4509-4515, 1996.
26. Partridge SE, Aquino-Parsons C, Luo C, et al. A pilot study comparing intratumoural oxygenation using the comet assay following 2.5% and 5% carbogen and 100% oxygen. *Int J Radiat Oncol Biol Phys* 49:575-580, 2001.
27. Bussink J, Kaanders JH, Rijken PF, et al. Vascular architecture and microenvironmental parameters in human squamous cell carcinoma xenografts: effects of carbogen and nicotinamide. *Radiother Oncol* 50:173-184, 1999.
28. Martin L, Lartigau E, Weeger P, et al. Changes in the oxygenation of head and neck tumours during carbogen breathing. *Radiother Oncol* 27:123-130, 1993.
29. Hoskin PJ, Saunders MI, Dische S. Hypoxic radiosensitizers in radical radiotherapy for patients with bladder carcinoma: hyperbaric oxygen, misonidazole, and accelerated radiotherapy, carbogen, and nicotinamide. *Cancer* 86:1322-1328, 1999.
30. Kaanders JHAM, Pop LA, Marres HAM, et al. ARCON: experience in 215 patients with advanced head-and-neck cancer. *Int J Radiat Oncol Biol Phys* 52:769-778, 2002.
31. Greenlee RT, Hill-Harmon MB, Murray T, Thun M. Cancer statistics, 2001. *CA Cancer J Clin* 51:15-36, 2001.
32. Visser O, Coebergh JWW, Otter R, Schouten LJ (Eds.). *Head and neck tumours in the Netherlands 1989-1995*. Lulof druktechniek, Almelo, The Netherlands, 1998.
33. Brennan JA, Boyle JO, Koch WM, et al. Association between cigarette smoking and mutation of the p53 gene in squamous cell carcinoma of the head and neck. *N Engl J Med* 332:712-717, 1995.
34. Spitz MR, Fueger JJ, Goepfert H, Hong WK, Newell GR. Squamous cell carcinoma of the upper aerodigestive tract. *Cancer* 61:203-208, 1988.

35. Wynder EL. The epidemiology of cancers of the upper alimentary and upper respiratory tracts. *Laryngoscope* 88 Suppl 8:50-51, 1978.
36. Blot WJ, McLaughlin JK, Winn DM, et al. Smoking and drinking in relation to oral and pharyngeal cancer. *Cancer Res* 48(11):3282-3287, 1988.
37. Forastiere A, Koch W, Trotti A, Sidransky D. Head and neck cancer. *N Engl J Med* 345(26):1890-1900, 2001.
38. Million RR, Cassisi NJ (Eds.). Management of head and neck cancer. J.B. Lippincott Company, Philadelphia, USA, 2nd edition, 61-74, 1994.
39. Pfister D, Strong E, Harrison L. Larynx preservation with combined chemo- and radiotherapy in advanced head and neck cancer. *J Clin Oncol* 9:830, 1991.
40. Karp D, Vaughan C, Carter R, et al. Larynx preservation with induction chemotherapy plus radiation as alternative to laryngectomy. *Am J Clin Oncol* 14:273, 1991.
41. Vaupel P. Blood flow and oxygenation status of head and neck carcinomas. *Adv Exp Med Biol* 428:89-95, 1997.
42. DeAngelis LM. Brain tumors. *N Engl J Med* 344:114-123, 2001.
43. Kokubo M, Shibamoto Y, Takahashi JA, Sasai K, Oya N, Hashimoto N, Hiraoka M. Efficacy of conventional radiotherapy for recurrent meningioma. *J Neurooncol* 48:51-55, 2000.
44. Sanson M, Cornu P: Biology of meningiomas. *Acta Neurochir (Wien)* 142:493-505, 2000.
45. Kleihues P, Cavenee WK (Eds.). Pathology and genetics of tumours of the nervous system. IARC Press, Lyon, France, 2000.
46. DeVita VT, Hellman S, Rosenberg SA (Eds.). Cancer. Principles and practice of oncology. Lippincott Williams and Wilkins, Philadelphia, USA, 6th edition, 2100-2160, 2001.
47. Mirimanoff RO, Dosoretz DE, Linggood RM, et al. Meningioma: analysis of recurrence and progression following neurosurgical resection. *J Neurosurg* 62:18, 1985.
48. Yamasaki F, Yoshioka H, Hama S, Sugiyama K, Arita K, Kurisu K. Recurrence of meningiomas. *Cancer* 89:1102-1110, 2000.
49. Ojemann SG, Sneed PK, Larson DA, Gutin PH, Berger MS, Verhey L, Smith V, Petti P, Wara W, Park E, McDermott MW. Radiosurgery for malignant meningioma: results in 22 patients. *J Neurosurg* 93 Suppl 3:62-67, 2000.
50. Roche PH, Regis J, Dufour H, Fournier HD, Delsanti C, Pellet W, Grisoli F, Peragut JC. Gamma knife radiosurgery in the management of cavernous sinus meningiomas. *J Neurosurg* 93 Suppl 3:68-73, 2000.
51. Cairncross JG, MacDonald DR. Successful chemotherapy for recurrent malignant oligodendroglioma. *Ann Neurol* 23:360-364, 1988.
52. Pech IV, Peterson K, Cairncross JG. Chemotherapy for brain tumors. *Oncology (Huntingt.)* 12:537-543, 547, 1998.

53. Soffietti R, Ruda R, Bradac GB, Schiffer D. PCV chemotherapy for recurrent oligodendrogliomas and oligoastrocytomas. *Neurosurgery* 43:1066-1073, 1998.
54. Chinot O. Chemotherapy for the treatment of oligodendroglial tumors. *Semin. Oncol* 28:13-18, 2001.



# 2

## MAGNETIC RESONANCE

Mark Rijpkema

## 2.1 A BRIEF HISTORICAL OVERVIEW

### 2.1.1 MAGNETISM

The record of the discovery in the Western world of the first magnetic material is a poem by Nicander of Colophon, described in a footnote in *Historiae Naturalis XXXVII*, the work of the Roman naturalist Pliny the Elder (23-79 AD) (1). Circa 1000 BC, a shepherd by the name of Magnes was tending sheep on the slopes of Mount Ida in the Troad in Mysia (now Turkey). Suddenly, he found that his iron tipped crook and the tacks in his sandals were strongly drawn to the earth. He dug up the ground to find stones that we now refer to as lodestones (magnetite, a magnetic oxide of iron,  $\text{Fe}_3\text{O}_4$ ). The unexplained nature of the magnetic attraction however has been exploited by story tellers for a long time, making it difficult to separate fact from fancy. Lodestones found their application in compasses in China and in the 12th century this knowledge came to the Western world. Understanding of the phenomenon 'magnetism' however would not be achieved until many centuries later (1-3). Today magnetic materials are applied in everyday life. We even know that bacteria, certain birds, butterflies and other insects have a magnetic sense of direction (4,5).

### 2.1.2 NUCLEAR MAGNETIC RESONANCE

The phenomenon of Nuclear Magnetic Resonance (NMR) was demonstrated for the first time in 1946 independently by Felix Bloch et al and Edward Purcell et al (6,7). In 1952 they were awarded the Nobel prize for physics for their discovery. They found that the nuclei of certain atoms, when placed in a magnetic field, absorbed energy in the radiofrequency range and re-emitted this energy during the transition to their original state. The phenomenon was called NMR; *nuclear* because the nucleus of an atom was involved, *magnetic* because a magnetic field was required, and *resonance* because of the direct dependence of the magnetic field strength and the radiofrequency.

NMR developed quickly as a scientific discipline. Bloch introduced the concepts of relaxation times and introduced the so-called Bloch equations in 1946 to describe the NMR phenomenon (8). NMR was used for chemical and physical molecular analysis and rapidly progressed to become the most powerful non-destructive analytical method in chemistry. The first potential medical application of NMR was described by Raymond Damadian in 1971, who reported that the NMR water signal of malignant tumours and normal tissues were different (9).

### 2.1.3 MAGNETIC RESONANCE IMAGING

In late 1972, a prospective contributor to the British scientific journal *Nature* received a letter from the editor of the journal that read as follows (10): "With regret I am returning your manuscript which we feel is not of sufficiently wide significance for inclusion in *Nature*. This action should not in any way be regarded as an adverse criticism of your work, nor even an indication of editorial policies on studies in this field [...]" The paper submitted was very short and described a new imaging technique dubbed zeugmatography, a method that was derived from the NMR technique. The author of the paper was Paul Lauterbur. As he wanted his paper published in *Nature* he wrote back to the editor proposing to change the style of the paper to make the applications more clear. Finally, the paper was accepted and published in the March 1973 issue in *Nature* under the title (11) "Image formation by induced local interaction; examples employing magnetic resonance". From reading this title one would not think that a revolutionary idea in medical imaging was hidden behind it; the foundation of magnetic resonance imaging, MRI. (Note -- With the introduction of NMR to clinical imaging, the adjective *nuclear* was dropped.)

Soon after Lauterbur's experiments (on a water sample), images were produced from small objects such as onions and peppers. In 1975 Richard Ernst proposed magnetic resonance imaging using phase and frequency encoding, and the Fourier Transform (12). This method is the basis of the current MRI techniques. A few years later Damadian completed construction of the first whole body scanner, which he dubbed *Indomitable*. July 3, 1977, Damadian made the first human MRI scan, which took almost 5 hours (13).

## 2.2 BASIC CONCEPTS OF MAGNETIC RESONANCE\*

### 2.2.1 SPIN, PRECESSION, AND RESONANCE

The secret of NMR\* resides in the nucleus of an atom. Certain nuclei possess the property of angular momentum, or spin. Simply put, some nuclei can be thought of as small spinning spheres. Since nuclei bear electric charges, their spinning produces a magnetic field analogous to the field produced when an electric current flows through a coil of wire. This results in a magnetic dipole moment oriented along the spinning axis. The nucleus of the hydrogen atom ( $^1\text{H}$ ) consists of a proton and possesses a magnetic moment. Because of its high natural abundance, sensitivity,

---

\* Main sources used in this section are listed as references (14-17), which are also suggested as further reading material.

\* In the remainder of this chapter 'NMR' will be referred to as 'MR', which is clinically more common.



and presence in water and fat in the human body, it is the most important nucleus in medical MR.

When exposed to a static magnetic field, the randomly oriented magnetic dipoles line up with the magnetic field. To be more precise, the magnetic moment does not align exactly with the axis of the external magnetic field but precesses around it (see figure 2.1) at a rate given by the Larmor relationship

$$\nu = \omega/2\pi = \gamma B_0/2\pi \quad (2.1)$$

where  $\nu$  is the resonance frequency in Hz,  $\omega$  is the angular frequency in radians per second,  $\gamma$  is the gyromagnetic ratio, and  $B_0$  is the static magnetic field.  $\gamma$  is a nuclear constant characteristic for each type of nucleus. For protons,  $\gamma/2\pi = 42.58$  MHz/T which means that at a field strength  $B_0$  of 1.5 T the Larmor frequency for proton spins is about 63.8 MHz. A collection of identical nuclei will precess with the Larmor frequency but with random phases relative to each other so that on average the net (macroscopic) magnetisation vector remains along the axis of the external magnetic field.

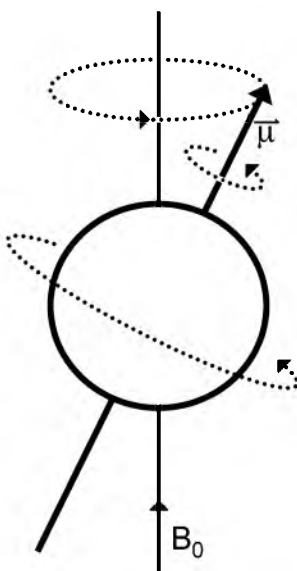


Figure 2.1. Schematic diagram of a hydrogen nucleus (proton) exposed to a magnetic field  $B_0$ . The spin of the positively charged proton results in a magnetic moment  $\vec{\mu}$ , which precesses around the axis of the magnetic field.

For a proton spin in a static magnetic field there are two possible basic states with orientations parallel and anti-parallel to the applied field, pertaining to a low and high energy state respectively. In MR, resonance occurs when radiofrequency (RF) energy is applied at the Larmor frequency, flipping the magnetic moments from their parallel (lower energy) to their anti-parallel (higher energy) states or vice versa.

In an external magnetic field more protons are in the lower energy state and the net magnetisation vector lies along the direction of the applied magnetic field. However, the only way to detect this magnetisation is to get it out of equilibrium. This can be

done by applying an specific RF field perpendicular to the main magnetic field. An RF pulse with a specific duration and amplitude will rotate the net magnetisation by an angle of  $90^\circ$  (often referred to as a 90 degree pulse, see figure 2.2). Following this pulse, the magnetisation will precess in the transverse plane at the Larmor frequency, and this precessing magnetisation can be picked up with an antenna (coil). The signal that is received is called the free induction decay (FID).

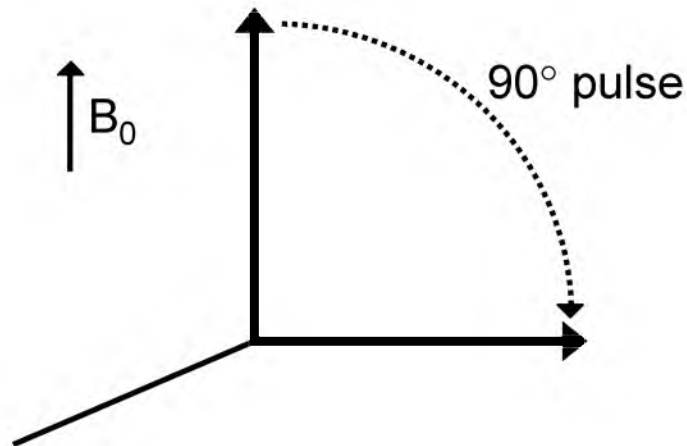


Figure 2.2. Schematic representation of the net magnetisation (indicated by the bold arrow) aligned to the external magnetic field  $B_0$  being tipped into the transverse plane. Transverse net magnetisation can be accomplished by application of a 90 degree RF pulse.

### 2.2.2 RELAXATION

When an excitation pulse is switched off, the spins start returning to their equilibrium. However, in their excited state, the nuclei can return to the ground state only by dissipating their excess energy to their surroundings. This process is called longitudinal ( $T_1$ ) relaxation.  $T_1$  relaxation is promoted by a surrounding nuclear environment with magnetic fields fluctuating at a frequency close to the Larmor frequency. These fluctuations are caused by rotational or translational motion of molecules. As the average rate at which molecules reorient is related to their size, the molecular environment of the nuclei (e.g. the presence of large molecules like proteins) determines their  $T_1$  relaxation time.

In addition to the inherent  $T_1$  of a tissue, MR contrast agents may be applied to modify this relaxation time. Gadolinium chelates are often used for this purpose. Gadolinium has a large magnetic moment because of its unpaired electrons, providing a strong fluctuating magnetic field at the Larmor frequency for protons in a magnetic field of  $\sim 1.5$  T. As a result, the  $T_1$  will drop when protons get near the contrast agent.

While the longitudinal magnetisation recovers to its equilibrium value, the transverse net magnetisation decays to zero. Nuclear magnetic moments contributing to the transverse net magnetisation get out of phase because of their mutual interaction, a process called T2 relaxation. All protons are affected by the magnetic fields of their neighbours, making them precess at slightly different Larmor frequencies. As a result, the magnetisation in the transverse plane begins to dephase, usually at a rate much faster than the longitudinal magnetisation recovers. The T2 of protons in water is primarily related to the intrinsic field caused by adjacent protons with low reorientation rates. For example, water molecules that are bound to biological macromolecules have efficient T2 relaxation and thus a shorter T2 relaxation time than 'free' water.

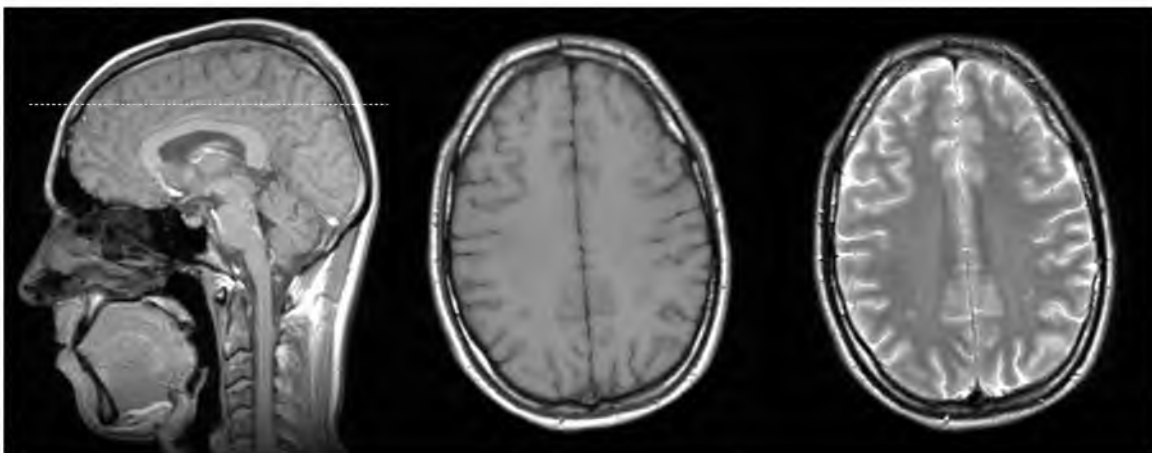


Figure 2.3. MR images of the author's head. Sagittal localizer image (left) indicating the position of the transversal slices (dashed line). Transversal T1 weighted image (centre) and T2 weighted image (right) of the brain.

The observed decay of the transverse magnetisation is usually faster than T2, due to imperfections in the main static magnetic field (field inhomogeneities). This also causes neighbouring protons to precess at different frequencies. The total rate of signal loss, due to a non-uniform magnetic field as well as T2 relaxation is characterised by T2\*. Besides having an effect on T1, MR contrast agents like Gadolinium chelates also alter the apparent relaxation time T2\*.

Differences in relaxation times provide contrast between different tissues in MR images. In figure 2.3 images are displayed showing differences in T1 (T1 weighted image) and differences in T2 (T2 weighted image) within the brain. Subtle differences in chemical, physical and biological properties of tissue may affect relaxation times. Tissue composition, structure, and surroundings, as well as inhomogeneities of the local magnetic fields within the tissue contribute to image contrast and may produce clinically useful differentiation between tissues.

### 2.2.3 PRINCIPLE OF IMAGING

The MR image represents the MR characteristics of tissue at a predefined position in the human body. To create an image of a specific slice within the body and also to localise individual voxels (volume elements) within the slice, all voxels have to experience a unique magnetic field. In conventional MR imaging three different functions are used for this purpose: slice selective excitation, frequency encoding, and phase encoding. These can be accomplished by applying temporary gradients in the magnetic field.

In slice selection, protons in the imaging slice are selectively excited by means of a combination of a frequency selective RF pulse and a magnetic field gradient perpendicular to the imaging plane. The bandwidth of the RF pulse and the amplitude of the slice selection gradient determine the slice thickness. Spatial encoding within this slice can be done by frequency encoding and phase encoding. When a gradient is switched on, spins at different locations will experience different magnetic fields, and will precess with different Larmor frequencies. This procedure is called frequency encoding and causes the resonance frequency to be proportional to the position of the spin. Phase encoding uses a gradient to induce a specific phase angle to the transverse magnetisation vector. This phase angle depends on the location of the individual spin and the duration and amplitude of the gradient. By applying frequency and phase encoding both the frequency and phase of the spins contain spatial information, which is recorded in the MR signal. In the process of MR imaging gradients with different strengths and/or durations are applied consecutively, and the MR signals recorded are stored in a raw data matrix called k-space. This data contains all spatial information and can be processed using Fourier Transformation to produce an image.

### 2.2.4 MAGNETIC RESONANCE SPECTROSCOPY

Whereas MR imaging mainly uses the signals from protons of water and fat to reconstruct an image, in MR spectroscopy the physical and chemical properties and concentrations of an extended set of metabolites are studied. Furthermore, MR spectroscopy can easily be applied to other nuclei than  $^1\text{H}$ ; nuclei potentially useful for biomedical application include  $^{13}\text{C}$ ,  $^{19}\text{F}$ , and  $^{31}\text{P}$ .

Chemical differences are manifest in the MR signal due to different shielding of the nucleus from the main magnetic field by the surrounding electrons. This results in an effective magnetic field

$$B_{\text{eff}} = B_0(1-\sigma) \quad (2.2)$$

where  $\sigma$  is the screening factor depending on the chemical environment of each nucleus. For example, in water, the electron cloud is drawn away from the hydrogen

nuclei (protons), leaving them fairly unshielded. The electrons of hydrogen in a  $\text{CH}_2$  group on a fatty acid chain are much closer to the hydrogen nucleus. These electrons shield the protons from the magnetic field and as a result their Larmor frequency is slightly different from those of water protons, by about 3 parts per million (ppm). This frequency shift is called 'chemical shift'. So, depending on its chemical environment, every nucleus resonates at a slightly different frequency. In MR spectroscopy signals are recorded at different frequencies, which are usually displayed in a spectrum. In figure 2.4 an example of an MR spectrum of the brain is shown. The horizontal axis of a spectrum represents the resonance frequency. The peak area reflects both the number of specific spins in a compound and the tissue content of that compound.

The property of chemical shift allows the MR spectroscopist to detect a wide variety of metabolites. Limiting factors for detection are the magnetic properties and the concentration of a compound. As the tissue levels of water and fat are much higher than those of other metabolites, MRS signals are much weaker than signals acquired using MRI. Therefore, in an MRS measurement multiple consecutive acquisitions are applied, and the resulting signals are averaged to obtain an acceptable level of signal with respect to noise (expressed as the signal-to-noise ratio, SNR).

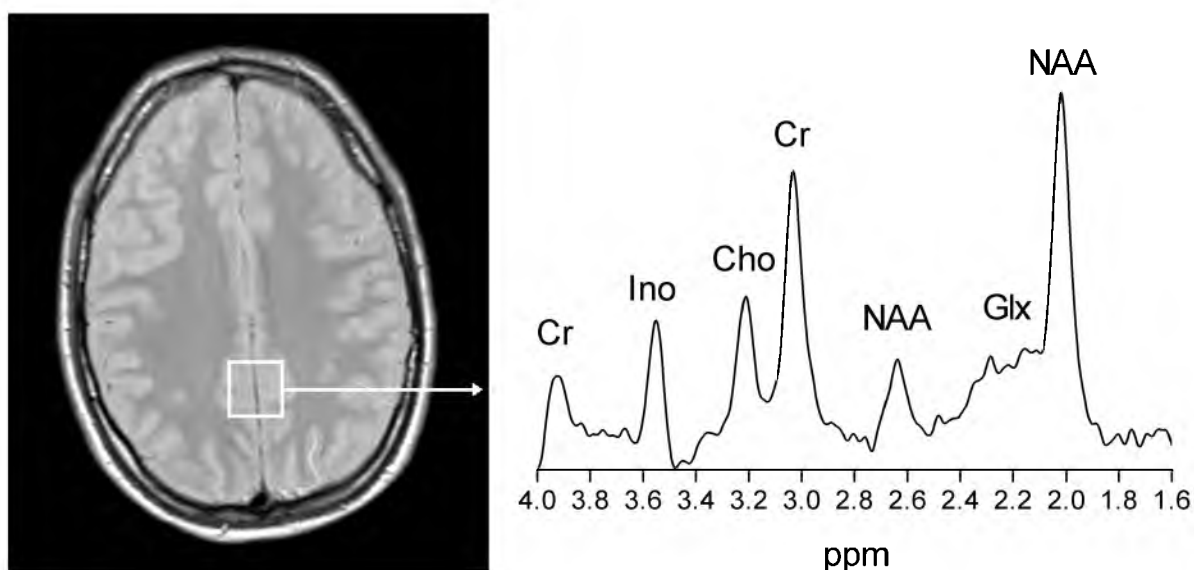


Figure 2.4. Transversal MR image (left) of the brain. The white square indicates the position from which the spectrum was obtained.  $^1\text{H}$  MR spectrum (right) of the grey matter region indicated in the MR image. The main brain metabolites NAA, Glx, Cr, Cho, and Ino are labelled, see section 2.3.4 for details. (Sequence parameters: STEAM SVS,  $\text{TR}=2000$  ms,  $\text{TE}=20$  ms, 128 acquisitions.)

To obtain *in vivo* MR spectra from a particular type of tissue it is necessary to limit or localise the volume from which the signal is detected. Two techniques are commonly applied for this purpose (18). Single voxel spectroscopy (SVS) uses slice selective RF pulses in three dimensions to select the volume of interest. In MR spectroscopic imaging (MRSI) gradients are used for spatial encoding, analogous to

the phase encoding technique used in MR imaging. Also a combination of phase encoding and slice selective pulses can be used. With MRSI, signals from multiple voxels in a grid can be obtained in one measurement. In this way, images of metabolite levels can be reconstructed, similar to MR images of anatomy.

## 2.3 MAGNETIC RESONANCE APPLICATIONS

### 2.3.1 BLOOD OXYGEN LEVEL DEPENDENT MRI

The blood oxygenation level dependent (BOLD) effect on MR signals was first demonstrated by Ogawa et al in a series of papers on a method to detect brain activation (19-21). In these papers the influence of the oxygenation level in venous blood on the signal intensity in MR images was shown. BOLD MRI is based on the magnetic properties of blood which are dependent on the oxygenation state of haemoglobin; deoxygenated haemoglobin is paramagnetic while oxyhaemoglobin is diamagnetic. Thus, deoxygenation results in an increased magnetic susceptibility difference between the vascular compartment and tissue (22). This susceptibility difference induces a local variation of the magnetic field strength around the vessels and capillaries, resulting in dephasing and signal loss in gradient echo (T2\* weighted) images (21). In this way, deoxyhaemoglobin acts as an endogenous contrast agent.

Ogawa et al showed the feasibility of the BOLD method to detect activity in the human occipital cortex after a visual stimulus; a method that grew out to a widely used practical technique in current brain research (functional MRI, fMRI (23-25)). Soon also tumours were assessed using this technique, first in laboratory animals (e.g. 26-28) and subsequently in humans (e.g. 29-31), mainly to assess the effect of oxygenating agents. The physiological basis of the BOLD signal has been investigated extensively (32-34), however its exact contrast mechanism in MRI remains complicated. The BOLD signal proved to be sensitive not only to oxygenation, but also to changes in vascular volume and flow (28,35,36). In this respect, also the acronym FLOOD (Flow and Oxygenation Dependent) was introduced (27).

BOLD measurements have been used to assess the effect of carbogen breathing in a variety of tumours in humans (29-31). In most tumours a significant signal enhancement was seen on T2\* weighted images, which was interpreted as an improved oxygenation. This was supported by studies of Al-Hallaq et al, who showed a correlation between microelectrode measurements of changes in tumour oxygenation due to carbogen breathing and BOLD MRI (37).

### 2.3.2 DYNAMIC CONTRAST ENHANCED MRI

The primary goal for the introduction of contrast agents in Magnetic Resonance Imaging was the possible improvement in medical diagnosis by better tissue characterisation. Most of the currently available contrast agents are paramagnetic and focus upon relaxation time and susceptibility changes. Their effect is caused by a metal ion which contains unpaired electrons (e.g.  $Gd^{3+}$  in Gd-DTPA has 7 unpaired electrons). The resulting shortening in relaxation times is usually measured by T1 weighted MR imaging.

Gadolinium-DTPA (Gd-DTPA) is an exogenous contrast agent that remains intravascular in normal brain tissue due to the blood brain barrier, but diffuses into the extravascular extracellular space (EES) in all other tissues. It normally does not cross the cell membrane and remains extracellular. Information on vascular structure and function can be acquired by dynamically monitoring the exchange of Gd-DTPA between blood plasma and the EES. Dynamic contrast enhanced MRI (DCE-MRI) has been widely used for the assessment of human tumours. Its diagnostic value has been shown in for example breast tumours (38,39), cervix tumours (40), and prostate carcinoma (41,42), both in tumour detection, identification, and staging.

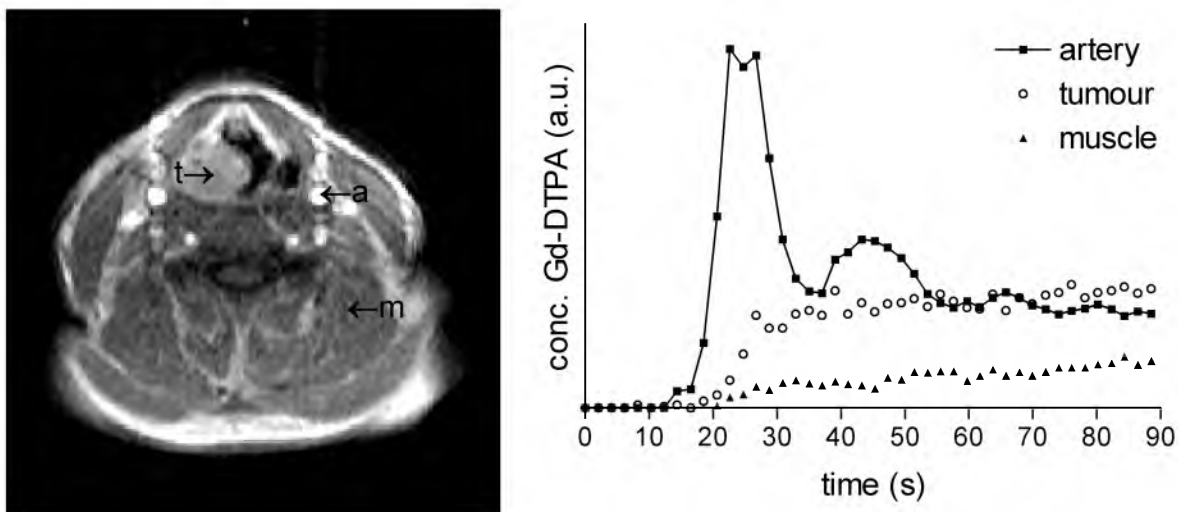


Figure 2.5. Transversal dynamic contrast enhanced MR image of a patient with a hypopharynx tumour, recorded one minute after Gd-DTPA contrast administration (left). Pixels from which the signal intensity versus times curves were obtained are labelled a (artery), t (tumour), and m (muscle). At the right, signal intensity changes in blood and the different tissues due to the contrast agent are plotted versus time.

The procedure for a DCE-MRI measurement is a combination of administration of the contrast agent and recording a series of fast MRI contrast enhanced images. For this purpose, Gd-DTPA is usually administered as an intravenous bolus injection. DCE-MRI data of a series of consecutive images can be visualised in signal intensity versus time curves, as shown in figure 2.5. As the signal intensity

changes reflect the local concentration of Gd-DTPA, this data can be used to characterise the vascular properties of different tissues. Also, the effects of agents or procedures with potential vasomodulating capabilities, e.g. carbogen breathing, may be investigated in this way.

### 2.3.3 PHYSIOLOGICAL PHARMACOKINETIC MODELS

Dynamic contrast enhanced MRI data can be used to gain insight in the underlying physiology of the tumour by applying a physiological pharmacokinetic model to the data. Several models have been developed to express this data in terms of physiological parameters. The most widely used are the model proposed by Larsson et al in 1990 (43) and the model proposed by Tofts and Kermode in 1991 (44). Although the two models are in general the same there are a few differences, mainly in the (physiological) assumptions that are being made. An extensive comparison of the models was discussed by the two authors in a joint study (45).

Both physiological pharmacokinetic models are commonly used to fit the concentration Gd-DTPA versus time data\*. For proper interpretation of the model results however, one has to be aware of the assumptions that are made in the formulation of the model. Three important assumptions are: 1. compartments contain a uniform distribution of Gd-DTPA, 2. Gd-DTPA in the EES has arrived directly from a nearby capillary, and 3. there is fast exchange of all mobile protons within a tissue. A more elaborate overview of the model assumptions has been discussed by Tofts (46).

In its simplest form, the model consists of two compartments, a vascular (blood plasma) and an extravascular (EES) compartment, as is shown in figure 2.6. A rate constant defines the exchange of contrast medium between these compartments. The change of the Gd-DTPA concentration in the EES is described by (43,44,47)

$$\frac{dC_t(t)}{dt} = K^{\text{trans}} \cdot C_p(t) - k_{\text{ep}} \cdot C_t(t) \quad (2.3)$$

with  $C_t$  : tissue concentration of Gd-DTPA (mM);  $C_p$  : arterial plasma concentration of Gd-DTPA (mM);  $k_{\text{ep}}$  : rate constant ( $\text{min}^{-1}$ ) between extravascular extracellular space and blood plasma;  $K^{\text{trans}}$  : volume transfer constant ( $\text{min}^{-1}$ ),  $K^{\text{trans}} = k_{\text{ep}} \cdot v_e$  and  $v_e$  = volume of EES per unit volume of tissue (47). By setting the concentration of Gd-DTPA at the time of bolus injection to 0, the general solution of equation 2.3 is (43,44,47)

---

\* Before DCE-MRI data is entered into the model, the measured signal intensity changes have to be converted into concentration of Gd-DTPA. Several mathematical methods can be used for this purpose, but description of these is beyond the scope of this chapter.



$$C_t(t) = K^{\text{trans}} \cdot \int_0^t C_p(\tau) \cdot e^{-k_{ep}(t-\tau)} \cdot d\tau \quad (2.4)$$

The function  $C_p(t)$  is called the arterial input function (AIF). According to the model, this AIF should be measured in feeding arterial vessels at the capillary level. However, this is generally not possible and the concentration changes of Gd-DTPA in blood are usually measured in a larger artery. An example of the bolus passage of Gd-DTPA in an artery is shown in figure 2.5.

In the Larsson model the Gd-DTPA uptake rate is governed by several physiological parameters (43,47)

$$k_{ep} = \frac{E \cdot F}{v_e} \quad \text{with the extraction fraction } E = 1 - e^{-\frac{P \cdot S}{F}} \quad (2.5)$$

with P: vascular permeability ( $\text{cm} \cdot \text{min}^{-1}$ ); S: vascular surface area ( $\text{cm}^2$ ); F: tumour blood flow ( $\text{ml} \cdot \text{min}^{-1}$ ) (47). For the sake of simplicity both haematocrit and tissue density are ignored here. The Gd-DTPA uptake rate can be displayed as a map by applying the physiological model to DCE-MRI data on a pixel-by-pixel basis. In this way spatial information can be obtained to identify and characterise tumour tissue and to map physiological changes in a tumour.

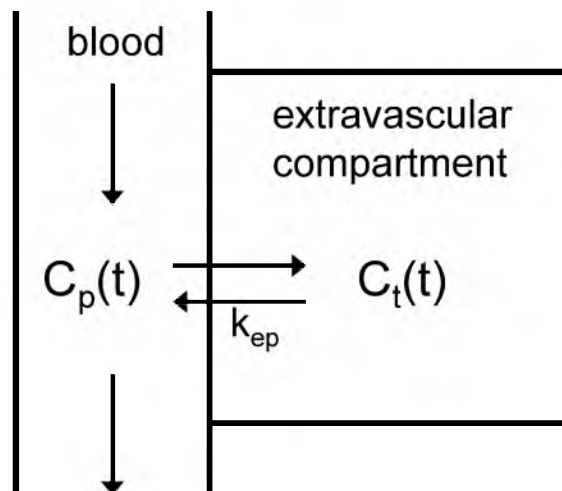


Figure 2.6. Physiological pharmacokinetic model containing two compartments: blood plasma (vascular compartment) and extravascular extracellular space (extravascular compartment), with Gd-DTPA concentrations of  $C_p(t)$  and  $C_t(t)$  respectively. The rate constant  $k_{ep}$  describes the exchange of Gd-DTPA between the two compartments.

#### 2.3.4 $^{31}\text{P}$ AND $^1\text{H}$ MAGNETIC RESONANCE SPECTROSCOPY

Among all biomedically relevant MR detectable nuclei,  $^1\text{H}$  offers the highest sensitivity for MR spectroscopy (MRS) because of its relatively high gyromagnetic ratio and natural abundance. In spite of this, the majority of pioneering studies in the

field of in vivo MRS dealt with the measurement of phosphorus ( $^{31}\text{P}$ ) containing metabolites, mainly because this was technically less complicated (48-50). The dominant signals in  $^{31}\text{P}$  MRS of human tissues originate from adenosine triphosphate (ATP), phosphocreatine (PCr), inorganic phosphate ( $\text{P}_i$ ), phosphodiester (PDE), and phosphomonoesters (PME). An example of a  $^{31}\text{P}$  MR spectrum is shown in figure 2.7. Both ATP and PCr have key functions in cellular energy metabolism; ATP as a direct energy source and PCr as an energy buffering compound to support ATP homeostasis. PME and PDE are believed to act as phospholipid precursors and catabolites respectively and may thus provide information on membrane metabolism (51).

Relative metabolite concentrations obtained from in vivo  $^{31}\text{P}$  MRS data have been used to study a wide range of physiological and pathophysiological phenomena, including cerebral ischemia (52,53) and tumour physiology.  $^{31}\text{P}$  MRS has been applied to numerous human cancers, both for tumour identification and monitoring treatment response (54-59). In general, metabolic characteristics of tumours include a high level of PME and PDE, and a low level of PCr with respect to normal tissues (55).

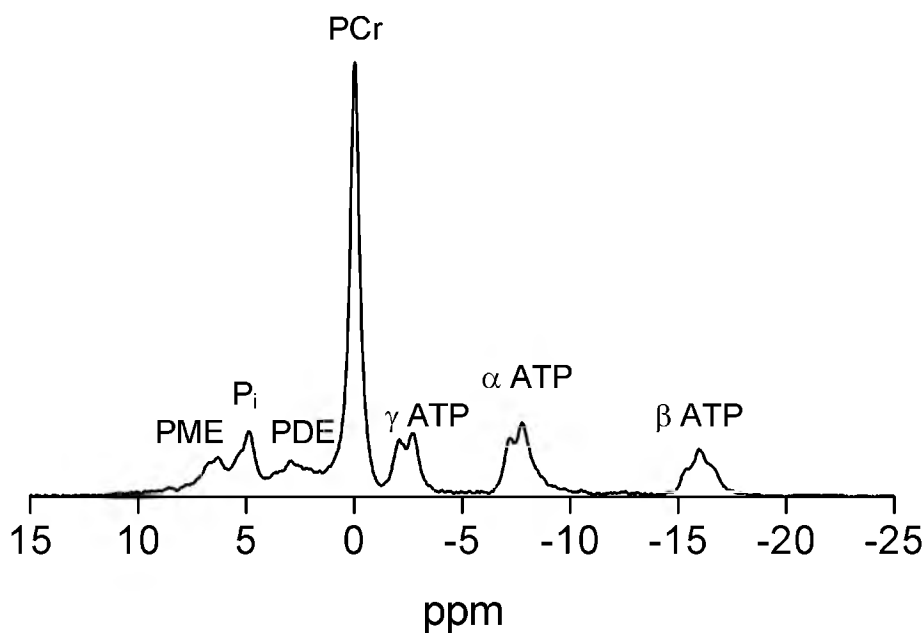


Figure 2.7.  $^{31}\text{P}$  MR spectrum of the author's neck. The signal was obtained mainly from muscle tissue. The metabolites ATP, PCr, PDE,  $\text{P}_i$ , and PME are labelled. (Sequence parameters: unlocalised BIRP (2kHz), TR=1800 ms, 500 acquisitions.)

The study of tissue metabolites by  $^1\text{H}$  MRS is more complicated because of the need to suppress the intense water and fat signals and by the large number of metabolites that produce signals in a relatively narrow chemical shift range. However, continued technical developments tackling these problems have made possible the detection and quantification of a wide range of metabolites. Nowadays,

$^1\text{H}$  MRS is in widespread use for the elucidation of pathophysiology starting from investigations of cell cultures, body fluids, isolated organs, whole animals, up to the study of human patients.

A major application of  $^1\text{H}$  MRS is the study of brain tumours, mainly because the brain is relatively easy to assess by MR and difficult to investigate by invasive methods. Clinical usefulness of  $^1\text{H}$  MR spectroscopy includes diagnosis, design of the most favourable treatment regimens for each patient, and posttreatment monitoring (60,61). MRS may provide additional information in cases in which the differential diagnosis of tumours by MRI is difficult (62). Metabolic information obtained by MR spectroscopy has proven to be promising in the accurate diagnosis of human brain tumours (63-65). Furthermore, MRS showed to be an important guide for clinical decision making (66).

A  $^1\text{H}$  MR spectrum provides a metabolic fingerprint of the tissue under analysis, as it contains many metabolites involved in a variety of cellular functions. For example, a common observation in  $^1\text{H}$  MR spectroscopy of brain tumours is a decreased level of NAA and an increased level of Cho (64,67). NAA is a major brain metabolite involved in cell signalling, regulation of interactions of brain cells, and the establishment and maintenance of the nervous system (68). The presence of NAA is used increasingly in clinical MRS studies as a neuronal marker. Elevated Cho levels are consistent with an increased choline turnover in relation to membrane biosynthesis by proliferating cells (62).

An example of a  $^1\text{H}$  MR spectrum of normal brain tissue is shown in figure 2.4. The main metabolites include N-acetylaspartate plus N-acetylaspartylglutamate (NAA), glutamine plus glutamate (Glx), creatine plus phosphocreatine (Cr), choline containing compounds (Cho), and myo-inositol (Ino). An elaborate overview of metabolites found in  $^1\text{H}$  MR spectra of normal and pathological tissues has been provided by several authors, e.g. (69-71). Also, different MRS techniques to obtain  $^1\text{H}$  MR spectra, and the clinical use of  $^1\text{H}$  MRS has been reviewed extensively in the past few years (60,64,72,73).

## REFERENCES

1. Mourino MR. From Thales to Lauterbur, or from the lodestone to MR Imaging: magnetism and medicine. *Radiology* 180:593-612, 1991.
2. Saini S, Frankel RB, Stark DD, Ferrucci JT. Magnetism: a primer and review. *A J R* 150:735-743, 1988.
3. Crombie AC. *Augustine to Galileo: Science in the Middle Ages and Science in the later Middle Ages and early modern times*. Harmondsworth, Middlesex, UK, 1970.
4. Blakemore RP, Frankel RB. Magnetic navigation in bacteria. *Sci Am* 246:58-65, 1981.
5. Etheredge JA, Perez SM, Taylor OR, Jander R. Monarch butterflies (*Danaus plexippus* L.) use a magnetic compass for navigation. *Proc Nat Acad Sci USA* 96:13845-13846, 1999.
6. Bloch F, Hansen WW, Packard M. The nuclear induction experiment. *Phys Rev* 70:474-485, 1946.
7. Purcell EM, Torrey HC, Pound RV. Resonance absorption by nuclear magnetic moments in a solid. *Phys Rev* 69:37-38, 1946.
8. Bloch F. Nuclear induction. *Phys Rev* 70:460-474, 1946.
9. Damadian R. Tumor detection by nuclear magnetic resonance. *Science* 171:1151-1153, 1971.
10. Rinck PA. *Magnetic Resonance in Medicine*. Blackwell Scientific Publications, Oxford, UK, 1-4, 1993.
11. Lauterbur PC. Image formation of induced local interactions: examples employing NMR. *Nature* 242:190-191, 1973.
12. Kumar A, Welti D, Ernst RR. NMR Fourier zeugmatography. *J Magn Reson* 18:69-83, 1975.
13. Damadian R, Goldsmith M, Minkoff L. NMR in cancer: XVI. FONAR image of the live human body. *Physiol Chem Phys* 9:97-100, 108, 1977.
14. Stark DD, Bradley WG. *Magnetic Resonance Imaging*. The CV Mosby Company, St. Louis, USA, 1988.
15. Rinck PA. *Magnetic Resonance in Medicine*. Blackwell Scientific Publications, Oxford, UK, 1993.
16. Gadian DG. *NMR and its applications to living systems*. Oxford university press, Oxford, UK, 1995.
17. Schild HH. *MRI made easy*. Schering AG, Berlin, Germany, 1990.
18. Sauter R, Schneider M, Wicklow K, Kolem H. Current status of clinically relevant techniques in magnetic resonance spectroscopy. *Electromedica* 60:32-54, 1992.
19. Ogawa S, Lee TM. Magnetic Resonance Imaging of blood vessels at high fields: in vivo and in vitro measurements and image simulation. *Magn Res Med* 19:9-18, 1990.

20. Ogawa S, Lee TM, Kay AR, Tank DW. Brain Magnetic Resonance Imaging with contrast dependent on blood oxygenation. *Proc Natl Acad Sci* 87:9868-9872, 1990.
21. Ogawa S, Lee TM, Nayak AS, Glynn P. Oxygenation-sensitive contrast in magnetic resonance image of rodent brain at high magnetic fields. *Magn Res Med* 14:68-78, 1990.
22. Weisskoff RM, Kuhne S. MRI susceptometry: image-based measurement of absolute susceptibility of MR contrast agents and human blood. *Magn Res Med* 24:375-383, 1992.
23. Orrison WWJ, Lewin JS, Sanders JA, Hartshorne MF. *Functional brain imaging*. Mosby, St. Louis, USA, 1995.
24. Kwong KK. Current issues in functional MRI. *NMR Biomed* 10:157-159, 1997.
25. Ogawa S, Menon RS, Kim SG, Ugurbil K. On the characteristics of functional magnetic resonance imaging of the brain. *Ann Rev Biophys Biomol Struct* 27:447-474, 1998.
26. Robinson SP, Rodrigues LM, Ojugo AS, McSheehy PMJ, Howe FA, Griffiths JR. The response to carbogen breathing in experimental tumour models monitored by gradient-recalled echo magnetic resonance imaging. *Br J Cancer* 75:1000-1006, 1997.
27. Howe FA, Robinson SP, Rodrigues LM, Griffiths JR. Flow and oxygenation dependent (FLOOD) contrast MR imaging to monitor the response of rat tumours to carbogen breathing. *Magn Reson Imag* 17:1307-1318, 1999.
28. Neeman M, Dafni H, Bukhari O, Braun RD, Dewhirst MW. In vivo BOLD contrast MRI mapping of subcutaneous vascular function and maturation: Validation by intravital microscopy. *Magn Reson Med* 45:887-898, 2001.
29. Griffiths JR, Taylor NJ, Howe FA, Saunders MI, Robinson SP, Hoskin PJ, Powell MEB, Thoumine M, Caine LA, Baddeley H. The response of human tumours to carbogen breathing, monitored by Gradient-Recalled Echo Magnetic Resonance Imaging. *Int J Radiat Oncol Biol Phys* 39:697-701, 1997.
30. Taylor NJ, Baddeley H, Goodchild KA, Powell MEB, Thoumine M, Culver LA, Stirling JJ, Saunders MI, Hoskin PJ, Phillips H, Padhani AR, Griffiths JR. BOLD MRI of human tumor oxygenation during carbogen breathing. *J Magn Res Imag* 14:156-163, 2001.
31. Rijpkema M, Kaanders J, Joosten F, van der Kogel A, Heerschap A. Effects of breathing a hyperoxic hypercapnic gas mixture on blood oxygenation and vascularity of head and neck tumors as measured by MRI. *Int J Radiat Oncol Biol Phys* 53(5):1185-1191, 2002.
32. Raichle ME. BOLD insights. *Nature* 412:128-130, 2001.
33. Logothetis NK, Pauls J, Augath M, Trinath T, Oeltermann A. Neurophysiological investigation of the basis of the fMRI signal. *Nature* 412:150-157, 2001.
34. Buxton RB, Frank LR. A model for the coupling between cerebral blood flow and oxygen metabolism during neural stimulation. *J Cerebr Blood Flow Metab* 17:64-72, 1997.
35. Duyn JH, Moonen CT, van Yperen GH, de Boer RW, Luyten PR. Inflow versus deoxyhemoglobin effects in BOLD functional MRI using gradient echoes at 1.5 T. *NMR Biomed* 7:83-88, 1994.

36. Lee SP, Duong TQ, Yang G, Iadecola C, Kim SG. Relative changes of cerebral arterial and venous blood volumes during increased cerebral blood flow: implications for BOLD fMRI. *Magn Res Med* 45:791-800, 2001.
37. Al Hallaq HA, River JN, Zamora M, Oikawa H, Karczmar GS. Correlation of magnetic resonance and oxygen microelectrode measurements of carbogen-induced changes in tumour oxygenation. *Int J Radiat Oncol Biol Phys* 41:151-159, 1998.
38. Degani H, Gusic V, Weinstein D, Fields S, Strano S. Mapping pathophysiological features of breast tumors by MRI at high spatial resolution. *Nat Med* 3:780-782, 1997.
39. Buckley DL, Drew PJ, Mussurakis S, Monson JR, Horsman A. Microvessel density of invasive breast cancer assessed by dynamic Gd-DTPA enhanced MRI. *J Magn Reson Imag* 7:461-464, 1997.
40. Mayr NA, Hawighorst H, Yuh WT, Essig M, Magnotta VA, Knopp MV. MR microcirculation assessment in cervical cancer: Correlations with histomorphological tumor markers and clinical outcome. *J Magn Reson Imag* 10:267-276, 1999.
41. Barentsz JO, Engelbrecht M, Jager GJ, Witjes JA, de LaRosette J, van der Sanden, BP, Huisman HJ, Heerschap A. Fast dynamic Gadolinium-enhanced MR Imaging of urinary bladder and prostate cancer. *J Magn Reson Imag* 10:295-304, 1999.
42. Padhani, AR, Gapinski CJ, Macvicar DA, Parker GJ, Suckling J, Revell PB, Leach MO, Dearnaley DP, Husband JE. Dynamic contrast enhanced MRI of prostate cancer: Correlation with morphology and tumour stage, histological grade and PSA. *Clin Radiol* 55: 99-109, 2000.
43. Larsson HB, Stubgaard M, Frederiksen JL, Jensen M, Henriksen O, Paulson OB. Quantitation of blood-brain barrier defect by Magnetic Resonance Imaging and Gadolinium-DTPA in patients with multiple sclerosis and brain tumors. *Magn Reson Med* 16:117-131, 1990.
44. Tofts PS, Kermode AG. Measurement of the blood-brain barrier permeability and leakage space using dynamic MR Imaging. 1. Fundamental Concepts. *Magn Reson Med* 17:357-367, 1991.
45. Larsson HBW, Tofts PS. Measurement of blood-brain barrier permeability using dynamic Gd-DTPA scanning --a comparison of methods. *Magn Reson Med* 24:174-176, 1992.
46. Tofts PS. Modeling tracer kinetics in dynamic Gd-DTPA MR Imaging. *J Magn Reson Imag* 7:91-101, 1997.
47. Tofts PS, Brix G, Buckley DL, Evelhoch JL, Henderson E, Knopp MV, Larsson HB, Lee TY, Mayr NA, Parker GJ, Port RE, Taylor J, Weisskoff RM. Estimating kinetic parameters from dynamic contrast-enhanced T(1)-weighted MRI of a diffusible tracer: standardized quantities and symbols. *J Magn Reson Imag* 10:223-232, 1999.
48. Moon RB, Richards JH. Determination of intracellular pH by <sup>31</sup>P magnetic resonance. *J Biol Chem* 248:7276-7278, 1973.
49. Hoult DI, Busby SJW, Gadian DG, Radda GK, Richards RE, Seeley PJ. Observations of tissue metabolites using <sup>31</sup>P nuclear magnetic resonance. *Nature* 252:285-287, 1974.

50. Henderson TO, Costello AJR, Omachi A. Phosphate metabolism in intact human erythrocytes: determination by phosphorus-31 nuclear magnetic resonance spectroscopy. *Proc Natl Acad Sci* 71:2487, 1974.
51. Podo F. Tumour phospholipid metabolism. *NMR Biomed* 12:413-439, 1999.
52. Martin E, Buchli R, Ritter S, Schmid R, Largo RH, Boltshauser E, Fanconi S, Duc G, Rumpel H. Diagnostic and prognostic value of cerebral 31P magnetic resonance spectroscopy in neonates with perinatal asphyxia. *Pediatr Res* 40:749-758, 1996.
53. Welch KMA, Levine SR, Martin G, Ordidge R, VandeLinde AMQ, Helpert JA. Magnetic resonance spectroscopy in cerebral ischemia. *Neurol Clin* 10:1-29, 1992.
54. Karczmar GS, Meyerhoff DJ, Speder A, Valone F, Wilkinson M, Shine N, Boska MD, Weiner MW. Response of tumors to therapy studied by 31P magnetic resonance spectroscopy. *Invest Radiol* 24:1020-1023, 1989.
55. Negendank W. Studies of human tumors by MRS: a review. *NMR Biomed* 5:303-324, 1992.
56. Negendank WG, Padavic-Shaller KA, Li CW, Murphy-Boesch J, Stoyanova R, Krigel RL, Schilder RJ, Smith MR, Brown TR. Metabolic characterization of human non-Hodgkin's lymphomas in vivo with the use of proton-decoupled phosphorus magnetic resonance spectroscopy. *Cancer Res* 55:3286-3294, 1995.
57. Moller HE, Vermathen P, Rummeny E, Wortler K, Wuisman P, Rossner A, Wormann B, Ritter J, Peters PE. In vivo 31P NMR spectroscopy of human musculoskeletal tumors as a measure of response to chemotherapy. *NMR Biomed* 9:347-358, 1996.
58. Maintz D, Heindel W, Kugel H, Jaeger R, Lackner KJ. Phosphorus-31 MR spectroscopy of normal adult human brain and brain tumors. *NMR Biomed* 15:18-27, 2002.
59. Shukla-Dave A, Poptani H, Loevner LA, Mancuso A, Serrai H, Rosenthal DI, Kilger A, Nelson D, Zakian K, Arias-Mendoza F, Rijpkema M, Koutcher JA, Brown TR, Heerschap A, Glickson JD. Prediction of treatment response of head and neck cancers by <sup>31</sup>P MRS from pretreatment relative phosphomonoester levels. *Acad Radiol* 9(6):688-694, 2002.
60. Smith ICP, Stewart LC. Magnetic resonance spectroscopy in medicine: clinical impact. *Prog NMR Spectroscopy* 40:1-34, 2002.
61. Leclerc X, Huisman TAGM, Sorensen G. The potential of proton magnetic resonance spectroscopy (<sup>1</sup>H-MRS) in the diagnosis and management of patients with brain tumors. *Curr Opin Oncol* 14:292-298, 2002.
62. Lee PL, Gonzalez RG. Magnetic resonance spectroscopy of brain tumors. *Curr Opin Oncol* 12:199-204, 2000.
63. Preul MC, Caramanos Z, Collins DL, Villemure JG, Leblanc R, Olivier A, Pokrupa R, Arnold D. Accurate, noninvasive diagnosis of human brain tumors by using proton magnetic resonance spectroscopy. *Nat Med* 2:323-325, 1996.
64. Nelson SJ, Vigneron DB, Dillon WP. Serial evaluation of patients with brain tumors using volume MRI and 3D 1H MRSI. *NMR Biomed* 12:123-138, 1999.

65. Norfray JF, Tomita T, Byrd SE, Ross BD, Berger PA, Miller RS. Clinical impact of MR spectroscopy when MR imaging is indeterminate for pediatric brain tumors. *Am J Roentgenol* 173:119-125, 1999.
66. Lin A, Bluml S, Mamelak AN. Efficacy of proton magnetic resonance spectroscopy in clinical decision making for patients with suspected malignant brain tumors. *J Neuro-Oncol* 45:69-81, 1999.
67. Negendank WG, Sauter R, Brown TR, et al. Proton magnetic resonance spectroscopy in patients with glial tumors: a multicenter study. *J Neurosurg* 84:449-458, 1996.
68. Baslow MH. Functions of N-acetyl-L-aspartate and N-acetyl-L-aspartylglutamate in the vertebrate brain: role in glial cell-specific signaling. *J Neurochem* 75:453-459, 2000.
69. Howe FA, Maxwell RJ, Saunders DE, Brwon MM, Griffiths JR. Proton spectroscopy in vivo. *Magn Reson Q* 9:31-59, 1993.
70. Ross B, Michaelis T. Clinical applicatios of magnetic resonance spectroscopy. *Magn Reson Q* 10:191-247, 1994.
71. Govindaraju V, Young K, Maudsley AA. Proton NMR chemical shifts and coupling constants for brain metabolites. *NMR Biomed* 13:129-153, 2000.
72. Kreis R. Quantitative localized <sup>1</sup>H-MR spectroscopy for clinical use. *Prog NMR Spectroscopy* 31:155-195, 1997.
73. Kaibara T, Tyson RL, Sutherland GR. Human cerebral neoplasms studied using MR spectroscopy: a review. *Biochem Cell Biol* 76:477-86, 1998.





# 3

## FUNCTIONAL MR IMAGING OF LARYNGEAL CANCER

Mark Rijpkema

Johannes Kaanders

Frank Joosten

Albert van der Kogel

Arend Heerschap

---

This chapter is based on:

Rijpkema M, Kaanders J. Functional MR imaging of laryngeal cancer.

In: Imaging of the larynx. Hermans R (Ed.), Springer, Berlin, Germany, 175-184, 2002.

Reprinted with permission.

### 3.1 INTRODUCTION

Almost all malignancies of the larynx are squamous cell carcinomas, located at the mucosal surface. The most applied treatment strategies include radiation therapy or total or partial laryngectomy (1). The choice of treatment depends on the initial stage of the tumour. Less advanced laryngeal tumours can be treated by radiotherapy whereas more advanced tumours are best treated by surgery. Recently, also Accelerated Radiotherapy with Carbogen and Nicotinamide (ARCON) is being applied on laryngeal tumours, with promising results (2).

An important factor in treatment planning of laryngeal carcinoma is the accuracy of pretherapeutic staging. Further characterisation of the tumour, for example the determination of tumour vascularity, may also assist in the diagnosis and choice of treatment (3). To assess the exact tumour extension and characterisation, clinical and endoscopic tumour evaluation have clear limitations. Therefore both Computed Tomography (CT) and Magnetic Resonance Imaging (MRI) are being used in the staging of head and neck tumours. Comparative studies of both imaging techniques show that in general MRI offers the highest sensitivity in staging squamous cell carcinomas of the larynx (4-6). Also, although estimations of perfusion of head and neck tumours by CT are feasible, this is more commonly studied by MRI (e.g. 7-9).

With conventional MRI, the differences in signal intensity between tumour, muscle, fat and normal cartilage enable delineation of the tumour. The diagnostic accuracy can be increased with the use of contrast agents, especially in the evaluation of malignant tumours (10-12). However, MRI offers techniques to study not only tumour anatomy but also various aspects of tumour physiology in more detail. This may be of importance in treatment selection and may have prognostic significance. In the next section two important techniques will be discussed: fast dynamic contrast enhanced imaging to study tumour vascularity and blood oxygen level dependent imaging to study tumour oxygenation.

### 3.2 FUNCTIONAL MR IMAGING

Functional MRI, defined as MR investigations of dynamic physiological processes, can be applied both to normal and abnormal tissues. A leading application of functional imaging is the study of the normal brain in response to stimuli, using imaging techniques that are sensitive to oxygenation. In tumours, several approaches can be used to monitor physiological processes dynamically. Dynamic contrast enhanced MRI (DCE-MRI) and blood oxygen level dependent (BOLD) MRI are often applied nowadays, although also other MR techniques, e.g. blood pool contrast enhanced imaging or diffusion weighted imaging can be used. DCE-MRI can be applied to assess changes in vascularity, including vascular permeability,

blood flow and blood volume. BOLD MRI can be used to assess changes in blood oxygenation status. In tumours, information about blood supply, vascular architecture and oxygenation status may be important factors determining the choice and outcome of therapy and may be helpful in selecting patients for various treatment strategies.

### 3.2.1 VASCULARITY

Tumours often feature a more chaotic vascular architecture than normal tissue and a heterogeneous blood supply. Shunting of blood flow within a tumour has been recognised together with variations in vascular permeability (7,13). Information on tumour vascularity may aid not only to the characterisation of tumours, but also to treatment planning. Tumour blood flow for example is of fundamental importance to the efficacy of chemotherapy (drug delivery) and radiotherapy (oxygen supply). Also, assessment of functional changes of tumour vasculature may be used to monitor treatment response.

Various aspects of vascularity, in particular vascular permeability and vascular surface area, can be assessed by DCE-MRI (14,15). Using this technique a contrast agent is administered and its uptake in tumour or normal tissue is monitored by fast imaging (temporal resolution ~seconds). Fast MR imaging techniques have not been applied frequently to laryngeal tumours yet. Most dynamic imaging studies so far employed a temporal resolution of 30 seconds or more. Using this technique images can be obtained with a high level of anatomical information, however the first pass effects of the contrast medium cannot be monitored. A higher temporal resolution can only be achieved at the expense of the spatial resolution. So, depending on the kind of information required, the best DCE-MRI technique can be applied. DCE-MRI techniques have been widely employed for the assessment of various human tumours in both detection, identification, and staging (16-19). For head and neck tumours, DCE-MRI has proven to be superior to conventional contrast enhanced imaging in delineating the margins and extent of tumour (8).

As a contrast medium, Gadolinium chelates are commonly used, in particular megluminegadopentetate (Gd-DTPA). This exogenous contrast agent remains intravascular in normal brain tissue due to the blood brain barrier, but in all other tissues it diffuses into the extravascular extracellular space (EES). In tumour tissue, the exchange of Gd-DTPA between blood plasma and the EES and the rate constant of this process can be studied. This Gd-DTPA uptake rate provides information about for example vascular permeability and vascular surface area. Usually Gd-DTPA is administered as a bolus to study first pass effects and fast MRI is applied until the contrast medium in the EES is in equilibrium with plasma.

In head and neck tumours, investigation of tumour vascularity by DCE-MRI has been used to improve the detection of tumours, to determine the tumour extension, and to make differential diagnosis. Time curves obtained from dynamic MRI were shown to indicate differentiated grades and cell proliferating activity in thyroid tumours (20). DCE-MRI has also proven to be useful in the evaluation of therapy of head and neck cancers (21). Most malignant lesions of the head and neck show early enhancement and early wash-out of contrast media on DCE-MRI (9). This information may aid in predicting the response of tumours to chemotherapeutic treatment. Also, DCE-MRI studies have shown to be useful in predicting the response to accelerated radiotherapy for head and neck cancer (7).

### 3.2.2 OXYGENATION

Tumour oxygenation is an important factor in the response of tumours to therapy, especially radiotherapy. Radiosensitivity is directly correlated to the oxygen concentration in the tumour; well-oxygenated cells are more radiosensitive than hypoxic cells (22). Increasing tumour oxygen levels may therefore improve the efficacy of radiotherapy. For laryngeal tumours, carbogen breathing and nicotinamide administration resulted in a significantly improved tumour response to accelerated radiotherapy (ARCON), most likely mediated by improved tumour oxygenation levels (2,23,24). Thus, information on the tumour oxygenation status is particularly valuable in predicting the outcome of radiotherapy and the effect of oxygenating agents.

Changes in tumour blood oxygenation, e.g. due to an oxygenation protocol can be assessed by BOLD MRI (25). This technique makes use of the different magnetic properties of oxyhaemoglobin and deoxyhaemoglobin. Unlike oxyhaemoglobin, deoxyhaemoglobin is paramagnetic and shortens the MRI time constant for the transverse magnetisation decay ( $T2^*$ ), resulting in an attenuation of MRI signals from tissue adjacent to (venous) blood vessels. Thus, deoxyhaemoglobin acts as an endogenous contrast agent, which can be monitored by gradient-echo MR imaging. Although the value of  $T2^*$  was shown to relate directly to the concentration of deoxyhaemoglobin in normal brain tissue of laboratory animals (26), in tumours this value may be mainly governed by the magnetic field distortions caused by tissue inhomogeneity. Especially in laryngeal tumours this may be an important factor, because the border between tissue and air tends to distort the magnetic field to a large extent. However, monitoring changes in the value of  $T2^*$  due to an oxygenating agent can be used to assess changes in local vascular oxygenation status.

So far, little information is available on BOLD MRI in patients with laryngeal cancer. Using oxygen electrodes, measurement of pretreatment oxygenation levels showed to be predictive of radiation response in patients with advanced squamous cell

carcinomas of the head and neck (27). Oxygenating agents will increase the blood oxygen level, which could result in a decrease of the deoxyhaemoglobin concentration and an increase of the value of  $T2^*$ . Therefore, the oxygenating effects on tumour tissue can be monitored noninvasively by measuring the change in the value of  $T2^*$ . BOLD MRI of tumours may thus assist in the prediction of radiotherapy outcome and be used to investigate the effect of oxygenating agents on radiosensitivity.

### 3.3 MRI METHODS

All data that is shown in this chapter has been recorded on a 1.5 T Siemens Vision whole body system (Siemens Medical Systems, Erlangen, Germany), using a CP-neck-array receive coil. For all studies from which this data has been obtained patients have given informed consent and approval has been obtained from the local ethics committee.

#### 3.3.1 DYNAMIC CONTRAST ENHANCED MRI

##### MRI PROTOCOL

The procedure for a DCE-MRI measurement is a combination of administration of a contrast agent and recording fast MRI contrast enhanced images. As a contrast agent, Gadolinium-DTPA is most commonly used. Intravenous injection of Gd-DTPA can be applied either by hand or by an automatic injection system. An automatic injection system has the clear advantage that the contrast agent can be administered in a more reproducible way, which may be important in comparing the signal enhancement curves of two measurements of the same patient, for example before and after therapy. Gd-DTPA is usually administered in a dose of 15 ml (0.5 M) of Gd-DTPA solution. This volume has to be administered as a bolus (e.g. 2.5 ml/sec.) to be able to study first pass effects of the contrast medium in the tumour.

Fast dynamic contrast enhanced MRI techniques can be classified into two methods: T1 weighted and  $T2^*$  weighted sequences. For dynamic contrast studies of the head and neck region,  $T2^*$  weighted sequences are difficult to implement because of magnetic field inhomogeneity effects. Furthermore,  $T2^*$  weighted imaging requires the Gd-DTPA contrast medium to remain intravascular for reliable assessment of the time-intensity curves (9); a prerequisite that is not met by laryngeal carcinomas. Under these conditions, T1 weighted imaging methods such as fast spin-echo and gradient-echo techniques are usually applied (8,28-30). To study the dynamics of the contrast medium in the tumour in detail, imaging sequences have to be fast. For the accurate measurement of tracer kinetic

parameters the temporal sampling requirement is about 4 seconds, and if also time-intensity curves of large blood vessels have to be measured, the sampling rate should be even higher (31). DCE-MRI data acquired this way is shown in figure 3.1 for a patient with a laryngeal tumour. The sequence parameters (2D FLASH, TR=50 ms, TE=4.4 ms,  $\alpha=60^\circ$ , slice thickness 7 mm, 7 slices, matrix  $256^2$ , FoV 210x280 mm) enabled reconstruction of an image every 2 seconds. The 6 images displayed in figure 3.1 are a subset of a data set of 44 consecutive images. The bolus passage of the contrast medium in the carotid and vertebral arteries can be recognised, as well as the dynamic contrast enhancement in the tumour.

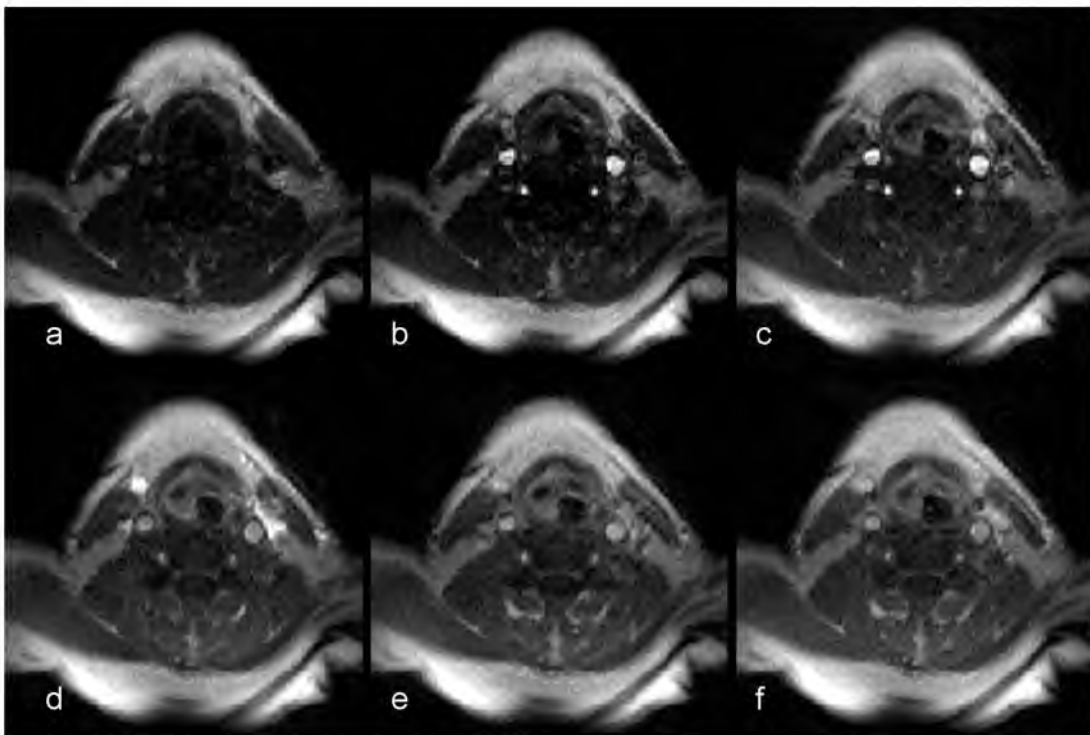


Figure 3.1. Six transversal dynamic contrast enhancement images of a patient with a laryngeal tumour (T3) obtained from a data set of 44 images. The images were acquired as described in section 3.3.1 with a temporal resolution of 2 seconds. Images a-f were recorded at  $t=4$ ,  $t=14$ ,  $t=16$ ,  $t=24$ ,  $t=60$ ,  $t=75$  seconds respectively. Dynamic contrast enhancement in both normal tissue, tumour tissue and large blood vessels can be recognised.

Especially when a mobile organ like the larynx is being imaged, artifacts may be introduced in the dynamic contrast enhancement images. Patients with laryngeal tumours may have trouble breathing, which may introduce motion artifacts. Also, the laryngeal region is extremely sensitive to artifacts caused by swallowing. These artifacts are very difficult to correct for after the data has been recorded. So, to reduce motion artifacts on the images, the total measurement time of the set of dynamic contrast enhancement images should be kept short. The first pass effects and the washout of the contrast medium however, have to be sampled for an accurate measurement of dynamic contrast enhancement parameters. In practice, with a short bolus and a sampling rate of 2 seconds, a total measurement time of 90 seconds suffices.

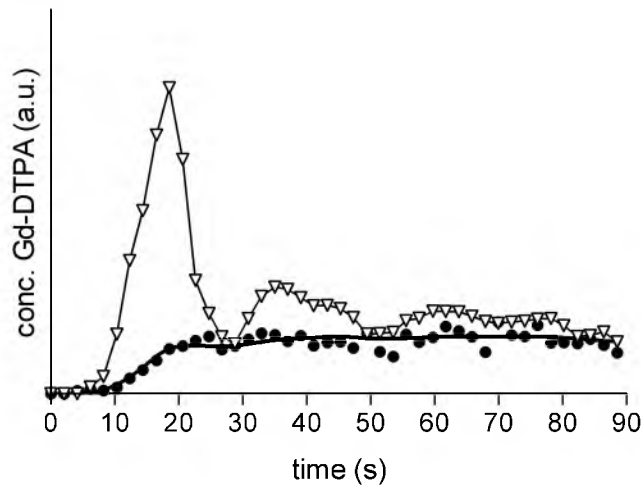


Figure 3.2. Gd-DTPA uptake curve (dots) of 1 pixel in the tumour region and the fit of this curve (solid line) according to the physiological model by Larsson et al (32). The arterial input function (triangles, connected with a line) is also shown. The data was obtained from the same patient as in figure 3.1.

#### DATA ANALYSIS

For clinical purposes, it may be sufficient to perform a parametric analysis of the DCE-MRI data, resulting in values of parameters such as maximum contrast enhancement and rate of enhancement. This approach may yield reliable data of clinical significance (e.g. 33). However, to minimise variations among patients and different measurements caused by variable systemic blood supply it is necessary to apply some kind of normalisation. As a reference the concentration-time curves of the contrast agent in the feeding vessels (arterial input function, AIF) can be used. The advantage of imaging laryngeal tumours compared to e.g. brain tumours or breast tumours is that multiple arteries are present in a transversal imaging slice through the tumour (vertebral and carotid arteries). Thus, the signal enhancement versus time curves in the tumour and in the arteries can be acquired simultaneously, without any additional measurements. The necessity to record the AIF for quantitative analysis of DCE-MRI data was recently shown by Port et al (34) and Rijpkema et al (30) for various tumours, including laryngeal carcinomas. The Gd-DTPA uptake curve of a laryngeal tumour and the coregistered AIF are plotted in figure 3.2, showing clearly the bolus passage of the contrast medium and the (rate of) Gd-DTPA uptake in the tumour. To gain insight in the underlying physiology of the tumour various physiological pharmacokinetic models have been proposed to describe the dynamic MR contrast enhancement. Using these models DCE-MRI data may be described in physiological terms such as vascular permeability and surface area, extracellular volume and tumour blood flow.



## PHYSIOLOGICAL PHARMACOKINETIC MODELS

The most commonly used physiological models in DCE-MRI are those described by Tofts and Kermode (35) and Larsson et al (32). The measured concentration-time curves of the contrast medium in the tumour and the AIF serve as input for these models. The output consists of quantified physiological parameters like the rate constant of contrast medium uptake, which is directly related to, for instance, the vascular permeability and surface area.

In its simplest form a physiological pharmacokinetic model describing dynamic contrast medium uptake contains two compartments: blood plasma and EES. A rate constant defines the exchange of contrast medium between these compartments. This rate constant  $k_{ep}$  (36) is one of the three principle parameters in the analysis of T1 weighted contrast enhancement data. The two other parameters are the volume transfer constant between blood plasma and EES ( $K^{trans}$ ) and the volume of EES per unit volume of tissue ( $v_e$ ). These three physiological parameters are related according to  $k_{ep} = K^{trans} / v_e$  (36). When a physiological model is applied to DCE-MRI

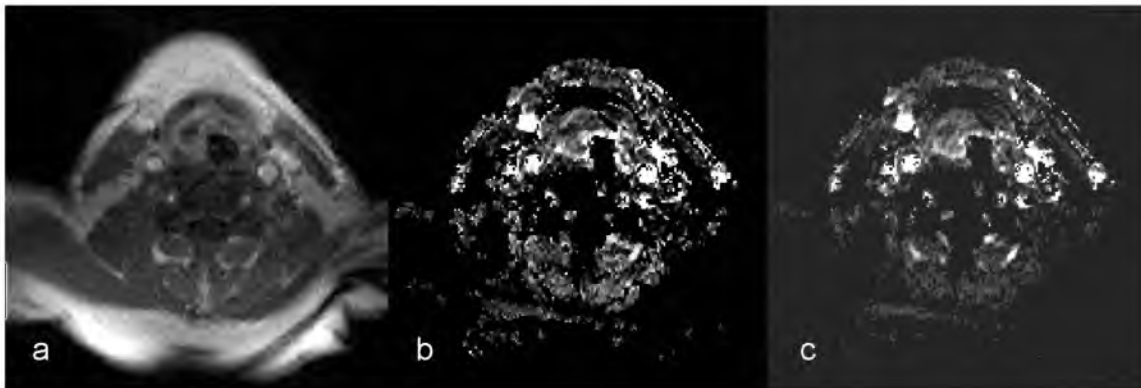


Figure 3.3. (a) T1 weighted dynamic contrast enhancement image of the same patient as in figure 3.1, recorded 75 seconds after Gd-DTPA contrast medium administration. The DCE-MRI data was analysed using the physiological model by Larsson et al (32). The results are shown in (b) map of the Gd-DTPA uptake rate ( $k_{ep}$ ) and (c) map of the volume transfer constant ( $K^{trans}$ ) of the same patient.

patient	stage	$k_{ep}$ ( $\text{min}^{-1}$ )
1	IV	$2.3 \pm 0.7$
2	III	$1.3 \pm 0.6$
3	II	$3.0 \pm 1.3$
4	III	$2.8 \pm 0.9$
5	IV	$1.9 \pm 1.7$
6	III	$2.4 \pm 2.5$
7	III	$2.3 \pm 1.0$
8	IV	$2.9 \pm 1.5$

Table 3.1. The contrast medium uptake rate  $k_{ep}$  ( $\text{min}^{-1}$ ) in laryngeal tumours of 8 patients ( $\pm$  SD). The T classification of the tumour according to the TNM classification system is also indicated. The contrast medium uptake rate may provide information on e.g. vascular permeability and surface area.

data on a pixel-by-pixel basis, maps can be reconstructed in which these parameters are displayed. In figure 3.3 a contrast enhancement image is displayed, together with maps of  $k_{ep}$  and  $K^{trans}$ , for the same patient as in figure 3.1. The tumour can readily be distinguished from the surrounding tissue in all three images. However, spatial inhomogeneity within the tumour is more easily recognised in the parameter maps (figure 3.3b and c).

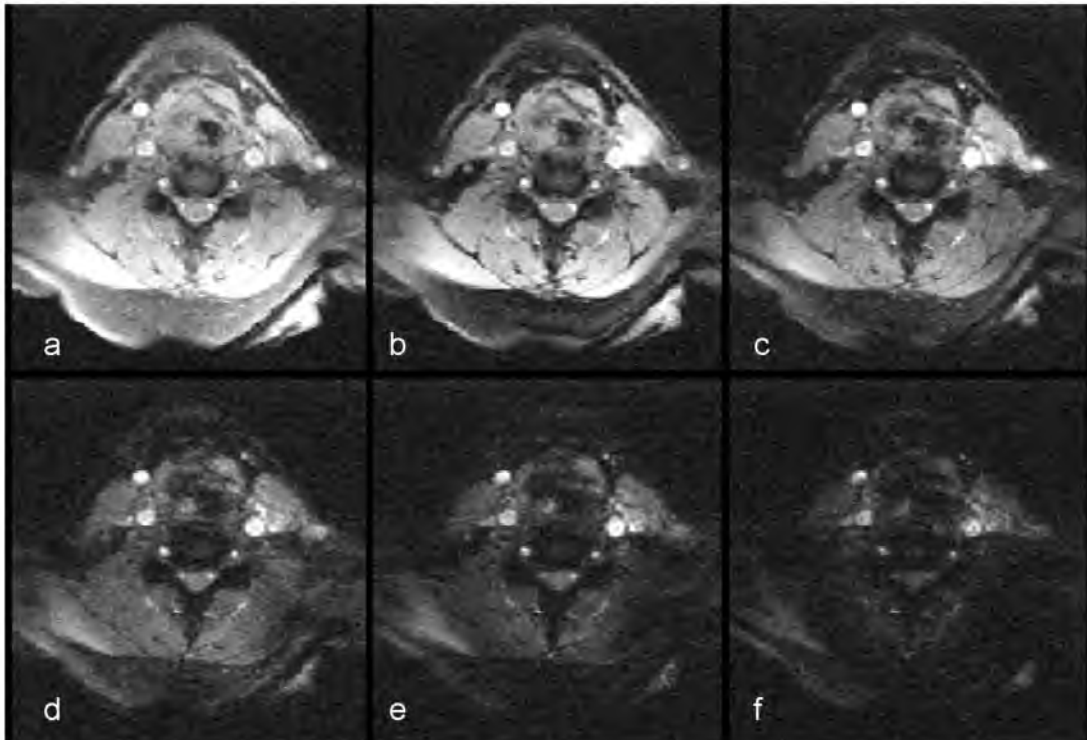


Figure 3.4. Six transversal T2\* weighted images from a data set of 16 images recorded using a multiple gradient-echo sequence. The data was obtained from the same patient as in figure 3.1. Images a-f were recorded with an echo time of 6, 9, 15, 21, 27, and 36 ms respectively. The signal decay at increasing echo times was used to calculate the value of T2\* (ms).

The characterisation of tumours by quantification of physiological parameters enables the direct comparison of tumour characteristics to those of other tumours. In table 3.1 the values of the Gd-DTPA uptake rate in laryngeal tumours is shown for 8 patients. The T classification of the tumour according to the TNM classification system (37), describing the extent of the tumour, is also shown. Because the amount of quantified physiological DCE-MRI data on laryngeal tumours is still limited no correlation with tumour TNM classification could be found yet. This correlation is complicated further since histological data obtained by biopsy may not be representative of the whole tumour, especially when a tumour is heterogeneous, whereas the physiological parameters obtained by DCE-MRI so far are an average of the whole tumour.

### 3.3.2 BLOOD OXYGEN LEVEL DEPENDENT MRI

MRI techniques to study tumour vascular oxygenation usually employ the BOLD effect. Using gradient-echo MRI changes in the value of the relaxation time  $T2^*$  can be determined, which correlate to changes in the deoxyhaemoglobin concentration. Although changes in  $T2^*$  are sensitive to changes in both blood volume, haematocrit, and oxygenation (38), the decrease in  $T2^*$  during hyperoxygenation was shown to be strongly correlated with increased tumour  $pO_2$  levels, as measured using oxygen electrodes (39). Conventional  $T2^*$  weighted MR imaging cannot distinguish accurately changes in blood oxygenation from changes in blood flow, because of inflow effects (40). To overcome this disadvantage a multiple gradient-echo MRI technique can be applied, which can quantify  $T2^*$  independently of effects of blood flow. In figure 3.4 data obtained with a multiple gradient-echo sequence is presented for a patient with a laryngeal tumour. In this figure 6 out of 16 images obtained with a 16-echo sequence are shown (sequence parameters: 16 echo FLASH, TR=65 ms, TE=6-51 ms,  $\alpha=20^\circ$ , 5 mm slice). Values of  $T2^*$  (ms) can be calculated from the monoexponential signal decay at increasing echo times. This calculation can be performed on a pixel-by-pixel basis, enabling reconstruction of a map of  $T2^*$ . In figure 3.5 a map is shown of the relaxation rate  $R2^*$  ( $R2^* = 1/T2^*$ ) obtained from the data set shown in figure 3.4. In this way, spatial information about tumour blood oxygenation changes can be visualised.

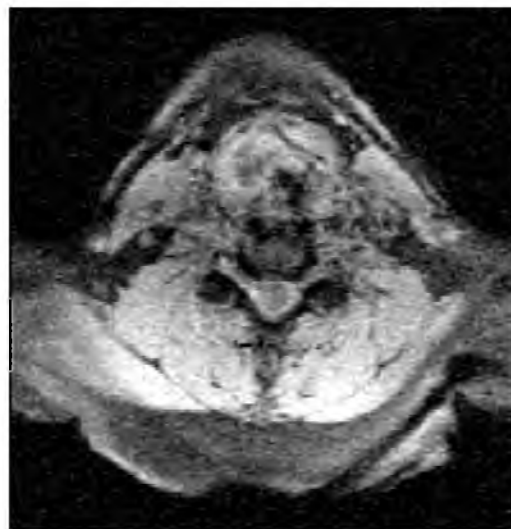


Figure 3.5. Map of the relaxation rate  $R2^*$  ( $R2^*=1/T2^*$ ) obtained from pixelwise analysis of the multiple gradient-echo data shown in figure 3.4. The  $R2^*$  map is shown instead of the  $T2^*$  map for display convenience.

In table 3.2 the values of  $T2^*$  in laryngeal tumours are listed for 8 patients. The tumour values were obtained by averaging all pixels within a selected tumour region on the  $T2^*$  maps. Although absolute  $T2^*$  values are difficult to interpret directly in terms of tumour oxygen levels (see section 3.2.2), they may serve as 'baseline values' in the investigation of the effect of oxygenating agents on tumour blood

oxygenation. An increase in the value of  $T2^*$  caused by an improved blood oxygenation may indicate the radiotherapeutical usefulness of the oxygenating agent. For example, changes in  $T2^*$  caused by breathing hyperoxic hypercapnic gas mixtures (e.g. 95-98%  $O_2$  plus 5-2%  $CO_2$ ) might predict whether the patient could benefit from radiotherapy treatment using these gas mixtures as a hyperoxygenation medium.

patient	$T2^*$ (ms)
1	$29.1 \pm 1.8$
2	$26.9 \pm 0.9$
3	$30.8 \pm 2.0$
4	$32.5 \pm 2.8$
5	$43.9 \pm 2.5$
6	$37.2 \pm 1.3$
7	$34.2 \pm 2.7$
8	$24.5 \pm 2.1$

Table 3.2. The MRI time constant for the transverse magnetisation decay ( $T2^*$ ) (ms) in laryngeal tumours of 8 patients ( $\pm$  SD). These values are particularly important in the investigation of the effects of oxygenation agents on tumour blood oxygenation.

### 3.4 LARYNGEAL CANCER: APPLICATION OF FUNCTIONAL MRI APPROACHES

An important treatment option for laryngeal cancer is radiotherapy. Although radiotherapy produces a high local control rate, in advanced carcinomas the radiation response is less good. Traditional prognostic factors, such as clinical staging, tumour size, and tumour extent, may not sufficiently predict results of radiotherapy (9). Blood flow and the presence of hypoxia in the tumour have long been considered important factors influencing the response to radiotherapy. Because functional MRI provides a way to assess tumour hypoxia by studying both functional changes in tumour vasculature and oxygenation status, the potential radiosensitising effect of oxygenating agents can be investigated.

For laryngeal tumours, increased tumour oxygenation levels achieved by carbogen breathing and nicotinamide administration resulted in a significantly improved tumour response to accelerated radiotherapy (ARCON), as was demonstrated by Kaanders and co-workers (2,23,24). Breathing a hyperoxic hypercapnic gas mixture like carbogen was hypothesised to increase the blood oxygen level which may reduce hypoxic regions in the tumour. The first results of their study show an actuarial local control rate at 3 years of 79% for T3 laryngeal carcinomas and 84% for T4 laryngeal carcinomas, higher than any previous report in the literature for this category of patients (24). Currently a randomised Phase III trial of this treatment is ongoing for laryngeal tumours.

Breathing a hyperoxic hypercapnic gas mixture may have an effect on both blood flow and oxygenation (41,42). To study these effects in the clinic a combination of BOLD MRI and DCE-MRI techniques seems suitable. Recently, the effects of breathing a hyperoxic hypercapnic gas mixture (98% O<sub>2</sub> + 2% CO<sub>2</sub>) were assessed by functional MRI techniques in patients with head and neck tumours (43). The main conclusion of this study was that breathing this gas mixture improved tumour blood oxygenation in these patients. No changes in tumour vascularity were found as assessed by the Gd-DTPA uptake rate. Furthermore, functional MRI proved to be a promising tool to investigate both tumour oxygenation and vascularity and might be developed into a predictive tool for testing treatments using hyperoxygenation for other types of tumours as well.

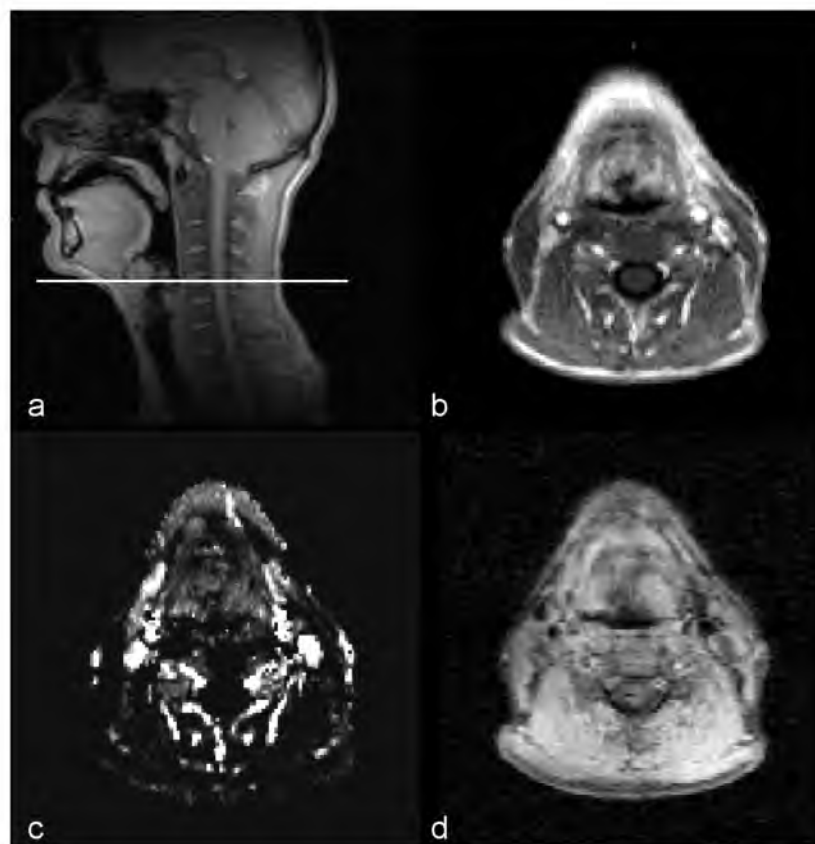


Figure 3.6. Functional MR images of a patient with a laryngeal tumour (T4). The images were recorded while the patient was breathing a hyperoxic hypercapnic gas mixture. (a) Sagittal image of the head and neck region showing the position of the transversal imaging slice used in both BOLD MRI and DCE-MRI. (b) Transversal dynamic contrast enhancement image of the same patient, recorded 1 minute after Gd-DTPA contrast medium administration. The image was acquired as described in section 3.3.1. (c) Volume transfer constant ( $K^{trans}$ ) map of the same patient, providing information on tumour vascularity (see section 3.3.1 for details). (d) Relaxation rate ( $R2^*$ ) map of the same patient (see section 3.3.2 for details).

As an example to show the use of different functional MRI techniques to monitor the effects of hyperoxygenation in laryngeal tumours, a case is presented of a patient with a T4 laryngeal tumour. In figure 3.6 the results of the MR imaging study of this patient is shown. To investigate the effects of breathing a hyperoxic hypercapnic

gas mixture on tumour oxygenation and vascularity, this patient was measured twice, once breathing air and once breathing a gas mixture consisting of 98% O<sub>2</sub> and 2% CO<sub>2</sub>. Tumour vascularity was assessed by DCE-MRI as described in section 3.3.1. Physiological parameter maps (e.g. K<sup>trans</sup>, figure 3.6b) were obtained from both the air breathing session and the session with breathing of the hyperoxic hypercapnic gas mixture. The values of the Gd-DTPA uptake rate  $k_{ep}$  are displayed in table 3.3. No significant differences could be detected, indicating that no extreme changes in vascularity occurred due to breathing the hyperoxic hypercapnic gas mixture.

Tumour oxygenation was assessed using BOLD MRI as described in section 3.3.2. The map of the relaxation rate R2\* is shown in figure 3.6d. The values of T2\* of the tumour obtained during air breathing and breathing the hyperoxic hypercapnic gas mixture proved to differ significantly (table 3.3); the value of T2\* increased during hypercapnic hyperoxygenation. Although the T2\* increase may seem small, it may reflect a much larger decrease in deoxyhaemoglobin concentration (26).

A powerful approach would be to combine the maps containing data on vascularity and oxygenation. A spatial relationship of the BOLD effect and the dynamic Gd-DTPA enhancement could provide useful physiological insight. However, in practice spatial correlation of the maps of the Gd-DTPA uptake rate and the (changes in) T2\* is problematic. Even small shifts of the patient position between the measurements could dramatically affect a pixel-to-pixel correlation.

	air	carbogen	significance
$k_{ep}$ (min <sup>-1</sup> )	2.3	2.2	N.S.
T2* (ms)	29.1	31.4	p=0.02

Table 3.3. The contrast medium uptake rate  $k_{ep}$  (min<sup>-1</sup>) and the MRI time constant for the transverse magnetisation decay (T2\*) (ms) of a patient with a laryngeal tumour. Data was obtained during air breathing and during breathing a hyperoxic hypercapnic gas mixture. The increased value of T2\* during breathing this gas mixture indicates an improved tumour blood oxygenation. Statistical significance was shown using Student's t-test. N.S. = not significant.

In this patient Gd-DTPA uptake did not reveal any effect on tumour vascularity due to breathing of the hyperoxic hypercapnic gas mixture. However, as the blood oxygenation level increased in the tumour during breathing this gas mixture, this patient could benefit from radiation treatment using this hyperoxygenating agent. In fact, this patient was treated using the ARCON therapy and has not shown tumour recurrence after three years. Of course this case only is no proof of the benefit of breathing a hyperoxic hypercapnic gas mixture or the validity of the MRI methods as a predictive tool. A more robust study to prove this is currently ongoing.

### 3.5 CONCLUSION

Functional MRI approaches of laryngeal cancer can be applied to study dynamic physiological processes and may aid in characterising physiological features of the tumour. Using dynamic contrast enhanced MRI various aspects of tumour vascularity can be assessed. Blood oxygen level dependent MRI enables investigation of blood oxygen levels in the tumour. Because for laryngeal carcinomas radiation treatment with hyperoxygenating agents has proven to be successful, studying the radiosensitising effects of these agents may provide valuable information. In this respect, functional MRI may be developed into a predictive tool for testing treatments using hyperoxygenation of laryngeal cancer.

## REFERENCES

- 1 Curtin HD. Imaging of the Larynx: Current Concepts Radiology 173(1):1-11, 1989.
- 2 Kaanders JH, Pop LA, Marres HA, et al. Accelerated Radiotherapy With Carbogen and Nicotinamide (ARCON) for Laryngeal Cancer. Radiother Oncol 48(2):115-122, 1998.
- 3 Endres D, Manaligod J, Simonson T, et al. The Role of Magnetic Resonance Angiography in Head and Neck Surgery. Laryngoscope 105(10):1069-1076, 1995.
- 4 Becker M, Zbaren P, Laeng H, et al. Neoplastic Invasion of the Laryngeal Cartilage: Comparison of MR Imaging and CT With Histopathologic Correlation. Radiology 194(3):661-669, 1995.
- 5 Zbaren P, Becker M, Lang H. Pretherapeutic Staging of Laryngeal Carcinoma Clinical Findings Computed Tomography and Magnetic Resonance Imaging Compared With Histopathology. Cancer 77(7):1263-1273, 1996.
- 6 Castelijns JA, Becker M, Hermans R. Impact of Cartilage Invasion on Treatment and Prognosis of Laryngeal Cancer. Eur Radiol 6(2):156-169, 1996.
- 7 Hoskin PJ, Saunders MI, Goodchild K, et al. Dynamic Contrast Enhanced Magnetic Resonance Scanning As a Predictor of Response to Accelerated Radiotherapy for Advanced Head and Neck Cancer. Br J Radiol 72(863):1093-1098, 1999.
- 8 Escott EJ, Rao VM, Ko WD, et al. Comparison of Dynamic Contrast-Enhanced Gradient-Echo and Spin-Echo Sequences in MR of Head and Neck Neoplasms. Am J Neuroradiol 18(8):1411-1419, 1997.
- 9 Baba Y, Yamashita Y, Onomichi M, et al. Dynamic Magnetic Resonance Imaging of Head and Neck Lesions. Top Magn Reson Imaging 10(2):125-129, 1999.
- 10 Weber AL. History of Head and Neck Radiology: Past Present and Future Radiology 218(1):15-24, 2001.
- 11 Hirsch JA, Loevner LA, Yousem DM, et al. Gadolinium-Enhanced Fat-Suppressed T1-Weighted Imaging of the Head and Neck: Comparison of Gradient and Conventional SE Sequences. J Comput Assist Tomogr 22(5):771-776, 1998.
- 12 Vogl T, Dresel S, Bilaniuk LT, et al. Grevers G, Kang K, and Lissner J Tumours of the Nasopharynx and Adjacent Areas: MR Imaging With Gd-DTPA. Am J Roentgenol 154(3):585-592, 1990.
- 13 Vaupel PW. Blood flow, oxygenation, tissue pH distribution, and bioenergetic status of tumours. Ernst Schering Research Foundation, Berlin, 1994.
- 14 Stubbs M. Application of Magnetic Resonance Techniques for Imaging Tumour Physiology. Acta Oncol 38(7):845-853, 1999.
- 15 Delorme S, Knopp MV. Non-Invasive Vascular Imaging: Assessing Tumour Vascularity Eur Radiol 8(4):517-527, 1998.
- 16 Degani H, Gusic V, Weinstein D, et al. Mapping Pathophysiological Features of Breast Tumours by MRI at High Spatial Resolution. Nat Med 3(7):780-782, 1997.



- 17 Buckley DL, Drew PJ, Mussurakis S, et al. Microvessel Density of Invasive Breast Cancer Assessed by Dynamic Gd-DTPA Enhanced MRI. *J Magn Reson Imaging* 7(3):461-464, 1997.
- 18 Barentsz JO, Engelbrecht M, Jager GJ, et al. A Fast Dynamic Gadolinium-Enhanced MR Imaging of Urinary Bladder and Prostate Cancer. *J Magn Reson Imaging* 10(3):295-304, 1999.
- 19 Mayr NA, Hawighorst H, Yuh WT, et al. MR Microcirculation Assessment in Cervical Cancer: Correlations With Histomorphological Tumour Markers and Clinical Outcome. *J Magn Reson Imaging* 10(3):267-276, 1999.
- 20 Kusunoki T, Murata K, Hosoi H, et al. Malignancies of Human Thyroid Tumours and Dynamic Magnetic Resonance Imaging (MRI). *Auris Nasus Larynx* 25(4):419-424, 1998.
- 21 Baba Y, Furusawa M, Murakami R, et al. Role of Dynamic MRI in the Evaluation of Head and Neck Cancers Treated With Radiation Therapy. *Int J Radiat Oncol Biol Phys* 37(4):783-787, 1997.
- 22 Gray LH, Conger AD, Ebert M, et al. The concentration of oxygen dissolved in tissues at the time of irradiation as a factor in radiotherapy. *Br J Radiol* 26: 638-648, 1953.
- 23 Kaanders JHAM, Bussink J, Pop LA, et al. Accelerated radiotherapy with carbogen and nicotinamide (ARCON): from mouse to man. *Int J Radiat Oncol Biol Phys* 46: 705, 2000.
- 24 Kaanders JHAM, Pop LAM, Marres HAM, et al. ARCON: experience in 215 patients with advanced head and neck cancer. *Int J Radiat Oncol Biol Phys* 52(3):769-778, 2002.
- 25 Ogawa S, Lee TM, Nayak AS, et al. Oxygenation-Sensitive Contrast in Magnetic Resonance Image of Rodent Brain at High Magnetic Fields. *Magn Reson Med* 14(1):68-78, 1990.
- 26 Punwani S, Ordidge RJ, Cooper CE, et al. MRI Measurements of Cerebral Deoxyhaemoglobin Concentration [Dhb]- Correlation With Near Infrared Spectroscopy (NIRS). *NMR Biomed* 11(6):281-289, 1998.
- 27 Nordmark M, Overgaard M, Overgaard J. Pretreatment Oxygenation Predicts Radiation Response in Advanced Squamous Cell Carcinoma of the Head and Neck. *Radiother Oncol* 41(1):31-39, 1996.
- 28 Takashima S, Noguchi Y, Okumura T, et al. Dynamic MR Imaging in the Head and Neck. *Radiology* 189(3):813-821, 1993.
- 29 Larsson HB, Stubgaard M, Sondergaard L, et al. In Vivo Quantification of the Unidirectional Influx Constant for Gd- DTPA Diffusion Across the Myocardial Capillaries With MR Imaging. *J Magn Reson Imaging* 4(3):433-440, 1994.
- 30 Rijpkema M, Kaanders JHAM, Joosten FBM, et al. Method for quantitative mapping of dynamic MRI contrast agent uptake in human tumours. *J Magn Reson Imaging* 14(4):457-463, 2001.
- 31 Henderson E, Rutt BK, Lee TY. Temporal Sampling Requirements for the Tracer Kinetics Modeling of Breast Disease. *Magn Reson Imaging* 16(9):1057-1073, 1998.
- 32 Larsson HB, Stubgaard M, Frederiksen JL, et al. Quantitation of Blood-Brain Barrier Defect by Magnetic Resonance Imaging and Gadolinium-DTPA in Patients With Multiple Sclerosis and Brain Tumours. *Magn Reson Med* 16(1):117-131, 1990.

- 33 Huisman HJ, Engelbrecht MR, Barentsz JO. Accurate estimation of pharmacokinetic contrast-enhanced dynamic MRI parameters of the prostate. *J Magn Reson Imaging* 13(4):607-614, 2001.
- 34 Port RE, Knopp MV, Brix G. Dynamic Contrast-Enhanced MRI Using Gd-DTPA: Interindividual Variability of the Arterial Input Function and Consequences for the Assessment of Kinetics in Tumours. *Magn Reson Med* 45(6):1030-1038, 2001.
- 35 Tofts PS, Kermode AG. Measurement of the Blood-Brain Barrier Permeability and Leakage Space Using Dynamic MR Imaging 1 Fundamental Concepts. *Magn Reson Med* 17(2):357-367, 1991.
- 36 Tofts PS, Brix G, Buckley DL, et al. Estimating Kinetic Parameters From Dynamic Contrast-Enhanced T(1)-Weighted MRI of a Diffusable Tracer: Standardized Quantities and Symbols. *J Magn Reson Imaging* 10(3):223-232, 1999.
- 37 Sobin LH, Wittekind C (eds). *TNM classification of malignant tumours*, 5th edn. Wiley-Liss, New York Chichester Weinheim Brisbane Singapore Toronto, pp 33-37, 1997.
- 38 Neeman M, Dafni H, Bukhari O, et al. In Vivo Contrast MRI Mapping of Subcutaneous Vascular Function and Maturation: Validation by Intravital Microscopy. *Magn Reson Med* 45(5):887-898, 2001.
- 39 Al Hallaq HA, River JN, Zamora M, et al. Correlation of Magnetic Resonance and Oxygen Microelectrode Measurements of Carbogen-Induced Changes in Tumour Oxygenation. *Int J Radiat Oncol Biol Phys* 41(1):151-159, 1998.
- 40 Robinson SP, Rodrigues LM, Howe FA, et al. Effects of Different Levels of Hypercapnic Hyperoxia on Tumour R(2)\* and Arterial Blood Gases. *Magn Reson Imaging* 19(2):161-166, 2001.
- 41 Horsman MR, Nordmark M, Khalil AA, et al. Reducing Acute and Chronic Hypoxia in Tumours by Combining Nicotinamide With Carbogen Breathing. *Acta Oncol* 33(4):371-376, 1994.
- 42 Bussink J, Kaanders JH, van der Kogel, AJ. Clinical Outcome and Tumour Microenvironmental Effects of Accelerated Radiotherapy With Carbogen and Nicotinamide. *Acta Oncol* 38(7):875-882, 1999.
- 43 Rijpkema M, Kaanders JHAM, Joosten FBM, et al. Effects of breathing a hyperoxic hypercapnic gas mixture on oxygenation and vascularity of head and neck tumours as measured by MRI. *Int J Radiat Oncol Biol Phys* 53(5):1185-1191, 2002.



# 4

## METHOD FOR QUANTITATIVE MAPPING OF DYNAMIC MRI CONTRAST AGENT UPTAKE IN HUMAN TUMOURS

Mark Rijpkema

Johannes Kaanders

Frank Joosten

Albert van der Kogel

Arend Heerschap

---

This chapter is based on:

Rijpkema M, Kaanders JHAM, Joosten FBM, van der Kogel AJ, Heerschap A. Method for quantitative mapping of dynamic MRI contrast agent uptake in human tumors. *J Magn Reson Imag* 14(4):457-463, 2001.

**ABSTRACT**

A method is presented for the acquisition and analysis of dynamic contrast enhanced (DCE) MRI data, focussed on the characterisation of tumours in humans. Gadolinium contrast was administered by bolus injection and its effect was monitored in time by fast T1 weighted MRI. A simple algorithm was developed for automatic extraction of the arterial input function (AIF) from the DCE-MRI data. This AIF was used in the pixelwise pharmacokinetic determination of physiological vascular parameters in normal and tumour tissue. Maps were reconstructed to show the spatial distribution of parameter values. To test the reproducibility of the method 11 patients with different types of tumours were measured twice, and the rate of contrast agent uptake in the tumour was calculated. The results show that normalising the DCE-MRI data using individual coregistered AIFs, instead of one common AIF for all patients, substantially reduces the variation between successive measurements. It is concluded that the proposed method enables the reproducible assessment of contrast agent uptake rates.

## INTRODUCTION

Dynamic contrast enhanced MRI (DCE-MRI) using Gadolinium has been widely used for the assessment of human tumours. Its diagnostic value has been shown in for example breast tumours (1-3), cervix tumours (4) and prostate carcinoma (5-7), both in tumour detection, identification and staging. Also, tumour treatment response has been monitored by DCE-MRI (8-10) and comparison with histology showed a relationship of DCE-MRI data with angiogenic characteristics like microvessel density (6,7,11).

For clinical purposes, it may be sufficient to perform a parametric analysis of the DCE-MRI data, resulting in values of parameters such as maximum contrast enhancement and rate of enhancement. However, to minimise variations among patients and different measurements caused by variable systemic blood supply it is necessary to apply some kind of normalisation. To do so, signal enhancement of healthy tissue may serve as a reference (12,13), but a more direct reference would be to measure concentration-time curves of the contrast agent in the feeding vessels (arterial input function, AIF). Furthermore, parametric analysis alone does not provide insight in the underlying physiology of the tumour. For this purpose various physiological pharmacokinetic models have been proposed to describe dynamic MR contrast enhancement. Using these models DCE-MRI data may be described in physiological terms such as vascular permeability and surface area, extracellular volume and blood flow.

The most commonly used physiological models in DCE-MRI are the ones described by Tofts et al (14) and Larsson et al (15). For both models the AIF is required. To obtain this function from the experiments the measurement protocol has to have sufficient temporal resolution (16), especially when the contrast agent is applied as a bolus injection. Accurate measurement of the AIF allows quantification of physiological parameters like rate constant of contrast medium uptake,  $k_{ep}$  (17), which is directly related to, for instance, the vascular permeability and surface area.

Often, the AIF cannot be measured directly and a general concentration-time curve is assumed to be valid for humans, usually the one described by Weinmann et al (18). However, as large differences may exist in the AIFs of different patients, or even in the same patient at a different time, simultaneous measurement of DCE-MRI data of tumour tissue and the AIF is essential for correcting inter- and inpatient differences (19,20). This normalisation of the DCE-MRI data is particularly important when one patient is measured more than once, for example to monitor the response to therapy.

In this study, we describe a method to measure both contrast medium uptake in human tumours and the AIF after bolus injection of Gadolinium. The rate constant of

Gadolinium uptake is calculated and displayed in a quantitative  $k_{ep}$  map. The reproducibility of the method was tested in patients with brain tumours, prostate tumours and tumours in the head-neck region.

## PATIENTS AND METHODS

MR imaging was performed on a 1.5 T Siemens Vision system. A total of 11 patients participated in this study. Data from 6 patients with a tumour in the head-neck region (1 larynx carcinoma, 3 hypopharynx carcinoma, 1 lymph node metastasis, 1 melanoma of the nasal cavity), 3 patients with prostate carcinoma, and 2 patients with a brain tumour (2 oligodendroglioma) was recorded and processed using the current method. All patients gave informed consent to participate to this study. Approval for the study was obtained from the local ethics committee.

After conventional T1 and T2 weighted imaging, Gadolinium-DTPA (Gd-DTPA, Magnevist®, Schering, Berlin, Germany) was administered by intravenous bolus injection (15 ml, 0.5 M, 2.5 ml/sec.) using a Spectris™ MR injection system (Medrad, Inc.). Both Gd-DTPA tissue uptake and bolus passage in large blood vessels were monitored using a T1 weighted FLASH sequence with a temporal resolution of 2 seconds. The sequence used was a 2D variant of the 3D TRICKS sequence described by Korosec et al (21). Briefly, k-space was divided in five sections which were sampled alternately, the central lines of k-space being acquired four times more frequent than the outer lines. Images were reconstructed using the sampled central lines of k-space; the outer lines of k-space were obtained by linear interpolation, as is shown in figure 4.1. Other sequence parameters were: TR=50 ms, TE=4.4 ms,  $\alpha=60^\circ$ , slice thickness 7 mm, 7 slices, matrix  $256^2$ , FoV 210x280 mm. DCE-MRI data was recorded for 90 seconds.

Before Gd-DTPA injection PD weighted images were recorded with the same sequence parameters as the DCE-MRI, except for the flip angle  $\alpha=8^\circ$  and the TR=200 ms. This image data was combined with the dynamic Gd-DTPA contrast enhancement image data to calculate concentration Gd-DTPA (a.u.) using the method described by Hittmair et al (22).

The concentration Gd-DTPA versus time curves were analysed using the Larsson (15) model. An algorithm developed in our laboratory was used to obtain the AIF from the image data set. The selection of arterial blood vessel pixels by this algorithm was based on the relative concentration Gd-DTPA (high in arteries) and time to bolus passage (short in arteries). First, the average maximum Gd-DTPA concentration,  $[Gd-DTPA]_{max,average}$ , was calculated for all pixels that showed contrast enhancement greater than zero. Then, a threshold was set at this  $[Gd-DTPA]_{max,average}$  plus two times the standard deviation of  $[Gd-DTPA]_{max,average}$ .

Although this factor of two was arbitrarily chosen, the algorithm proved to be quite insensitive to this threshold because the Gd-DTPA concentration in blood vessels is usually much higher than in tissue. In practice, virtually all pixels above this threshold were located in arteries and veins, as was confirmed by the radiologist. In the second step contributions from arteries and veins were separated from each other. To do so, a threshold was set at the time to the maximum Gd-DTPA concentration. This level was stepwise shortened with one inter-image interval until no pixels in a clearly visible vein were selected by the algorithm. The AIF was calculated as the average of the remaining selected pixels.

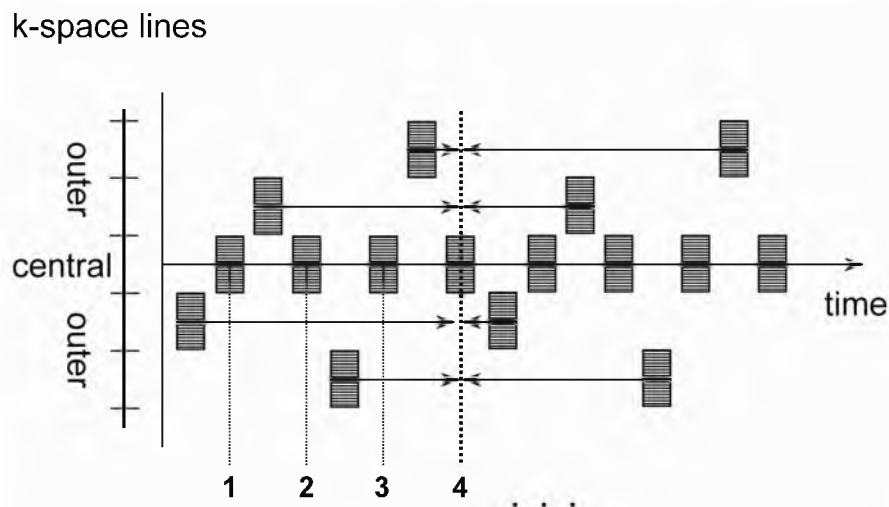


Figure 4.1. Diagram showing the acquisition order of the k-space sections (y-axis) and the interpolation used to reconstruct the MR images in time (x-axis). Central lines in k-space (section marked 'central') and outer lines (section marked 'outer') were sampled alternately. Reconstruction of an image (in this example image number 4) was done using the sampled central lines of k-space to which the outer lines were added by linear interpolation as indicated by the arrows.

For patients with tumours in the head-neck region the AIF found originated largely from pixels in the carotid artery and vertebral artery. These arteries were measured in the same transversal DCE-MRI slice as the tumour. In a similar way, for patients with prostate tumours, the AIF found originated from pixels in the external iliac artery. To obtain the AIF for brain tumours, one transversal DCE-MRI slice was positioned caudally to the slice showing the tumour in such way that the basilar artery and the internal carotid artery were visible. The AIF was then calculated as in the head and neck tumour patients.

Data was transferred to a SUN Ultra 10 workstation (UltraSPARC-IIi, 440 MHz, 1 Gb RAM) where the Larsson model was implemented in a Matlab routine. The function

$$C_t(t) = f \cdot K^{\text{trans}} \cdot \int_0^t C_p(\tau - \Delta T) \cdot e^{-k_{ep}(t-\tau)} \cdot d\tau = f \cdot K^{\text{trans}} \cdot e^{-k_{ep}(t)} * C_p(t - \Delta T) \quad (4.1)$$

was used to describe the transport of Gd-DTPA across the capillary membrane.  $C_t$  : tissue concentration of Gd-DTPA (mM);  $C_p$  : arterial plasma concentration of Gd-



DTPA (mM);  $k_{ep}$  : rate constant ( $s^{-1}$ ) between extravascular extracellular space (EES) and blood plasma;  $K^{trans}$  : volume transfer constant ( $s^{-1}$ );  $v_e$  : volume of EES per unit volume of tissue,  $k_{ep}=K^{trans}/v_e$  (17).  $\Delta T$  (s) is the time delay of the tissue enhancement curve relative to the AIF (23). Factor  $f$  is a scaling factor and is dependent on the MR method used and the relaxation properties of the tissue. The  $*$  denotes a convolution operation. For  $C_p(t)$  the raw data of the AIF as described above was used, without fitting this data.

The fit results were reconstructed into maps of  $k_{ep}$  ( $s^{-1}$ ),  $K^{trans}$  (a.u. $\cdot s^{-1}$ ) and  $v_e$  (a.u.) on a pixel-by-pixel basis. No smoothing or averaging was performed. The calculation time was less than 2 hours for most data sets.

To test the reproducibility of the method all patients were measured twice, with at least 24 hours between the sessions. To compare the results of the two measurements the average  $k_{ep}$  of the tumour was calculated. For this purpose, up to 100 pixels were randomly selected from enhancing tumour regions on the T1 weighted DCE-MRI image recorded 90 seconds after Gd-DTPA administration. The  $k_{ep}$  values of these pixels were averaged and the tumour was characterised by the mean  $k_{ep}$  and its standard deviation.

## RESULTS

On the T1 weighted MR image, which was obtained 90 seconds after Gd-DTPA administration, the presence of a head and neck tumour can readily be detected as illustrated in figure 4.2a for a patient with a hypopharynx tumour. The white line in figure 4.2b indicates the border of the tumour as determined by the radiologist. For further analysis of this tumour region by DCE-MR imaging the AIF was determined by the algorithm described in the previous section. 33 pixels were selected in the vertebral and carotid arteries as indicated in black in figure 4.2b. Pixels located in the arteries that were not selected by the algorithm either showed extreme artifacts or a bolus passage less than one inter-image interval (2 sec) earlier than in the veins. The AIF calculated from the selected pixels is shown in figure 4.2d. The solid line through the AIF data (squares) only connects the data points. The Gd-DTPA uptake data of 1 pixel in the tumour region is also shown in this figure (circles). The result of the fit according to equation 4.1, using for  $C_p(t)$  the AIF, is indicated by the solid line through the tumour data points. The value of  $k_{ep}$  derived from this fit was  $1.52 \text{ min}^{-1}$ . Values of  $k_{ep}$  derived for all pixels were reconstructed into a  $k_{ep}$  map (figure 4.2c).

In the  $k_{ep}$  map of the patient with a hypopharynx tumour (figure 4.2c) the tumour can be clearly distinguished from the surrounding tissue, suggesting its diagnostic value. The  $k_{ep}$  map also shows several lymph nodes (e.g. one located laterally to the

tumour and indicated by the arrow in figure 4.2c), which suggests a potential importance of this method in detecting metastases. Furthermore, spatial inhomogeneity in Gd-DTPA uptake rates within the tumour can be seen, which can be visualised in quantitated  $k_{ep}$  histograms. This tool may be an important asset in the evaluation of treatment response and prediction of treatment outcome by distinguishing areas with high Gd-DTPA uptake rates from necrotic areas with low uptake rates. As an example, the  $k_{ep}$  histogram of all pixels of the tumour of patient 1 is shown in figure 4.3.

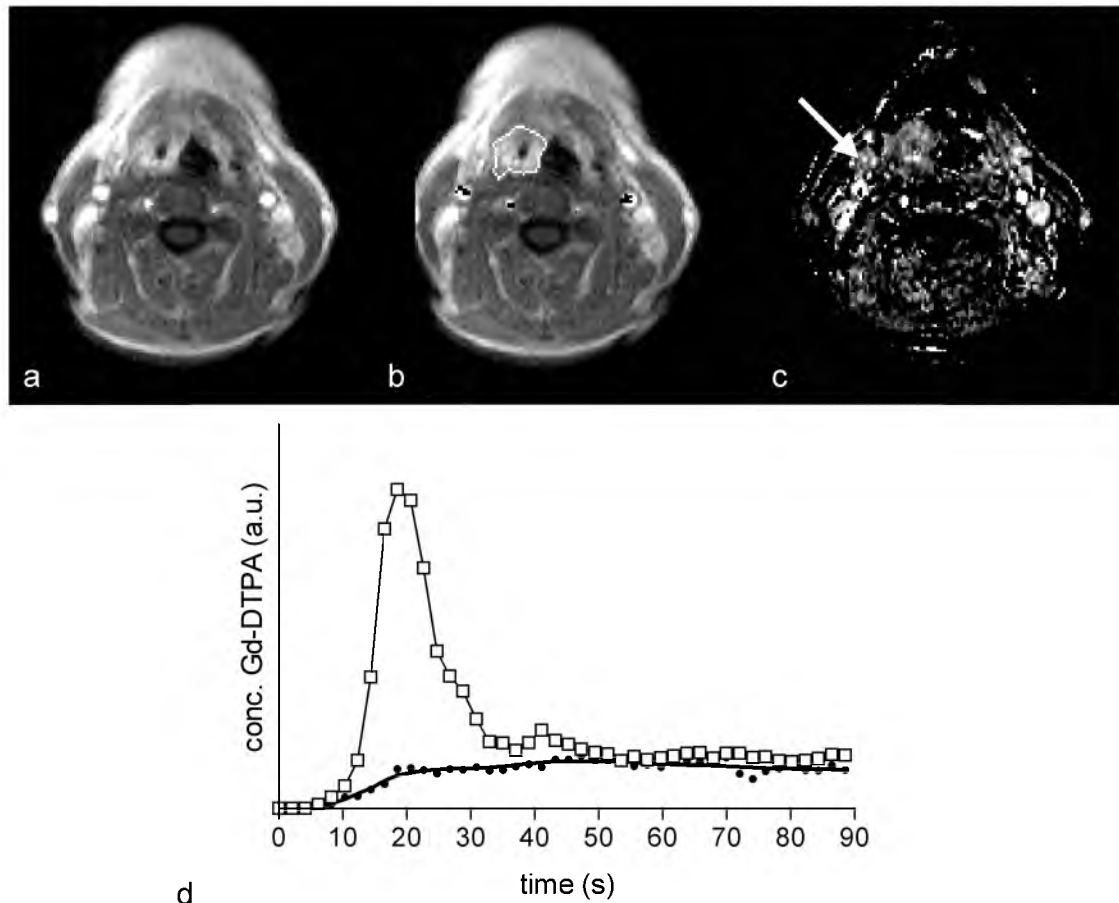


Figure 4.2. (a) T1 weighted DCE image of a patient with a hypopharynx tumour recorded 90 seconds after Gd-DTPA administration. (b) The same image, with the AIF pixels as selected by the algorithm shown in black. The white line marks the ROI of the tumour. The central part of the tumour (consisting of air) was excluded from the analysis. (c) The  $k_{ep}$  map of the same patient. The arrow indicates a clearly visible lymph node, suggesting potential importance of mapping the Gd-DTPA uptake rate in detecting metastases. (d) Gd-DTPA uptake curve (circles) of 1 pixel of the tumour region and of the fit of this curve according to equation 4.1 (solid line). The AIF (squares, connected with a line) is also shown.

The reproducibility of the present method was tested in 11 patients with tumours in the brain, prostate and head and neck region. The results of this test are shown in figure 4.4. In ten of the eleven patients no significant difference in the mean value of  $k_{ep}$  was found between the two measurement sessions (Student's t-test,  $p > 0.05$ ); in one patient this difference was significant ( $p = 0.02$ ). The standard deviation of the

mean  $k_{ep}$  for each patient reflects the fit error and the measurement error including motion artifacts. Also, inhomogeneity of the tumour will contribute to the value of this standard deviation. For this reason small changes in the average  $k_{ep}$  may remain undetected.

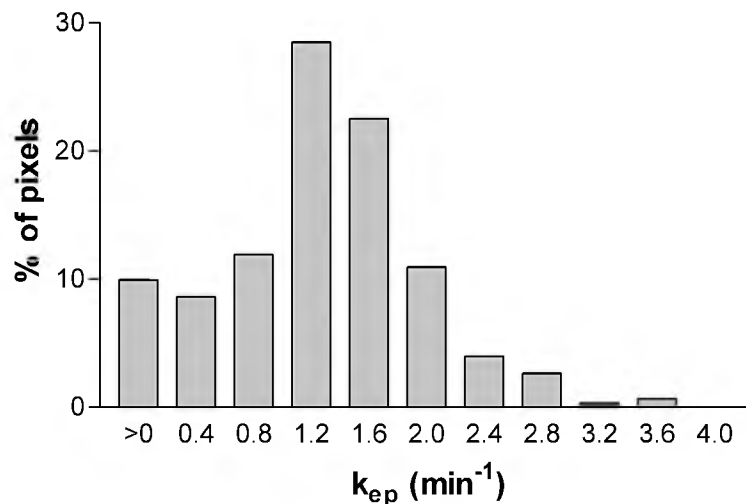


Figure 4.3. Histogram of all pixels of the tumour region shown in figure 4.2, visualising the distribution of  $k_{ep}$  values. Spatial inhomogeneity in Gd-DTPA uptake rates within the tumour is clearly visible. Low values of  $k_{ep}$  may correspond to necrotic areas which often show slow contrast enhancement (if any), high values of  $k_{ep}$  usually indicate tumour areas containing many (permeable) vessels, which may coincide with active growing tumour tissue.

The necessity to normalise DCE-MRI data individually for further (pharmacokinetic) assessment followed from an analysis using a general concentration-time curve as AIF, instead of using coregistered AIFs for each examination. This general AIF was obtained by averaging 20 AIFs of patients with tumours in the head-neck region. Again, reproducibility of the method was tested. The results are shown in figure 4.5. Statistically significant differences between the two measurement sessions were found in 6 out of 11 patients (Student's t-test,  $p < 0.05$ ), showing a poor reproducibility using this general AIF method and the inaccuracy made when assuming no intra- and interindividual differences.

Furthermore, significant differences in the actual values of  $k_{ep}$  were found between the two data analysis methods, using a coregistered AIF (figure 4.4) and using a general AIF (figure 4.5). Assuming the first method will generate more accurate 'true' values of  $k_{ep}$ , errors up to a factor 2 are being made in the second method.

## DISCUSSION

We demonstrated the application of a DCE-MRI method which allows reconstruction of quantitative spatial maps of the rate of Gd-DTPA contrast uptake in tissue ( $k_{ep}$ ) after bolus injection of Gd-DTPA. Values of  $k_{ep}$  were normalised using a

coregistered AIF enabling comparison of intra- and interpatient data. This method proved to yield very reproducible results.

A key factor in the present method is measuring the AIF after bolus injection of Gd-DTPA. Especially in large arteries flow and pulsation artifacts may be visible. Because of these artifacts manually selecting all pixels in an artery led to non-reproducible results. Pixels near the vascular wall often showed less extended artifacts than pixels in the centre of large arteries, possibly because of the decreased blood flow near the vascular wall. Implementation of a simple automated algorithm to select the AIF pixels (search for rapid and large contrast enhancement) increased reproducibility to a high level. The algorithm has two main advantages in comparison with manual selection of AIF pixels. Firstly, all arteries in the image are used to obtain the AIF. Also contributions from small arteries consisting of only a few pixels are included, leading to a more robust AIF. Secondly, extreme artifacts which may exist in arteries are automatically discarded, leading to more reproducible results. In all patients practically all pixels that were selected by the algorithm were located in arteries clearly visible on MRI, demonstrating the feasibility of the algorithm for this purpose. A similar method to select AIF pixels has been described by Rempp et al (24), who applied dynamic T2\* weighted MR imaging of the normal brain after a bolus injection of Gd-DTPA. In their study however, a gamma variate function was used to extract the measured concentration-time curves. Threshold values of the parameters of this function were defined using an interactive computer program to select AIF pixels.

A difficulty in acquiring the AIF is the T2\* shortening in regions of high Gd-DTPA concentration. Extreme T2\* shortening may lead to signal decrease, especially at the top of the bolus passage. Although pixels showing extreme T2\* effects are automatically discarded by the algorithm, the top value of the selected AIF may be attenuated to some extent. However, even a 50% decrease or increase of the top value of the AIF led to only 10% change in the value of  $k_{ep}$ , as was tested in three patients. The sequence used in the present study had already been optimised to reduce T2\* effects. Avoiding these effects further may be done by either using a different type of sequence (e.g. 25) or to lower the dose of the bolus Gd-DTPA.

Another method to apply the contrast medium is by infusion. Knopp et al (26) and Hoffman et al (27) showed good DCE-MRI results using a 1-minute infusion of Gd-DTPA and incorporating the shape of the AIF by modelling its monoexponential decay. In this way, accurate estimation of the AIF may be facilitated (19), as artifacts will be less. However, first pass dynamics cannot be measured in this approach. Furthermore, as Henderson et al (16) discussed, a rapid bolus injection may reduce the error in estimations of Gd-DTPA uptake.

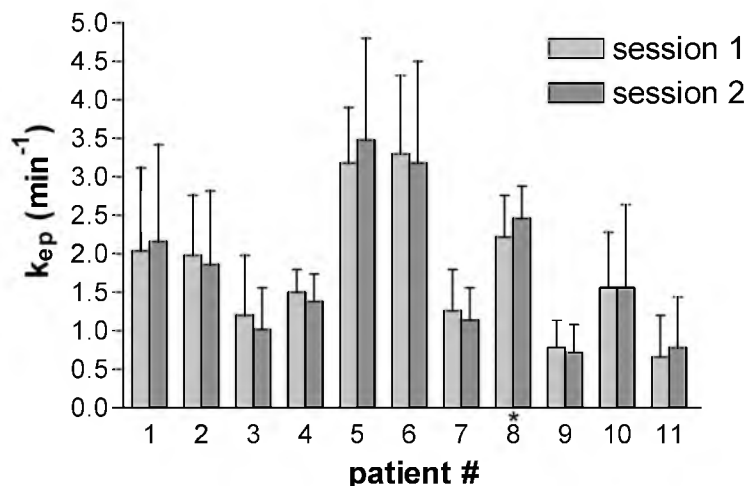


Figure 4.4. Graph showing the results of the reproducibility test of the proposed method. Eleven patients were measured twice (session 1 and 2) and  $k_{ep}$  values were calculated for the tumour region. No statistically significant differences were found between the two measurement sessions in all but one patient (marked \*, Student's t-test,  $p > 0.05$ ). Patient numbers: (1) larynx carcinoma, (2-4) hypopharynx carcinoma, (5) lymph node metastasis, (6) melanoma, (7-9) prostate carcinoma, (10-11) brain tumour.

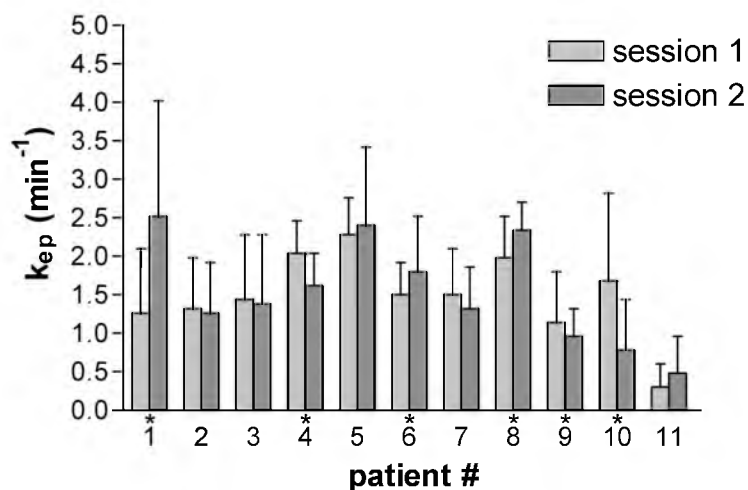


Figure 4.5. Graph showing the results of the reproducibility test of the data analysis method using a generalised AIF. Eleven patients were measured twice (session 1 and 2) and  $k_{ep}$  values were calculated for the tumour region. In 6 out of 11 patients statistically significant differences were found between the sessions (marked \*, Student's t-test,  $p < 0.05$ ), showing a poor reproducibility.

Larsson et al (25) and Fritz-Hansen et al (28) showed the feasibility of MRI measurement of the AIF compared to arterial blood sampling in healthy volunteers and the necessity to normalise DCE-MRI data using this AIF. Port et al (20) also demonstrated the need for monitoring arterial kinetics of Gd-DTPA individually when determining contrast medium exchange rates between blood and tumour in patients with mammary tumours. When the first pass of the contrast agent is not sampled, for example when DCE-MRI data is recorded with low temporal resolution, differences in AIFs may be less pronounced. In studies using laboratory animals

(29-31) AIFs may be more similar and less interindividual differences may exist due to their more identical (genetic) background. Simpson et al (32) showed that substantial errors are introduced using a common AIF instead of individual AIFs in rats, but that these errors can be minimised with proper experimental strategies.

When analysing DCE-MRI data using the Tofts or Larsson model one has to be aware of the assumptions that are being made in these models (33). In this respect, physiological interpretation of the parameters in the model may not be trivial. The rate constant  $k_{ep}$  is not solely dependent on vascular permeability, but may be governed by other physiological parameters as well (34,35). In particular, as one MRI voxel generally contains both tissue and blood vessels, perfusion of these vessels may become an important contributing factor. Thus, without prior knowledge, a  $k_{ep}$  map can neither be interpreted simply as a permeability map nor as a perfusion map. Physiological specificity may be increased by including a plasma volume term ( $v_p C_p$ ) into the data analysis (equation 4.1), but this will only make a valuable contribution to the analysis when this term can be determined with good precision (33). Su et al (29) proposed a method to separate contributions from blood vessels and extravascular components to the Gd-DTPA uptake rate in rats, assuming a generalised AIF. Recently, Li et al (36) showed a method to generate permeability maps corrected for contributions from vessels in brain tumour patients.

Pixelwise mapping of  $k_{ep}$  would allow one to perform a pixel-to-pixel analysis of data of the same patient at different sessions. In practice this is quite difficult, because an exact slice match is necessary for this purpose. Even a small shift can be problematic for performing a pixel-to-pixel analysis, especially in regions of interest with large heterogeneity. In this case, histograms of  $k_{ep}$  (see figure 4.3) may prove valuable to provide a way in the analysis of the distribution of the Gd-DTPA uptake rates in the tumour region.

Besides  $k_{ep}$  maps also  $K^{trans}$  and  $v_e$  maps were generated from the DCE-MRI data in this study. However, due to the scaling factor  $f$  (see equation 4.1) these parameters could not be expressed in absolute quantitated values. To do so, knowledge would be required not only about the T1 before Gd-DTPA injection, but also about the tissue relaxivity, which can generally only be approximated (33).

In conclusion, a method is described to measure reproducibly both Gd-DTPA uptake in human tumours and the AIF after bolus injection of Gd-DTPA, and to generate maps of physiological parameters from this DCE-MRI data.

## ACKNOWLEDGEMENTS

The authors thank Gerhard Laub (Siemens Medical Systems) for supplying the MR sequence. HenkJan Huisman, Boudewijn van der Sanden and Rene in 't Zandt are acknowledged for helpful discussions. Ferdi van Dorsten, Hanneke van Laarhoven and Janneke Schuurin are acknowledged for providing the data sets and the technicians of the departments of Radiology and Radiotherapy for their assistance.

## REFERENCES

1. Degani H, Gusic V, Weinstein D, Fields S, Strano S. Mapping pathophysiological features of breast tumors by MRI at high spatial resolution. *Nat Med* 3:780-782, 1997.
2. Buckley DL, Drew PJ, Mussurakis S, Monson JR, Horsman A. Microvessel density of invasive breast cancer assessed by dynamic Gd-DTPA enhanced MRI. *J Magn Reson Imaging* 7:461-464, 1997.
3. Den Boer JA, Hoenderop RK, Smink J, et al. Pharmacokinetic analysis of Gd-DTPA enhancement in dynamic three-dimensional MRI of breast lesions. *J Magn Reson Imaging* 7:702-715, 1997.
4. Mayr NA, Hawighorst H, Yuh WT, Essig M, Magnotta VA, Knopp, MV. MR microcirculation assessment in cervical cancer: correlations with histomorphological tumor markers and clinical outcome. *J Magn Reson Imaging* 10:267-276, 1999.
5. Barentsz JO, Engelbrecht M, Jager GJ, et al. Fast dynamic Gadolinium-enhanced MR imaging of urinary bladder and prostate cancer. *J Magn Reson Imaging* 10:295-304, 1999.
6. Turnbull LW, Buckley DL, Turnbull LS, Liney GP, Knowles AJ. Differentiation of prostatic carcinoma and benign prostatic hyperplasia: correlation between dynamic Gd-DTPA-enhanced MR imaging and histopathology. *J Magn Reson Imaging* 9:311-316, 1999.
7. Padhani AR, Gapinski CJ, Macvicar DA, et al. Dynamic contrast enhanced MRI of prostate cancer: correlation with morphology and tumour stage, histological grade and PSA. *Clin Radiol* 55:99-109, 2000.
8. Baba Y, Furusawa M, Murakami R, et al. Role of dynamic MRI in the evaluation of head and neck cancers treated with radiation therapy. *Int J Radiat Oncol Biol Phys* 37:783-787, 1997.
9. Hoskin PJ, Saunders MI, Goodchild K, Powell ME, Taylor NJ, Baddeley H. Dynamic contrast enhanced magnetic resonance scanning as a predictor of response to accelerated radiotherapy for advanced head and neck cancer. *Br J Radiol* 72:1093-1098, 1999.
10. Hawighorst H, Knopp MV, Debus J, et al. Pharmacokinetic MRI for assessment of malignant glioma response to stereotactic radiotherapy: initial results. *J Magn Reson Imaging* 8:783-788, 1998.
11. Hawighorst H, Knapstein PG, Weikel W, et al. Angiogenesis of uterine cervical carcinoma: characterisation by pharmacokinetic magnetic resonance parameters and histological microvessel density with correlation to lymphatic involvement. *Cancer Res* 57:4777-4786, 1997.
12. Su MY, Muhler A, Lao X, Nalcioglu O. Tumor characterisation with dynamic contrast-enhanced MRI using MR contrast agents of various molecular weights. *Magn Reson Med* 39:259-269, 1998.
13. Kovar DA, Lewis M, Karczmar GS. A new method for imaging perfusion and contrast extraction fraction: input functions derived from reference tissues. *J Magn Reson Imaging* 8:1126-1134, 1998.



14. Tofts PS, Kermode AG. Measurement of the blood-brain barrier permeability and leakage space using dynamic MR imaging. 1. Fundamental concepts. *Magn Reson Med* 17:357-367, 1991.
15. Larsson HB, Stubgaard M, Frederiksen JL, Jensen M, Henriksen O, Paulson OB. Quantitation of blood-brain barrier defect by magnetic resonance imaging and Gadolinium-DTPA in patients with multiple sclerosis and brain tumors. *Magn Reson Med* 16:117-131, 1990.
16. Henderson E, Rutt BK, Lee TY. Temporal sampling requirements for the tracer kinetics modeling of breast disease. *Magn Reson Imaging* 16:1057-1073, 1998.
17. Tofts PS, Brix G, Buckley DL, et al. Estimating kinetic parameters from dynamic contrast-enhanced T(1)-weighted MRI of a diffusable tracer: standardized quantities and symbols. *J Magn Reson Imaging* 10:223-232, 1999.
18. Weinmann HJ, Laniado M, Mutzel W. Pharmacokinetics of GdDTPA/Dimeglumine after intravenous injection into healthy volunteers. *Physiol Chem Phys Med NMR* 16:167-172, 1984.
19. Evelhoch JL. Key factors in the acquisition of contrast kinetic data for oncology. *J Magn Reson Imaging* 10:254-259, 1999.
20. Port RE, Knopp MV, Hoffmann U, Milker-Zabel S, Brix G. Multicompartment analysis of Gadolinium chelate kinetics: blood-tissue exchange in mammary tumors as monitored by dynamic MR imaging. *J Magn Reson Imaging* 10:233-241, 1999.
21. Korosec FR, Frayne R, Grist TM, Mistretta CA. Time-resolved contrast-enhanced 3D MR angiography. *Magn Reson Med* 36:345-351, 1996.
22. Hittmair K, Gomiscek G, Langenberger K, Recht M, Imhof H, Kramer J. Method for the quantitative assessment of contrast agent uptake in dynamic contrast-enhanced MRI. *Magn Reson Med* 31:567-571, 1994.
23. Larsson HB, Stubgaard M, Sondergaard L, Henriksen O. In vivo quantification of the unidirectional influx constant for Gd-DTPA diffusion across the myocardial capillaries with MR imaging. *J Magn Reson Imaging* 4:433-440, 1994.
24. Rempp KA, Brix G, Wenz F, Becker CR, Gueckel F, Lorenz WJ. Quantification of regional cerebral blood flow and volume with dynamic susceptibility contrast-enhanced MR imaging. *Radiology* 193:637-641, 1994.
25. Larsson HB, Fritz-Hansen T, Rostrup E, Sondergaard L, Ring P, Henriksen O. Myocardial perfusion modeling using MRI. *Magn Reson Med* 35:716-726, 1996.
26. Knopp MV, Weiss E, Sinn HP, et al. Pathophysiologic basis of contrast enhancement in breast tumors. *J Magn Reson Imaging* 10:260-266, 1999.
27. Hoffmann U, Brix G, Knopp MV, Hess T, Lorenz WJ. Pharmacokinetic mapping of the breast: a new method for dynamic MR mammography. *Magn Reson Med* 33:506-514, 1995.
28. Fritz-Hansen T, Rostrup E, Larsson HB, Sondergaard L, Ring P, Henriksen O. Measurement of the arterial concentration of Gd-DTPA using MRI: a step toward quantitative perfusion imaging. *Magn Reson Med* 36:225-231, 1996.

29. Su MY, Jao JC, Nalcioglu O. Measurement of vascular volume fraction and blood-tissue permeability constants with a pharmacokinetic model: studies in rat muscle tumors with dynamic Gd-DTPA enhanced MRI. *Magn Reson Med* 32:714-724, 1994.
30. Vallee JP, Sostman HD, MacFall JR, et al. Quantification of myocardial perfusion by MRI after coronary occlusion. *Magn Reson Med* 40:287-297, 1998.
31. Taylor NJ, Rowland IJ, Tanner SF, Leach MO. A rapid interleaved method for measuring signal intensity curves in both blood and tissue during contrast agent administration. *Magn Reson Med* 30:744-749, 1993.
32. Simpson NE, He Z, Evelhoch JL. Deuterium NMR tissue perfusion measurements using the tracer uptake approach: I. Optimisation of methods. *Magn Reson Med* 42:42-52, 1999.
33. Tofts PS. Modeling tracer kinetics in dynamic Gd-DTPA MR imaging. *J Magn Reson Imaging* 7:91-101, 1997.
34. Taylor JS, Tofts PS, Port R, et al. MR imaging of tumor microcirculation: promise for the new millennium. *J Magn Reson Imaging* 10:903-907, 1999.
35. van der Sanden BP, Rozijn TH, Rijken PF, et al. Noninvasive assessment of the functional neovasculature in 9L-glioma growing in rat brain by dynamic 1H magnetic resonance imaging of Gadolinium uptake. *J Cereb Blood Flow Metab* 20:861-870, 2000.
36. Li KL, Zhu XP, Waterton JC, Jackson A. Ultrafast quantitative 3D mapping of blood volume and endothelial permeability in brain tumours. *ISMRM Workshop on MR in Experimental and Clinical Cancer Research in the New Millennium*, Geiranger, Norway, p.24, 2000.



# 5

## EFFECTS OF BREATHING A HYPEROXIC HYPERCAPNIC GAS MIXTURE ON BLOOD OXYGENATION AND VASCULARITY OF HEAD AND NECK TUMOURS AS MEASURED BY MRI

Mark Rijpkema

Johannes Kaanders

Frank Joosten

Albert van der Kogel

Arend Heerschap

---

This chapter is based on:

Rijpkema M, Kaanders J, Joosten F, van der Kogel A, Heerschap A. Effects of breathing a hyperoxic hypercapnic gas mixture on blood oxygenation and vascularity of head and neck tumors as measured by MRI. *Int J Radiat Oncol Biol Phys* 53(5):1185-1191, 2002.

**ABSTRACT**

For head and neck tumours breathing a hyperoxic hypercapnic gas mixture and administration of nicotinamide has been shown to result in a significantly improved tumour response to accelerated radiotherapy (ARCON, Accelerated Radiotherapy with CarbOgen and Nicotinamide). This may be caused by improved tumour oxygenation, possibly intermediated by vascular effects. In this study, both blood oxygenation and vascular effects of breathing a hyperoxic hypercapnic gas mixture (98% O<sub>2</sub> + 2% CO<sub>2</sub>) were assessed by Magnetic Resonance Imaging (MRI) in patients with head and neck tumours. Tumour vascularity and oxygenation were investigated by dynamic Gadolinium-DTPA contrast enhanced MRI and Blood Oxygen Level Dependent (BOLD) MRI respectively. Eleven patients with primary head and neck tumours were each measured twice; with and without breathing the hyperoxic hypercapnic gas mixture. BOLD MR imaging revealed a significant increase of the MRI time constant of transverse magnetisation decay (T2\*) in the tumour during hypercapnic hyperoxygenation, which correlates to a decrease of the deoxyhaemoglobin concentration. No changes in overall tumour vascularity were observed, as measured by the Gadolinium-DTPA contrast agent uptake rate in the tumour. In conclusion, breathing a hyperoxic hypercapnic gas mixture improves tumour blood oxygenation in patients with head and neck tumours, which may contribute to the success of the ARCON therapy.

## INTRODUCTION

Both tumour blood flow and oxygenation are important factors determining the outcome of cancer therapy. As well-oxygenated cells are more radiosensitive than hypoxic cells (1), increasing tumour oxygen levels may improve the efficacy of radiotherapy. Hypoxia may occur in cells that are located relatively far away from a blood vessel ('chronic' or 'diffusion limited' hypoxia (2)) or it may be induced by local fluctuations of blood flow ('acute' or 'perfusion limited' hypoxia (3,4)). Both mechanisms underlying hypoxia have to be dealt with to realise the best clinical outcome for radiotherapy.

Studies by Kaanders and co-workers (5,6) showed that treatment results in advanced head and neck tumours can be improved successfully by accelerated radiotherapy with carbogen and nicotinamide (ARCON). The mechanism of action of carbogen and nicotinamide is thought to be an increase in tumour oxygenation and thus a reduction of hypoxic regions in the tumour. The first results of their study show an actuarial local control rate of 80% at 3 years for carcinomas of the larynx, higher than any previous report in the literature for this category of patients (6). Also for patients with bladder carcinoma ARCON therapy resulted in a significant improvement of local control, progression free survival, and overall survival (7). For both tumour types randomised Phase III trials are ongoing.

Breathing a hyperoxic hypercapnic gas mixture like carbogen (95% O<sub>2</sub> + 5% CO<sub>2</sub>) may have an effect on both tissue oxygenation and blood flow (8-10). The oxygen component in the gas mixture causes arterial haemoglobin to be fully oxygenated, and increases the blood oxygen tension (pO<sub>2</sub>) to a large extent (11-14). The effect of carbogen breathing on blood flow is more complex (9,15). Simplistically, CO<sub>2</sub> is a vasodilator at a vascular level and may increase blood flow, whereas high concentrations of oxygen have a potential to decrease blood flow (16,17). Recently however, using intravital microscopy tumour vascular response to hyperoxygenation and hypercapnia was shown to be heterogeneous and dependent on vascular function and maturation (14).

Magnetic Resonance Imaging (MRI) provides non-invasive ways to study tumour physiology. Both functional changes in tumour vasculature and oxygenation status can be studied to assess treatments of tumour hypoxia. Furthermore, the high spatial resolution of MRI enables investigations of the heterogeneous vascular response throughout the tumour. MRI techniques to study tumour vascular oxygenation usually employ the Blood Oxygen Level Dependent (BOLD) effect (18). This effect is based on the different magnetic properties of deoxyhaemoglobin and oxyhaemoglobin. Unlike oxyhaemoglobin, deoxyhaemoglobin is paramagnetic and shortens the MR time constant for the transverse magnetisation decay (apparent spin-spin relaxation time, T<sub>2</sub><sup>\*</sup>), resulting in an attenuation of MRI signals from water

in tissue adjacent to blood vessels. The BOLD effect in human tumours has been assessed by gradient-echo MRI (19). Using this technique changes in the value of  $T_2^*$  can be determined, which correlate directly to changes in the deoxyhaemoglobin concentration (20) and thus provide information on changes in local vascular oxygenation.

In tumours, newly formed blood vessels usually show structural and functional abnormalities with regard to their spatial distribution, morphology, dimensions and permeability (21). To study various aspects of tumour vascularity including blood flow, permeability, and vascular volume, dynamic Gadolinium-DTPA contrast enhanced MRI can be used (22). This technique has been widely employed for the assessment of human tumours both in detection, identification, and staging (e.g. 23-25).

Both BOLD MRI and Gadolinium-DTPA contrast MRI have been used extensively to study the effects of oxygenating agents and blood flow enhancement on tumour hypoxia in laboratory animal models (e.g. 13,26-28). Tumour blood flow may respond heterogeneously when challenged with a hyperoxic hypercapnic gas mixture, which may be due to the association of blood vessels with smooth muscle cells (14). In this respect, also the 'steal' effect is well-recognised: blood flow may be increased locally at the expense of an adjacent location, depending on the tumour vascular bed (13,29). The effect of breathing a hyperoxic hypercapnic gas mixture on tumour oxygenation seems to be more clear, resulting in an improved oxygenation status in most experimental tumours. In mice, not only tumour  $pO_2$  was shown to increase during carbogen breathing, but also radiation response was enhanced under these conditions (30).

Although the clinical ARCON therapy leads to promising results in tumour treatment, the precise mechanism of action of breathing a hyperoxic hypercapnic gas mixture remains unclear. Animal studies suggest that an improved tumour oxygenation may contribute to the success of the ARCON therapy by reducing hypoxic regions in tumour. In humans, little information on the effects of breathing a hyperoxic hypercapnic gas mixture is currently available. MRI may be a suitable tool to investigate both changes in blood oxygenation and vascularity and may assist in the prediction of response to treatments using hyperoxygenation. In this study, BOLD MRI and Gadolinium-DTPA contrast enhanced MRI techniques were combined to assess the effects of breathing a hyperoxic hypercapnic gas mixture on the oxygenation and vascularity of head and neck tumours.

## METHODS AND MATERIALS

Eleven patients (10 males, 1 female) with squamous cell carcinomas of the larynx (n=6), hypopharynx (n=3) and oropharynx (n=2) were included in the study. The mean age was 56 years (45-67 years). All patients met the eligibility criteria of the ARCON clinical trial (31) and gave informed consent to participate to this study. Approval for the study was obtained from the local ethics committee.

MR imaging was performed on a 1.5 T Siemens Vision whole body system (Siemens Medical Systems, Erlangen, Germany) using a CP-neck-array coil. All patients were studied twice; once breathing air and once breathing a gas mixture of 98% O<sub>2</sub> and 2% CO<sub>2</sub>. This hyperoxic hypercapnic gas mixture is also used in the ARCON clinical trial for head and neck tumours. The time between the two sessions was at least 24 hours. Gadolinium-DTPA (Gd-DTPA, Magnevist®, Schering, Berlin, Germany) was administered by intravenous bolus injection (15 ml, 0.5 M, 2.5 ml/s) using a Spectris™ MR injection system (Medrad, Inc.). This MRI contrast agent is routinely used for vascular investigations.

In the first session conventional T1, T2, and proton density weighted images were recorded and after administration of the contrast medium Gd-DTPA tissue uptake was monitored for 90 seconds (FLASH, TR=50 ms, TE=4.4 ms,  $\alpha=60^\circ$ , 7 mm slice, 2 seconds temporal resolution). In the second session 28 multiple gradient-echo images (16 echo FLASH, TR=65 ms, TE=6-51 ms,  $\alpha=20^\circ$ , 5 mm slice (32)) were recorded for 14 minutes whilst breathing air. Subsequently breathing of the hyperoxic hypercapnic gas mixture was started and 12 gradient-echo images were recorded for another 6 minutes, followed by Gd-DTPA contrast enhanced imaging as in the first session.

T2\* values (ms) were calculated from the gradient-echo imaging data (32). The value of T2\* in the tumour was obtained by averaging all pixels within the selected tumour region. Although the mask for supplying the hyperoxic hypercapnic gas mixture was positioned carefully, air leaks might occur in the experimental setup. Therefore, patients were checked for inhaling the gas mixture properly by measuring the T2\* in venous blood. If no statistically significant increase (Student's t-test) in the value of T2\* in the jugular vein was observed during hypercapnic hyperoxygenation the measurement was considered a technical failure.

The dynamic Gd-DTPA contrast image data was analysed as described by Rijpkema et al (33). The rate of contrast medium uptake ( $k_{ep}$  (s<sup>-1</sup>) (34)) was calculated using the physiological pharmacokinetic model of Larsson et al (35). The concentration-time characteristics of the contrast medium in arterial blood were used to normalise the data. Maps of  $k_{ep}$  were reconstructed from the value of  $k_{ep}$  for each pixel. The Gd-DTPA uptake rate of the tumour during air breathing and



breathing the hyperoxic hypercapnic gas mixture was calculated by averaging the values of  $k_{ep}$  in Gd-DTPA enhancing regions of the tumour.

To uncover spatial heterogeneity pixels in the tumour region were selected from the  $T2^*$  and  $k_{ep}$  data and displayed as histograms of  $T2^*$  and Gd-DTPA uptake rate. In this way the effects of hypercapnic hyperoxygenation on the relative distribution of these parameters could be assessed in more detail.

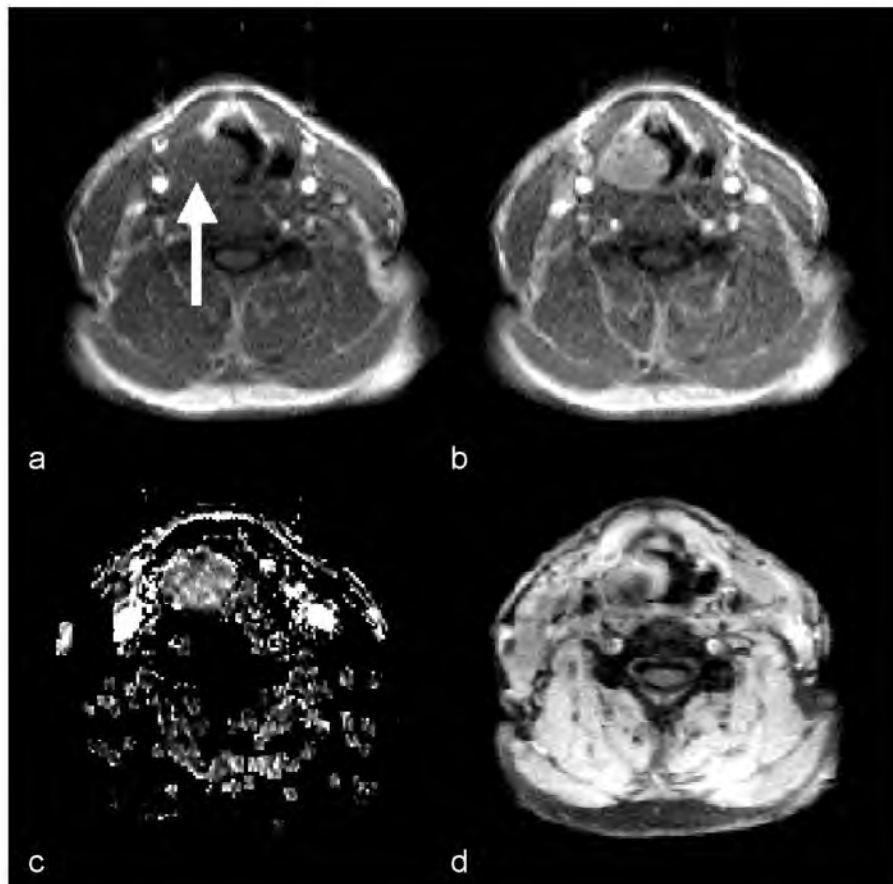


Figure 5.1. (a) Transversal MR image of a patient with a hypopharynx tumour, recorded before Gd-DTPA contrast administration. The arrow indicates the tumour. The image was obtained at the end of a 10-minutes period of breathing the hyperoxic hypercapnic gas mixture. (b) Dynamic contrast enhanced MR image of the same patient, recorded one minute after Gd-DTPA contrast administration. MR signal intensity in the tumour region is clearly enhanced. (c) Map of the Gd-DTPA uptake rate  $k_{ep}$  of the same patient, providing information on tumour vascularity. The  $k_{ep}$  map was calculated from the contrast enhanced MRI data set as shown in figures 5.1a and 5.1b. (d) The  $R2^*$  map at the same slice position of the same patient during breathing the hyperoxic hypercapnic gas mixture, showing clear heterogeneity within the tumour.

## RESULTS

Eleven patients were measured successfully using the current MRI protocol. From the 17 initially selected patients, 6 dropped out of the study or were eliminated from the study for technical reasons. In two patients severe claustrophobia necessitated

the early abort of the MRI measurement, in two patients no significant increase in the value of T2\* in the jugular vein was observed during breathing the hyperoxic hypercapnic gas mixture and the measurement was considered a technical failure, in one patient measurements were discontinued because of artifacts on the MR images caused by a metal implant in the mandible, and one patient was unable to breathe the hyperoxic hypercapnic gas mixture and dropped out of the ARCON study. Four patients were slightly claustrophobic or unusually restless during the MR measurement and the protocol was shortened by recording fewer gradient-echo images during air breathing, to a minimum of 15 images (7.5 minutes).

patient	$k_{ep}$ (tumour, air) ( $\text{min}^{-1}$ )	$\Delta k_{ep}$ (%)
1	$2.3 \pm 0.7$	$-7.7 \pm 4.2$
2	$3.0 \pm 1.3$	$6.0 \pm 6.1$
3	$2.8 \pm 0.9$	$12.8 \pm 11.0$
4	$1.3 \pm 0.6$	$4.5 \pm 8.3$
5	$1.3 \pm 0.7$	$-14.3 \pm 8.2$
6	$2.6 \pm 0.9$	$-11.4 \pm 6.6$
7	$1.4 \pm 0.5$	$8.3 \pm 6.6$
8	$1.8 \pm 0.4$	$6.7 \pm 4.5$
9	$2.3 \pm 1.0$	$5.1 \pm 7.1$
10	$2.9 \pm 1.1$	$10.0 \pm 7.2$
11	$1.4 \pm 0.4$	$4.2 \pm 3.0$

Table 5.1. Values of the Gd-DTPA uptake rate  $k_{ep}$  of the tumour during air breathing and the change due to breathing the hyperoxic hypercapnic gas mixture. Values are presented as mean  $\pm$  standard deviation.  $\Delta k_{ep} = k_{ep}(\text{hyperoxic hypercapnic gas mixture}) - k_{ep}(\text{air})$ , expressed as % with respect to  $k_{ep}(\text{air})$ . In none of the patients the hypercapnic hyperoxia induced change in Gd-DTPA uptake rate was statistically significant (Student's t-test,  $p > 0.05$ ).

MR signal intensity in the tumour region clearly enhanced after Gd-DTPA administration, as is shown in figures 5.1a (pre-contrast) and 5.1b (post-contrast) for a patient with a hypopharynx tumour. This contrast enhanced MRI data was used to reconstruct maps of the rate of contrast agent uptake,  $k_{ep}$ , as shown in figure 5.1c for the same patient. The average values of the Gd-DTPA uptake rate of the tumour during air breathing and breathing the hyperoxic hypercapnic gas mixture were calculated from the corresponding  $k_{ep}$  maps. In table 5.1 the values of  $k_{ep}$  during air breathing and the hypercapnic hyperoxia induced change in  $k_{ep}$  are listed for all patients. The standard deviation of the average value of  $k_{ep}$  in table 5.1 reflects both the heterogeneity of the tumour and the measurement error including motion artifacts. Both small decreases and increases in the Gd-DTPA uptake rate were found as a result of breathing the hyperoxic hypercapnic gas mixture but none were statistically significant (Student's t-test,  $p > 0.05$ ). There was a mean increase in Gd-DTPA uptake rate in the tumour of all patients of 2.2% ( $\pm 9\%$ ), which was also not statistically significant (ANOVA, split plot design;  $p = 0.54$ ). In the distribution

histograms of  $k_{ep}$  values no evident changes in the profile of Gd-DTPA uptake rates were observed visually.

The gradient-echo MR images were used to reconstruct maps of  $R2^*$  ( $R2^*=1/T2^*$ ), as is shown in figure 5.1d. On images recorded during air breathing the tumour was selected and values of the  $T2^*$  of the tumour were calculated. After switching to breathing the hyperoxic hypercapnic gas mixture, data obtained in the first minute was discarded to allow oxygen levels in blood to reach a new equilibrium. The remaining  $R2^*$  maps were processed as those obtained during air breathing. Table 5.2 lists the average values of  $T2^*$  in the tumour during air breathing and the change in  $T2^*$  due to breathing the gas mixture. In all patients an increase in  $T2^*$  was observed, which was statistically significant in 7 out of 11 cases (Student's t-test,  $p<0.05$ ). The mean increase in  $T2^*$  in the tumour of all patients was 5.5% ( $\pm 2.6\%$ ) which was highly significant (ANOVA, split plot design;  $p<0.001$ ).

patient	$T2^*$ (air) (ms)	$\Delta T2^*$ (%)	
1	29.1 $\pm$ 1.8	8.2 $\pm$ 2.9	*
2	31.1 $\pm$ 2.0	0.6 $\pm$ 2.5	
3	32.5 $\pm$ 2.8	6.9 $\pm$ 3.4	
4	26.9 $\pm$ 0.9	7.5 $\pm$ 1.9	♦
5	37.3 $\pm$ 1.5	5.9 $\pm$ 1.2	♦
6	38.2 $\pm$ 1.1	6.1 $\pm$ 1.6	♦
7	31.1 $\pm$ 2.1	5.9 $\pm$ 2.0	*
8	36.6 $\pm$ 2.6	7.9 $\pm$ 3.5	*
9	34.2 $\pm$ 2.7	7.4 $\pm$ 6.7	
10	37.2 $\pm$ 1.3	3.1 $\pm$ 1.3	*
11	45.2 $\pm$ 3.2	1.4 $\pm$ 2.3	

Table 5.2. Values of  $T2^*$  in the tumour during air breathing and the change due to breathing the hyperoxic hypercapnic gas mixture. Values are presented as mean  $\pm$  standard deviation.  $\Delta T2^* = T2^*(\text{hyperoxic hypercapnic gas mixture}) - T2^*(\text{air})$ , expressed as % with respect to  $T2^*(\text{air})$ . In 7 out of 11 patients the hypercapnic hyperoxia induced increase in  $T2^*$  was statistically significant (Student's t-test, \*  $p<0.05$ , ♦  $p<0.01$ ).

To assess this increase in the value of  $T2^*$  due to breathing the hyperoxic hypercapnic gas mixture in more detail histograms of  $T2^*$  were created of all pixels in the tumour region. In figure 5.2 the  $T2^*$  histogram of the tumour of the same patient as in figure 5.1 is shown. Values of  $T2^*$  shorter than 20 ms could not be calculated. In particular the high values of  $T2^*$  seem to be more abundant in the data recorded during breathing the gas mixture. This phenomenon was observed in all patients and may account for the hypercapnic hyperoxia induced increase in the average value of  $T2^*$ .

The results in table 5.1 and 5.2 show significant differences between patients in both the Gd-DTPA uptake rate and the value of  $T2^*$  (ANOVA, split plot design; both

$p < 0.001$ ). Correlations between the values of  $T2^*$  and  $k_{ep}$  were not found (Pearson correlation,  $p > 0.05$ ). Also, pixelwise matching of the  $R2^*$  map and the  $k_{ep}$  map did not lead to a strong correlation in any of the patients (Pearson's correlation coefficient  $< 0.3$ ).

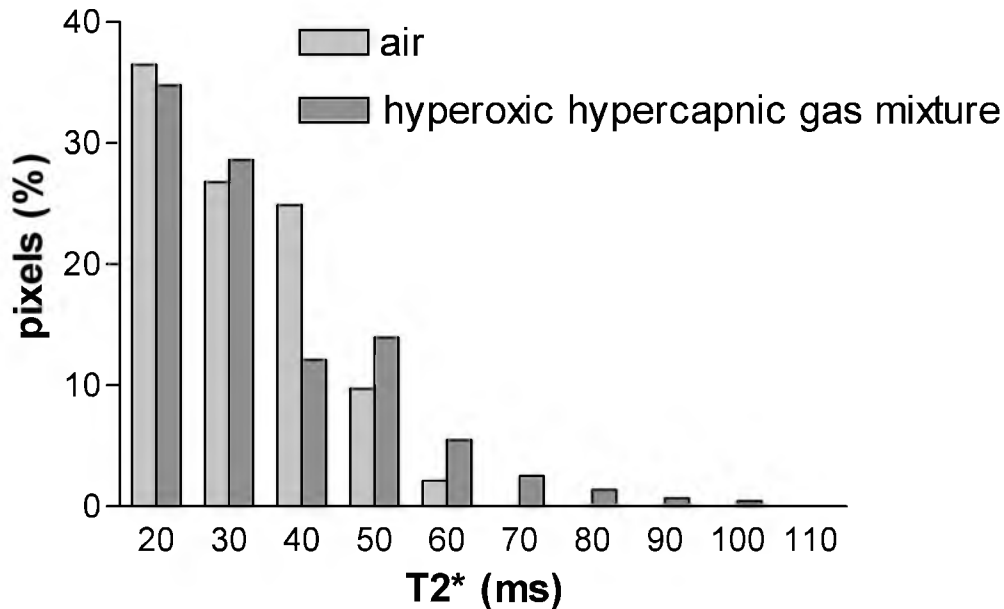


Figure 5.2. The  $T2^*$  histogram of the tumour of the same patient as shown in figure 5.1, visualising the distribution of values of  $T2^*$  (ms) during air breathing and breathing the hyperoxic hypercapnic gas mixture.

## DISCUSSION

Most other work on the effects of breathing hyperoxic hypercapnic gas mixtures on tumour oxygenation and vascularity has been done in laboratory animals using carbogen gas (95%  $O_2$  + 5%  $CO_2$ ). Due to the high  $CO_2$  content carbogen is difficult to breathe for patients during the prolonged time necessary to acquire the MRI data. In our experience the hyperoxic gas mixture containing 2%  $CO_2$  is better tolerated by most patients. Near infrared spectroscopy studies in mice showed that the oxyhaemoglobin / deoxyhaemoglobin ratio significantly increases when breathing the 2%  $CO_2$  hyperoxic gas mixture compared to air breathing. This ratio remains nearly constant however when the  $CO_2$  content is increased to 5%, suggesting that the gas mixture containing 2%  $CO_2$  and 98%  $O_2$  is sufficient for maximum oxygenation (13). This was also shown by blood gas analyses in rats breathing different hyperoxic hypercapnic gas mixtures (36). Furthermore, radiosensitisation in mice was shown not to be affected by reduction of the  $CO_2$  content from 5% even to 1% (37).

Tumour blood oxygen levels were assessed using multiple gradient-echo BOLD MRI. Although the BOLD effect may not only be governed by the oxygenation status but also by flow effects (38-40), measuring the value of  $T2^*$  with a multiple echo sequence is thought to be quite insensitive for flow (41). Thus, multiple gradient-echo MRI may be an important tool for the assessment of the local oxygenation status. Measurement of pretreatment oxygenation levels using oxygen electrodes already showed to be predictive of radiation response in both head and neck carcinomas and carcinomas of the uterine cervix (42,43).

Breathing a hyperoxic hypercapnic gas mixture causes a dramatic increase in the concentration of dissolved oxygen in the plasma and a decrease in the amount of deoxyhaemoglobin (11,13,44). This decrease of the deoxyhaemoglobin concentration is reflected in an increase of  $T2^*$  (20). The  $T2^*$  increase of 5.5%, as observed in this study, may represent a much larger change in deoxyhaemoglobin concentration, as other factors such as local magnetic field inhomogeneities and tissue structure also contribute to the basal value of  $T2^*$ . Apart from blood oxygenation, the deoxyhaemoglobin concentration is also sensitive to blood volume and haematocrit. A variable response to hypercapnia and hyperoxia was observed in vessel diameters and haematocrit in laboratory animal models (14). However, BOLD MRI signal intensity correlated significantly with the fraction of oxygenated haemoglobin (14) and the effect of hyperoxic conditions on blood volume was shown to be inferior to the blood oxygenation increase (45). Thus, the decrease in deoxyhaemoglobin concentration suggests a substantial increase in blood  $pO_2$  in head and neck tumours due to breathing a hyperoxic hypercapnic gas mixture. The question remains whether this is a good representation of tumour tissue  $pO_2$ , which is dependent on both oxygen supply and consumption. Information on the way microregional oxygen gradients are affected by hyperoxygenation is still limited. However, Al Hallaq et al (29) showed the carbogen-induced increase in  $T2^*$  to be strongly correlated with increased tumour  $pO_2$  levels, as measured in rats using oxygen micro-electrodes. Thus, changes in the value of  $T2^*$  may provide information about tumour oxygen levels during breathing of a hyperoxic hypercapnic gas mixture.

While arterial blood may have a much longer  $T2^*$  than generally found in tissue, in venous blood the  $T2^*$  may be as short as 12 ms (46). In the  $T2^*$  histogram of the tumour (figure 5.2) the higher values of  $T2^*$  during breathing of the hyperoxic hypercapnic gas mixture may reflect well-perfused regions containing blood with low deoxyhaemoglobin levels. One might expect that capillaries and small vessels during air breathing contain blood with oxygen levels somewhere between arterial and venous blood levels, although in tumours large heterogeneity in oxyhaemoglobin levels may be present (47). If in capillaries more haemoglobin remains oxygenated because of the high amount of dissolved oxygen in the plasma during breathing the hyperoxic hypercapnic gas mixture, the  $T2^*$  values

corresponding to these vessels will increase. Thus, presenting data as histograms allows investigation of tumour heterogeneity, both with respect to baseline values and hypercapnic hyperoxia induced changes. This may be important information for the selection of treatment strategies and prediction of treatment response.

Dynamic Gd-DTPA contrast enhanced MRI was used to study changes in tumour vascularity. This method already showed to be of value as a predictor of response to radiotherapy for head and neck tumours (48). In this study, contrast enhancement data was analysed using a physiological pharmacokinetic model (35), resulting in values of the rate of Gd-DTPA uptake. This contrast medium uptake rate is dependent on multiple physiological factors, including tumour blood flow, volume of extravascular extracellular space, vascular surface area and permeability (34,35). In general there is insufficient physiological information to establish which of these factors mainly governs the rate of Gd-DTPA uptake. Thus, changes in the uptake rate during breathing a hyperoxic hypercapnic gas mixture may only become manifest if substantial vascular changes occur.

In most laboratory animal models oxygen levels measured in tumour tissue and blood increased dramatically during carbogen breathing as measured either polarographically or by blood gas analysis (e.g. 12,13,30,49), although non-significant changes have also been observed (e.g. 50). A heterogeneous response of tumour blood flow to breathing hyperoxic hypercapnic gas mixtures has been reported (e.g. 12,13,40), probably reflecting the variable types of tumours and tumour-host interactions. While increases in tumour blood flow are usually explained in terms of vasodilatation, decreases in tumour blood flow can be explained by the steal effect, which may occur when the tumour vascular bed runs in parallel to the vasculature of the host. Also vasoconstriction of tumour vasculature and reduced tumour blood flow in response to carbogen breathing have been reported (14, 51). It is difficult however to extrapolate these results directly to primary tumours in humans, because in humans the relationship between tumour and normal tissue vasculature may be fundamentally different.

The results of the present study show no apparent change in tumour vascularity (table 5.1) as measured by the dynamic Gd-DTPA contrast uptake rate. This implies that a dramatic hypercapnic hyperoxia induced decrease of blood flow, which could be disadvantageous for therapy, did not occur. In the ARCON therapy breathing the hyperoxic hypercapnic gas mixture is combined with administration of nicotinamide (5,7,52). This vasomodulator has been shown to improve radiosensitivity by enhancing tissue microcirculation (53-55). The effect of nicotinamide on tumour vascularity was not investigated in this study. In several human tumours carbogen breathing was shown to induce no overall change in blood flow and only small transient fluctuations in individual tumour blood flow, as measured by laser Doppler

flowmetry (15). When combining carbogen with nicotinamide however, tumour blood flow did increase (56).

The present results indicate that in head and neck tumours the primary mechanism of action of breathing the hyperoxic hypercapnic gas mixture is an improvement of the tumour blood oxygenation level which may result in a reduction of hypoxia. In healthy volunteers, analysis of arterial blood samples showed a slight increase in the oxygen saturation of haemoglobin and a large increase in blood  $pO_2$  (11). In head and neck tumours oxygen tension increased during carbogen breathing, as was shown using oxygen electrodes (57). Using the comet assay a reduction in the hypoxic fraction in response to breathing different hyperoxic hypercapnic gas mixtures was found in hypoxic tumours (58). This was also shown in hypoxic marker studies (vascular architecture and microenvironmental parameters, VAMP) using laryngeal squamous cell carcinoma xenografts, in which carbogen breathing reduced diffusion limited hypoxia (9,59).

In conclusion, breathing a hyperoxic hypercapnic gas mixture was shown to improve tumour blood oxygenation in patients with head and neck tumours, which may contribute to the success of the ARCON therapy. No substantial changes in overall tumour vascularity were found, as measured by the Gadolinium-DTPA contrast uptake rate in the tumour. MRI enables non-invasive investigation of both tumour blood oxygenation and vascularity and may assist in the prediction of response to treatments using hyperoxygenation for other tumour types as well.

#### ACKNOWLEDGEMENTS

The authors would like to thank James Goldfarb for supplying the multiple gradient-echo sequence. Also, the MRI and ARCON technicians of the departments of radiology and radiotherapy are acknowledged for their assistance.

## REFERENCES

1. Gray LH, Conger AD, Ebert M, et al. The concentration of oxygen dissolved in tissues at the time of irradiation as a factor in radiotherapy. *Br J Radiol* 26:638-648, 1953.
2. Thomlinson RH, Gray LH. The histological structure of some human lung cancers and the possible implications for radiotherapy. *Br J Cancer* 9:539-549, 1955.
3. Brown JM. Evidence for acutely hypoxic cells in mouse tumours, and a possible mechanism of reoxygenation. *Br J Radiol* 52:650-656, 1979.
4. Chaplin DJ, Olive PL, Durand RE. Intermittent blood flow in a murine tumour: radiobiological effects. *Cancer Res* 47:597-601, 1987.
5. Kaanders JH, Pop LA, Marres HA, et al. Accelerated radiotherapy with carbogen and nicotinamide (ARCON) for laryngeal cancer. *Radiother Oncol* 48:115-122, 1998.
6. Kaanders JHAM, Pop LA, Marres HAM, et al. ARCON: experience in 215 patients with advanced head-and-neck cancer. *Int J Radiat Oncol Biol Phys* 52:769-778, 2002.
7. Hoskin PJ, Saunders MI, Dische S. Hypoxic radiosensitizers in radical radiotherapy for patients with bladder carcinoma: hyperbaric oxygen, misonidazole, and accelerated radiotherapy, carbogen, and nicotinamide. *Cancer* 86:1322-1328, 1999.
8. Horsman MR, Nordmark M, Khalil AA, et al. Reducing acute and chronic hypoxia in tumours by combining nicotinamide with carbogen breathing. *Acta Oncol* 33:371-376, 1994.
9. Bussink J, Kaanders JH, Rijken PF, et al. Vascular architecture and microenvironmental parameters in human squamous cell carcinoma xenografts: effects of carbogen and nicotinamide. *Radiother Oncol* 50:173-184, 1999.
10. Fenton BM, Lord EM, Paoni SF. Enhancement of tumour perfusion and oxygenation by carbogen and nicotinamide during single- and multifraction irradiation. *Radiat Res* 153:75-83, 2000.
11. Kaanders JH, van der Maazen RW. A convenient and reliable method for carbogen breathing in man. *Radiother Oncol* 29:341-343, 1993.
12. Robinson SP, Rodrigues LM, Ojugo AS, et al. The response to carbogen breathing in experimental tumour models monitored by gradient-recalled echo magnetic resonance imaging. *Br J Cancer* 75:1000-1006, 1997.
13. van der Sanden BP, Heerschap A, Hoofd L, et al. Effect of carbogen breathing on the physiological profile of human glioma xenografts. *Magn Reson Med* 42:490-499, 1999.
14. Neeman M, Dafni H, Bukhari O, et al. In vivo BOLD contrast MRI mapping of subcutaneous vascular function and maturation: Validation by intravital microscopy. *Magn Reson Med* 45:887-898, 2001.
15. Powell ME, Hill SA, Saunders MI, et al. Effect of carbogen breathing on tumour microregional blood flow in humans. *Radiother Oncol* 41:225-231, 1996.
16. Milone SD, Newton GE, Parker JD. Hemodynamic and biochemical effects of 100% oxygen breathing in humans. *Can J Physiol Pharmacol* 77:124-130, 1999.



17. Watson NA, Beards SC, Altaf N, et al. The effect of hyperoxia on cerebral blood flow: a study in healthy volunteers using magnetic resonance phase-contrast angiography. *Eur J Anaesthesiol* 17:152-159, 2000.
18. Ogawa S, Lee TM, Nayak AS, et al. Oxygenation-sensitive contrast in magnetic resonance image of rodent brain at high magnetic fields. *Magn Reson Med* 14:68-78, 1990.
19. Griffiths JR, Taylor NJ, Howe FA, et al. The response of human tumours to carbogen breathing, monitored by Gradient-Recalled Echo Magnetic Resonance Imaging. *Int J Radiat Oncol Biol Phys* 39:697-701, 1997.
20. Punwani S, Ordidge RJ, Cooper CE, et al. MRI measurements of cerebral deoxyhaemoglobin concentration [dHb]-- correlation with near infrared spectroscopy (NIRS). *NMR Biomed* 11:281-289, 1998.
21. Vaupel PW. Blood flow, oxygenation, tissue pH distribution and bio-energetic status of tumours. Ernst Schering Research Foundation: Berlin; 1994.
22. Delorme S, Knopp MV. Non-invasive vascular imaging: assessing tumour vascularity. *Eur Radiol* 8:517-527, 1998.
23. Degani H, Gusic V, Weinstein D, et al. Mapping pathophysiological features of breast tumours by MRI at high spatial resolution. *Nat Med* 3:780-782, 1997.
24. Barentsz JO, Engelbrecht M, Jager GJ, et al. Fast dynamic gadolinium-enhanced MR imaging of urinary bladder and prostate cancer. *J Magn Reson Imaging* 10:295-304, 1999.
25. Mayr NA, Hawighorst H, Yuh WT, et al. MR microcirculation assessment in cervical cancer: correlations with histomorphological tumour markers and clinical outcome. *J Magn Reson Imaging* 10:267-276, 1999.
26. Howe FA, Robinson SP, Griffiths JR. Modification of tumour perfusion and oxygenation monitored by gradient recalled echo MRI and <sup>31</sup>P MRS. *NMR Biomed* 9:208-216, 1996.
27. Al Hallaq HA, Zamora M, Fish BL, et al. MRI measurements correctly predict the relative effects of tumour oxygenating agents on hypoxic fraction in rodent BA1112 tumours. *Int J Radiat Oncol Biol Phys* 47:481-488, 2000.
28. Robinson SP, Howe FA, Stubbs M, et al. Effects of nicotinamide and carbogen on tumour oxygenation, blood flow, energetics and blood glucose levels. *Br J Cancer* 82:2007-2014, 2000.
29. Al Hallaq HA, River JN, Zamora M, et al. Correlation of magnetic resonance and oxygen microelectrode measurements of carbogen-induced changes in tumour oxygenation. *Int J Radiat Oncol Biol Phys* 41:151-159, 1998.
30. Nordmark M, Maxwell RJ, Horsman MR, et al. The effect of hypoxia and hyperoxia on nucleoside triphosphate/inorganic phosphate, pO<sub>2</sub> and radiation response in an experimental tumour model. *Br J Cancer* 76:1432-1439, 1997.
31. Kaanders JH, Pop LA, Marres HA, et al. Radiotherapy with carbogen breathing and nicotinamide in head and neck cancer: feasibility and toxicity. *Radiother Oncol* 37:190-198, 1995.

32. Prasad PV, Chen Q, Goldfarb JW, et al. Breath-hold  $R2^*$  mapping with a multiple gradient-recalled echo sequence: application to the evaluation of intrarenal oxygenation. *J Magn Reson Imaging* 7:1163-1165, 1997.
33. Rijpkema M, Kaanders JHAM, Joosten FBM, et al. Method for quantitative mapping of dynamic MRI contrast agent uptake in human tumours. *J Magn Reson Imaging* 14:457-463, 2001.
34. Tofts PS, Brix G, Buckley DL, et al. Estimating kinetic parameters from dynamic contrast-enhanced T(1)-weighted MRI of a diffusable tracer: standardized quantities and symbols. *J Magn Reson Imaging* 10:223-232, 1999.
35. Larsson HB, Stubgaard M, Frederiksen JL, et al. Quantitation of blood-brain barrier defect by magnetic resonance imaging and gadolinium-DTPA in patients with multiple sclerosis and brain tumours. *Magn Reson Med* 16:117-131, 1990.
36. Robinson SP, Rodrigues LM, Howe FA, et al. Effects of different levels of hypercapnic hyperoxia on tumour  $R(2)^*$  and arterial blood gases. *Magn Reson Imaging* 19:161-166, 2001.
37. Hill SA, Collingridge DR, Vojnovic B, et al. Tumour radiosensitization by high-oxygen-content gases: influence of the carbon dioxide content of the inspired gas on  $pO_2$ , microcirculatory function and radiosensitivity. *Int J Radiat Oncol Biol Phys* 40:943-951, 1998.
38. Duyn JH, Moonen CT, van Yperen GH, et al. Inflow versus deoxyhemoglobin effects in BOLD functional MRI using gradient echoes at 1.5 T. *NMR Biomed* 7:83-88, 1994.
39. Robinson SP, Collingridge DR, Howe FA, et al. Tumour response to hypercapnia and hyperoxia monitored by FLOOD magnetic resonance imaging. *NMR Biomed* 12:98-106, 1999.
40. Howe FA, Robinson SP, Rodrigues LM, et al. Flow and oxygenation dependent (FLOOD) contrast MR imaging to monitor the response of rat tumours to carbogen breathing. *Magn Reson Imaging* 17:1307-1318, 1999.
41. Lebon V, Carlier PG, Brillault-Salvat C, et al. Simultaneous measurement of perfusion and oxygenation changes using a multiple gradient-echo sequence: application to human muscle study. *Magn Reson Imaging* 16:721-729, 1998.
42. Nordsmark M, Overgaard M, Overgaard J. Pretreatment oxygenation predicts radiation response in advanced squamous cell carcinoma of the head and neck. *Radiother Oncol* 41:31-39, 1996.
43. Hockel M, Schlenger K, Aral B, et al. Association between tumour hypoxia and malignant progression in advanced cancer of the uterine cervix. *Cancer Res* 56:4509-4515, 1996.
44. Tadamura E, Hatabu H, Li W, et al. Effect of oxygen inhalation on relaxation times in various tissues. *J Magn Reson Imaging* 7:220-225, 1997.
45. Kennan RP, Scanley BE, Gore JC. Physiologic basis for BOLD MR signal changes due to hypoxia/hyperoxia: separation of blood volume and magnetic susceptibility effects. *Magn Reson Med* 37:953-956, 1997.
46. Reeder SB, Faranesh AZ, Boxerman JL, et al. In vivo measurement of  $T^*2$  and field inhomogeneity maps in the human heart at 1.5 T. *Magn Reson Med* 39:988-998, 1998.

47. Mueller-Klieser W, Vaupel P, Manz R, et al. Intracapillary oxyhemoglobin saturation of malignant tumours in humans. *Int J Radiat Oncol Biol Phys* 7:1397-1404, 1981.
48. Hoskin PJ, Saunders MI, Goodchild K, et al. Dynamic contrast enhanced magnetic resonance scanning as a predictor of response to accelerated radiotherapy for advanced head and neck cancer. *Br J Radiol* 72:1093-1098, 1999.
49. Vaupel P, Kallinowski F, Okunieff P. Blood flow, oxygen and nutrient supply, and metabolic microenvironment of human tumors: a review. *Cancer Res* 49:6449-6465, 1989.
50. Brizel DM, Lin S, Johnson JL, et al. The mechanisms by which hyperbaric oxygen and carbogen improve tumour oxygenation. *Br J Cancer* 72:1120-1124, 1995.
51. Dunn TJ, Braun RD, Rhemus WE, et al. The effects of hyperoxic and hypercarbic gases on tumour blood flow. *Br J Cancer* 80:117-126, 1999.
52. Bernier J, Denekamp J, Rojas A, et al. ARCON: accelerated radiotherapy with carbogen and nicotinamide in head and neck squamous cell carcinomas. The experience of the Co-operative group of radiotherapy of the european organization for research and treatment of cancer (EORTC). *Radiother Oncol* 55:111-119, 2000.
53. Horsman MR, Chaplin DJ, Brown JM. Tumour radiosensitization by nicotinamide: a result of improved perfusion and oxygenation. *Radiat Res* 118:139-150, 1989.
54. Chaplin DJ, Horsman MR, Trotter MJ. Effect of nicotinamide on the microregional heterogeneity of oxygen delivery within a murine tumour. *J Natl Cancer Inst* 82:672-676, 1990.
55. Kelleher DK, Vaupel PW. Nicotinamide exerts different acute effects on microcirculatory function and tissue oxygenation in rat tumours. *Int J Radiat Oncol Biol Phys* 26:95-102, 1993.
56. Powell ME, Hill SA, Saunders MI, et al. Human tumour blood flow is enhanced by nicotinamide and carbogen breathing. *Cancer Res* 57:5261-5264, 1997.
57. Lartigau E, Lusinchi A, Weeger P, et al. Variations in tumour oxygen tension (pO<sub>2</sub>) during accelerated radiotherapy of head and neck carcinoma. *Eur J Cancer* 34:856-861, 1998.
58. Partridge SE, Aquino-Parsons C, Luo C, et al. A pilot study comparing intratumoural oxygenation using the comet assay following 2.5% and 5% carbogen and 100% oxygen. *Int J Radiat Oncol Biol Phys* 49:575-580, 2001.
59. Bussink J, Kaanders JH, van der Kogel AJ. Clinical outcome and tumour microenvironmental effects of accelerated radiotherapy with carbogen and nicotinamide. *Acta Oncol* 38:875-882, 1999.

# 6

## BOLD MRI RESPONSE TO HYPERCAPNIC HYPEROXIA IN PATIENTS WITH MENINGIOMAS: CORRELATION WITH GADOLINIUM-DTPA UPTAKE RATE

Mark Rijpkema

Janneke Schuurung

Pieter Bernsen

Hans Bernsen

Richard van der Maazen

Johannes Kaanders

Albert van der Kogel

Arend Heerschap

---

This chapter is based on:

Schuuring J, Rijpkema M, Bernsen H, Bernsen P, van der Maazen R, Kaanders J, van der Kogel A, Heerschap A. Effect of breathing a hyperoxic hypercapnic gas mixture on the oxygenation of meningiomas; preliminary results. *J NeuroOncol* 57(2):127-132, 2002.

and

Rijpkema M, Schuurung J, Bernsen PL, Bernsen HJ, Kaanders JHAM, van der Kogel AJ, Heerschap A. BOLD MRI response to hypercapnic hyperoxia in patients with meningiomas: correlation with Gadolinium-DTPA uptake rate. Submitted.

**ABSTRACT**

Because meningiomas tend to recur after (partial) surgical resection, radiotherapy is increasingly being applied for the treatment of these tumours. Radiation dose levels are limited however to avoid radiation damage to the surrounding normal tissue. The radiosensitivity of tumours can be improved by increasing tumour oxygen levels. The aim of this study was to investigate if breathing a hyperoxic hypercapnic gas mixture could improve the oxygenation of meningiomas, as monitored by BOLD MRI. In addition, dynamic Gd-DTPA contrast enhanced MRI was used to assess changes in tumour vascularity under hyperoxic hypercapnic conditions. Ten meningioma patients were each studied twice; without and with breathing a gas mixture consisting of 2% CO<sub>2</sub> and 98% O<sub>2</sub>. Values of T<sub>2</sub>\* and the Gd-DTPA uptake rate k<sub>ep</sub> were calculated under both conditions. In six tumours a significant increase in the value of T<sub>2</sub>\* in the tumour was found, suggesting an improved tumour blood oxygenation, which exceeded the effect in normal brain tissue. Contrarily, two tumours showed a significant T<sub>2</sub>\* decrease. The change in T<sub>2</sub>\* was found to correlate with both k<sub>ep</sub> and with the change in k<sub>ep</sub>. The overall effect of hypercapnic hyperoxia on meningiomas will be a balance between oxygenation and vascular effects. Improved oxygenation of blood entering the tumour may be counteracted by a reduction in tumour blood volume and flow. The current MRI protocol may assist in radiation treatment selection in patients with meningiomas.

## INTRODUCTION

Meningiomas account for 15-20% of all intracranial tumours (1,2). Most of these tumours are benign, but within this group great variations in cellular morphology, architectural pattern, vascularity, and metaplastic changes have been described (1,3). MRI has been frequently used to identify and characterise meningiomas. Hyperintensity, isointensity and hypointensity on T<sub>1</sub> and T<sub>2</sub> weighted images have all been reported and data on correlations between MR signal intensity and histological features is still controversial (3-5). Also the presence of oedema is highly variable from one meningioma to another (2). With Gadolinium-DTPA (Gd-DTPA) infusion, meningiomas usually show clear contrast enhancement, sharply demarcating the tumour from normal brain tissue (5).

The first choice of treatment for meningiomas is surgical resection, occasionally in combination with preoperative embolisation (5). However, meningiomas often recur, even after macroscopic total removal (6,7). Recently, there has been an increased interest in stereotactic radiosurgery and radiotherapy for the treatment of meningiomas in which complete resection is impossible (8,9). Although in general there is a good response to radiotherapy, sometimes higher doses of radiation are needed to improve control rates (6). Radiation dose levels are limited however to avoid radiation damage to the normal central nervous system (6,10). The radiosensitivity of tumours can be improved by increasing tumour oxygen levels (11). This may be achieved by breathing high oxygen content gases, which have been shown to improve oxygenation in several human tumours (12,13). For head and neck tumours, breathing a hyperoxic hypercapnic gas mixture like carbogen in combination with nicotinamide administration resulted in a significantly improved tumour response to accelerated radiotherapy (Accelerated Radiotherapy with Carbogen and Nicotinamide, ARCON, 14). Preliminary results of breathing a hyperoxic hypercapnic gas mixture to increase tumour blood oxygenation in meningiomas already seemed promising (15). Hyperoxic hypercapnic conditions during radiotherapy might allow optimisation of radiation schemes.

The effects of breathing hyperoxic hypercapnic gas mixtures on tumour oxygenation and blood flow can be studied noninvasively by MRI (16). Changes in oxygenation can be measured by blood oxygen level dependent (BOLD) MR imaging, using the paramagnetic deoxyhaemoglobin as an endogenous contrast agent (17). Deoxyhaemoglobin shortens the MR time constant for the transverse magnetisation decay (apparent spin-spin relaxation time, T<sub>2</sub><sup>\*</sup>), which can be assessed by gradient-echo MRI. BOLD T<sub>2</sub><sup>\*</sup> measurements have been shown to correlate with tumour pO<sub>2</sub> levels and deoxyhaemoglobin concentration in laboratory animal models (18,19). Tumour blood flow may respond heterogeneously when challenged with a hyperoxic hypercapnic gas mixture. The vasodilatory effect of CO<sub>2</sub> may be dependent on the association of blood vessels with smooth muscle cells (18,20). In this respect, also

the 'steal' effect is well-recognised: blood flow may be increased locally at the expense of an adjacent location, depending on the tumour vascular bed (20). Changes in blood flow, vascular volume, and permeability, can be studied by dynamic Gd-DTPA contrast enhanced MRI. This technique is widely used for the assessment of human tumours both in detection, identification, and staging.

The aim of this study was to investigate the effects of breathing a hyperoxic hypercapnic gas mixture on the oxygenation of meningiomas using BOLD MRI. In addition, dynamic Gd-DTPA contrast enhanced MRI was used to assess changes in tumour vascular function under hyperoxic hypercapnic conditions. This MRI protocol may assist in the selection of appropriate meningioma patients for radiation treatment using hyperoxygenation.

## METHODS

Ten meningioma patients (3 males, 7 females) were included in the study. The mean age was 54 years (table 6.1). Approval for the study was obtained from the local ethics committee and informed consent was obtained from all patients. MR imaging was performed on a 1.5 T Siemens Vision whole body system using a CP-head coil. All patients were studied twice; without and with breathing a gas mixture consisting of 2% CO<sub>2</sub> and 98% O<sub>2</sub>. Gadolinium-DTPA was administered by intravenous bolus injection (6 ml, 0.5 M, 1 ml/s).

	sex	age	tumour location	histological subtype*	tumour volume (ml)	oedema volume (ml)
1	f	48	convexity cerebellar	n.a.	10.5	0.0
2	m	63	convexity parietal	n.a.	9.3	0.0
3	f	70	convexity parieto-occipital	microcystic	29.9	37.5
4	f	45	convexity frontal	meningothelial	22.4	19.1
5	f	43	posterior fossa	meningothelial	20.1	0.0
6	f	49	sphenoid wing	meningothelial	16.2	102.6
7	f	55	convexity parietal	transitional	58.3	0.0
8	m	68	olfactory groove	transitional	64.8	66.4
9	f	50	parasagittal	hemangioblastic	30.9	109.1
10	m	51	lateral ventricle	atypical	7.9	50.7

Table 6.1. Clinical and tumour related data of the meningioma patients. \*n.a.: data not available.

In the first session Gd-DTPA tissue uptake was monitored (FLASH, TR=50 ms, TE=4.4 ms, 7 mm slice) while the patient was breathing air. In the second session gradient-echo images (2D FLASH, TR=65 ms, 16 echoes, TE=6-51 ms, 5 mm slice) were recorded continuously for 8-10 minutes whilst breathing air, then breathing of the hyperoxic hypercapnic gas mixture was started and images were recorded for

another 5-8 minutes, followed by Gd-DTPA contrast enhanced imaging as in the first session. Altogether, patients had to breathe the hyperoxic hypercapnic gas mixture for 12 minutes. The time between the two sessions was one week.

$T_2^*$  values (ms) were calculated pixelwise from the gradient-echo imaging data and displayed as a map. The value of  $T_2^*$  of the tumour under normal and hyperoxic hypercapnic conditions was obtained by averaging all pixels within the selected tumour region. Also, the change in  $T_2^*$  during hypercapnic hyperoxia was calculated for normal brain tissue on the contralateral side of the brain. As air leaks might occur in the experimental setup while supplying the hyperoxic hypercapnic gas mixture, patients were checked for inhaling the gas mixture properly. For this purpose the  $T_2^*$  of venous blood was measured in the transverse sinus or the sagittal sinus. If no statistically significant (Student's t-test,  $p < 0.05$ ) increase in the  $T_2^*$  of venous blood was observed during breathing of the hyperoxic hypercapnic gas mixture the measurement was considered a technical failure. Changes in  $T_2^*$  were expressed as  $\Delta T_2^*$  (ms) =  $T_2^*$ (hyperoxic hypercapnic gas mixture) -  $T_2^*$ (air).

The dynamic Gd-DTPA contrast image data was analysed as described by Rijpkema et al (21). Using a physiological pharmacokinetic model the rate of contrast medium uptake ( $k_{ep}$  ( $\text{min}^{-1}$ )) was determined. In perfused tumour tissue this Gd-DTPA uptake rate reflects physiological parameters such as vascular permeability, vascular surface area and tumour blood flow (22). Maps of  $k_{ep}$  were reconstructed from the value of  $k_{ep}$  for each pixel. The geometric mean of the Gd-DTPA uptake rates under normal and hyperoxic hypercapnic conditions was calculated after log transformation of all pixel values in Gd-DTPA enhancing regions of the tumour. Changes in  $k_{ep}$  were represented as  $\Delta k_{ep} = k_{ep}$ (hyperoxic hypercapnic gas mixture) -  $k_{ep}$ (air), expressed as % with respect to  $k_{ep}$ (air). Statistically significant differences were shown using Student's t-test. Pearson's correlation coefficient was used to assess significant correlations.

## RESULTS

Ten patients successfully completed the entire MRI protocol. From the twelve initially selected patients, two dropped out of the study because no significant increase in the value of  $T_2^*$  in the transverse sinus was observed during breathing of the hyperoxic hypercapnic gas mixture and the measurement was considered a technical failure. A transversal turbo inversion recovery (with magnitude reconstruction) image of a patient with a meningioma located in the right hemisphere is shown in figure 6.1a. Dynamic Gd-DTPA uptake was monitored in a series of images at 2 second intervals for 90 seconds. The last image of this series is displayed in figure 6.1b, showing signal enhancement in the tumour region. This contrast enhanced MRI data was used to reconstruct maps of the rate of contrast



agent uptake,  $k_{ep}$ , as shown in figure 6.1c for the same patient. The average values of the Gd-DTPA uptake rate of the tumour during air breathing and breathing the hyperoxic hypercapnic gas mixture were calculated from the corresponding  $k_{ep}$  maps. Large variations were found in the values of  $k_{ep}$  between meningiomas, ranging from 0.24 to 3.11  $\text{min}^{-1}$  (mean 1.21  $\text{min}^{-1}$ ). Changes in the Gd-DTPA uptake rate as a result of breathing the hyperoxic hypercapnic gas mixture were diverse. In three tumours an increase in  $k_{ep}$  was found, while in seven tumours  $k_{ep}$  decreased. The average  $\Delta k_{ep}$  was 1% (range -57 to +89%).

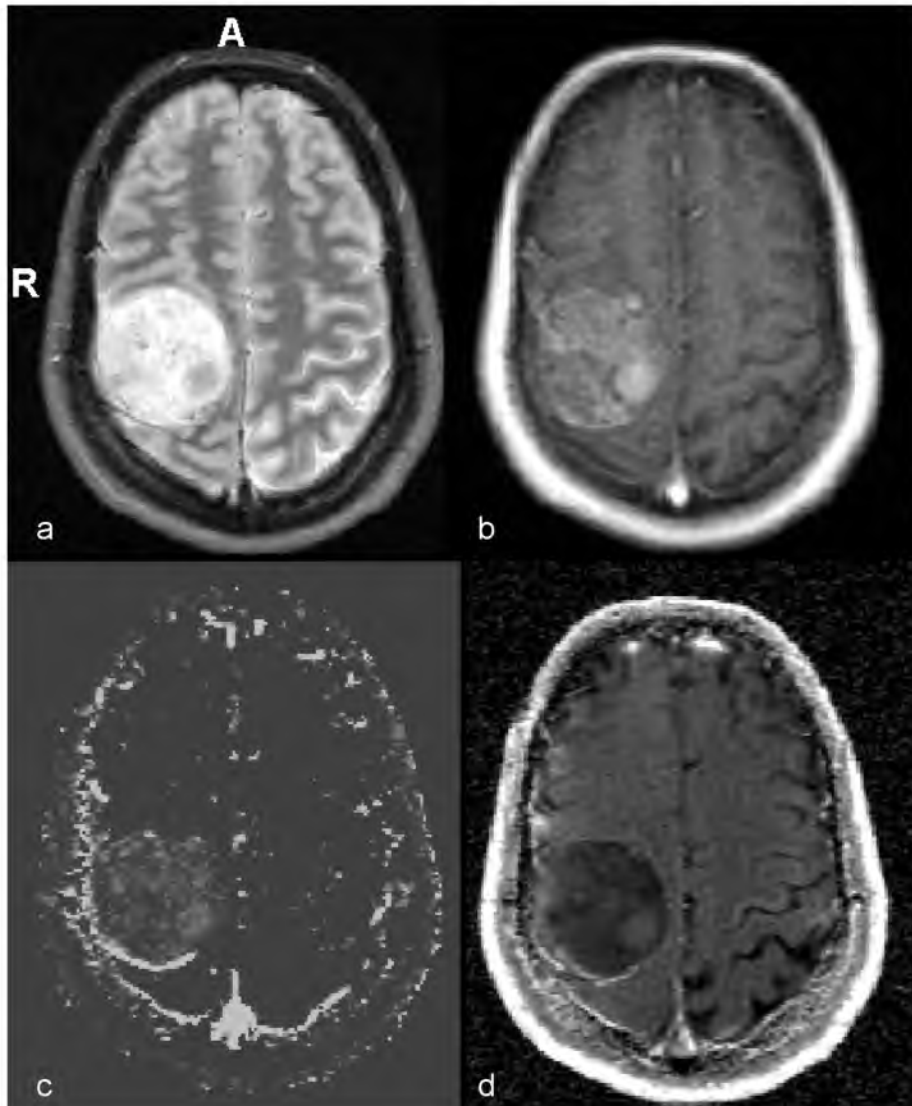


Figure 6.1. Transversal MR images of a patient with a meningioma in the right hemisphere. R: right, A: anterior. (a) Turbo inversion recovery (with magnitude reconstruction) image clearly showing the tumour. (b) T<sub>1</sub> weighted image recorded 90 seconds after Gd-DTPA contrast administration during breathing a hyperoxic hypercapnic gas mixture consisting of 2% CO<sub>2</sub> and 98% O<sub>2</sub>. (c) Map showing the Gd-DTPA uptake rate, as calculated from the dynamic Gd-DTPA enhanced data. (d) The R<sub>2</sub><sup>\*</sup> map (R<sub>2</sub><sup>\*</sup>=1/T<sub>2</sub><sup>\*</sup>) calculated from the BOLD MRI data recorded during breathing of the hyperoxic hypercapnic gas mixture.

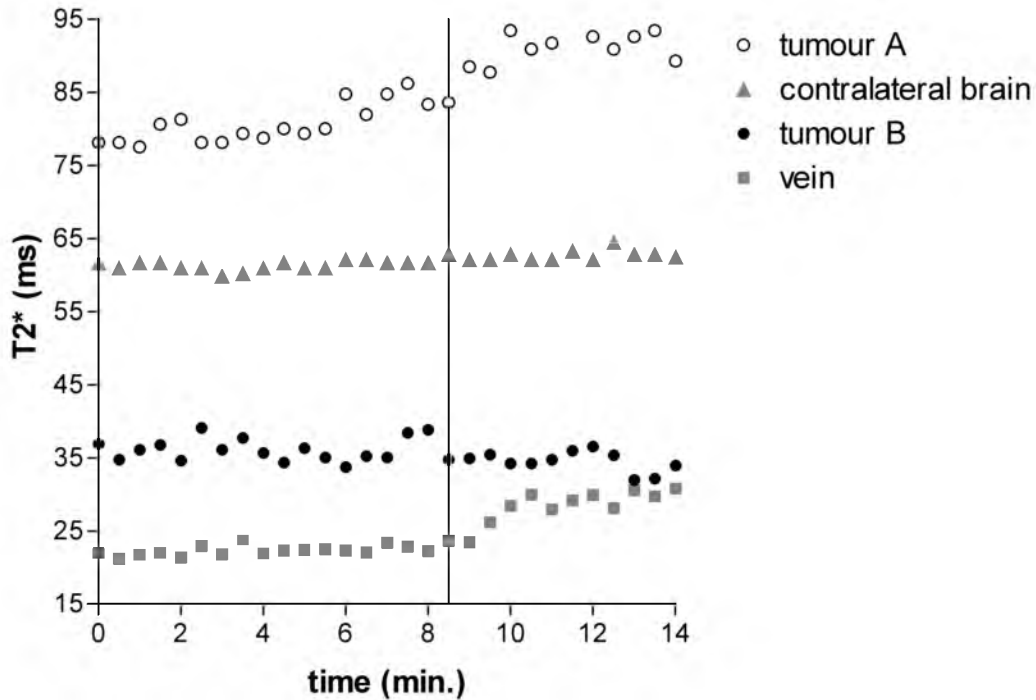


Figure 6.2. Graph showing the  $T_2^*$  changes in blood, tumour tissue, and contralateral brain tissue during hypercapnic hyperoxia. Breathing of the hyperoxic hypercapnic gas mixture was started after 8.5 minutes of air breathing. In the sagittal sinus the value of  $T_2^*$  increased significantly in all patients during breathing of the hyperoxic hypercapnic gas mixture, indicating an improved blood oxygenation. This is shown here in grey squares for patient A. Contralateral brain tissue (triangles) showed a slight  $T_2^*$  increase of 2 ms in this patient. In the tumour (tumour A, open circles) an increase was observed in  $T_2^*$ . Contrarily, the tumour of another patient (tumour B, black circles) showed a decrease in  $T_2^*$  under hyperoxic hypercapnic conditions.

The  $T_2^*$  weighted MR images were used to reconstruct maps of  $R_2^*$  ( $R_2^* = 1/T_2^*$ ), as is shown in figure 6.1d. The basal values of  $T_2^*$  however reflect not only tumour characteristics such as oxygenation and vascular and tissue architecture, but also local homogeneity of the magnetic field, especially when proximal to sinuses in the head. Therefore, only the change in  $T_2^*$  was evaluated.  $T_2^*$  maps obtained in the first minute after switching to breathing the hyperoxic hypercapnic gas mixture were discarded to allow oxygen levels in blood to reach a new equilibrium. Under hyperoxic hypercapnic conditions all patients showed a statistically significant increase of the value of  $T_2^*$  in either the sagittal or the transverse sinus relative to air breathing. In six tumours also a significant increase in the average value of  $T_2^*$  in the tumour was observed, suggesting an improved tumour blood oxygenation. Contrarily, two tumours showed a significant  $T_2^*$  decrease and in two tumours no statistically significant change in  $T_2^*$  was observed. The average  $\Delta T_2^*$  over all tumours was 3.7 ms (range -1.9 to +11.3 ms). Normal brain tissue measured on the contralateral side of the brain showed a small but significant  $T_2^*$  increase in all patients due to breathing the hyperoxic hypercapnic gas mixture, with a mean increase of 2.3 ms (standard deviation 0.6 ms). In figure 6.2 the  $T_2^*$  changes in venous blood and contralateral brain tissue during hypercapnic hyperoxia are shown

for one patient. The  $T_2^*$  versus time plots of a tumour region that showed a  $T_2^*$  increase and a tumour region that showed a  $T_2^*$  decrease under hyperoxic hypercapnic conditions are also shown.

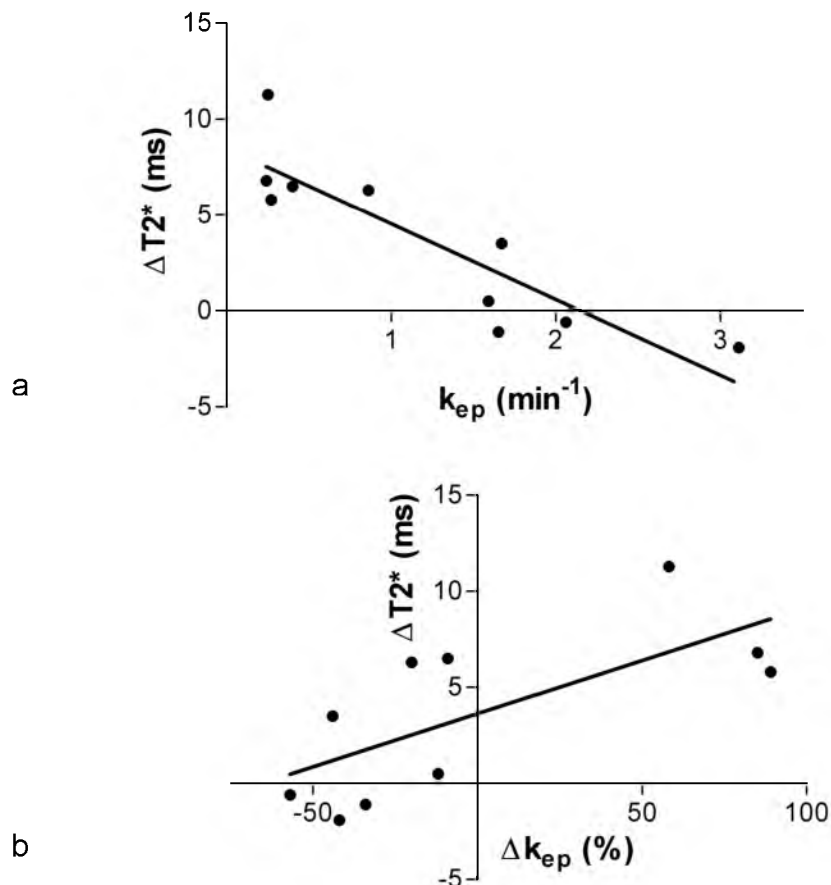


Figure 6.3. (a) Graph showing the correlation of the Gd-DTPA uptake rate  $k_{ep}$  during air breathing with the hypercapnic hyperoxia induced change in  $T_2^*$  in meningiomas. The correlation was highly significant (Pearson's  $r=-0.88$ ,  $p=0.001$ ). (b) The change in  $k_{ep}$  due to breathing the hyperoxic hypercapnic gas mixture showed a moderate correlation with the change in  $T_2^*$  in tumour tissue (Pearson's  $r=0.69$ ,  $p=0.024$ ).

Interestingly, correlations were found between the change in  $T_2^*$  and the (change in) Gd-DTPA uptake rate. The change in  $T_2^*$  was found to correlate negatively with  $k_{ep}$ , with a Pearson's correlation coefficient of  $-0.88$  ( $p=0.001$ , figure 6.3a). Thus, tumours with a high Gd-DTPA uptake rate tend to show a negative  $T_2^*$  response to hypercapnic hyperoxia. The change in  $k_{ep}$  correlated positively with the change  $T_2^*$  (Pearson's  $r=0.69$ ,  $p=0.024$ , figure 6.3b). Consequently, a negative correlation was found between  $k_{ep}$  and  $\Delta k_{ep}$  (Pearson's  $r=-0.79$ ,  $p=0.007$ , data not shown), indicating that in tumours with a high Gd-DTPA uptake rate the uptake is decreased during hypercapnic hyperoxia compared to normal conditions. No statistically significant correlations were found with patient's age, histological subtype of the tumour,

volume of the tumour, volume of oedema, the basal value of  $T_2^*$ , or the  $T_2^*$  increase in contralateral normal brain tissue.

## DISCUSSION

Tumour oxygenation is mainly influenced by the arterial oxygen supply to the tissue, which depends on arterial oxygen content and tissue perfusion (23). Increasing the arterial  $pO_2$  by breathing a hyperoxic hypercapnic gas mixture should therefore improve the  $O_2$  diffusion from microvessels to the cells (24). However, tumour vasculature may exhibit structural and functional abnormalities and blood flow through tumours is anything but uniform (20). Most tumours show an increased tumour oxygenation in response to breathing hyperoxic hypercapnic gas mixtures (1-5%  $CO_2$ , 99-95%  $O_2$ ), but also decreased tumour oxygenation has been reported in various human tumours (13,25). The impact of hypercapnic hyperoxia on blood flow may also be heterogeneous. In laboratory animal models vascular effects including vasodilation, vasoconstriction, steal phenomena, and blood pressure changes have been observed (18,20,26-28). The effects of breathing a hyperoxic hypercapnic gas mixture on tumour blood oxygenation and blood flow have been assessed by MRI in both laboratory animal models and humans. Although most studies show a clear increase in  $T_2^*$  under hyperoxic hypercapnic conditions, also non-significant changes have been reported (16,18,28-30).

In meningiomas, blood flow and oxygenation may show large variations. Using orthogonal polarisation spectral imaging, meningiomas were characterised by chaotic and dilated vessels with almost no erythrocyte movement (31). A striking architectural feature of meningiomas was that sections in which vessels were tortuous and close together were adjacent to sections in which no vessels were present (31). Using contrast enhanced MRI and CT, blood flow and blood volume were found to be highly variable (32,33). The same was found for the arterial blood supply and degree of vasodilation, as assessed by angiographic techniques (5,34). Although meningiomas are in general well vascularised, dynamic contrast enhanced MRI showed variations in Gd-DTPA uptake rates similar to the results of the present study (35,36). No correlation was found between the degree of contrast enhancement and histopathological features, vascularity, or consistency of meningiomas (3,4). Haemoglobin concentration showed high interindividual variability in meningiomas and saturation ranged from 10-40%, as measured by NIR reflection measurements (37).

One could expect that breathing a hyperoxic hypercapnic gas mixture results in an increase in  $T_2^*$ , as observed in e.g. head and neck tumours (16). Blood entering the tumour will be better oxygenated, resulting in a decrease of the deoxyhaemoglobin concentration under hyperoxic hypercapnic conditions. The Gd-DTPA uptake rate

may either remain constant or increase under these conditions, because of a potential CO<sub>2</sub> induced increase in blood volume and flow (23,38). These effects on T<sub>2</sub>\* and k<sub>ep</sub> were observed in most of the meningiomas in this study (see figure 6.3b). All of these tumours however had a relatively low Gd-DTPA uptake rate (figure 6.3a), suggesting no extremely high vascular permeability, blood volume, or flow. As these meningiomas showed a larger increase in T<sub>2</sub>\* than normal brain tissue, the combination of radiotherapy with hyperoxygenation may be a treatment option for these patients to improve radiation response (15). However, in some patients also an opposite effect was observed. Meningiomas with a relatively high Gd-DTPA uptake rate showed a decrease in T<sub>2</sub>\* (figure 6.3a), suggesting a worsened tumour blood oxygenation. In these tumours also a decrease in the Gd-DTPA uptake rate was found under hyperoxic hypercapnic conditions. This may be explained by a steal effect as a result of the CO<sub>2</sub> induced vasodilation in the surrounding normal tissue (20,23), which may cause reduction of tumour blood flow and a further desaturation of the blood (28,39). Also, tumour blood volume may decrease as a result of vascular collapse (28). Because many tumour blood vessels have weak walls (20,40), they may collapse if blood pressure is reduced. Especially those meningiomas with a high interstitial pressure due to highly permeable vessels (resulting in a high Gd-DTPA uptake rate) may show this phenomenon. Assuming that no substantial changes in oxygen consumption occur under hyperoxic hypercapnic conditions, a decrease in both blood flow and blood volume may result in a decrease of tumour blood oxygenation (23,28).

The overall effect of breathing a hyperoxic hypercapnic gas mixture on meningiomas will be a balance between oxygenation and vascular effects. In some tumours the improved oxygenation of blood entering the tumour may be the dominant effect, while in others reduced tumour blood volume and flow may counteract this result. All these effects may contribute to the response of tumours to hypercapnic hyperoxia. In 6 out of 10 meningioma patients, hypercapnic hyperoxia was shown to induce an improved tumour blood oxygenation exceeding the effect on normal brain tissue, a prerequisite to consider radiotherapy combined with hyperoxygenation. The presence of both vascular effects and oxygenation effects and the heterogeneous response to hypercapnic hyperoxia necessitates individual assessment of the effects of breathing a hyperoxic hypercapnic gas mixture on meningiomas. Thus, BOLD MRI and dynamic contrast enhanced MRI may guide treatment selection for patients with meningiomas.

#### ACKNOWLEDGEMENTS

The authors would like to thank the MRI and ARCON technicians of the departments of radiology and radiotherapy for their assistance. The neurosurgeons

from the Nijmegen Neurosurgical Centre are gratefully acknowledged for their assistance in patient recruitment.

## REFERENCES

1. Manivel JC, Sung JH. Pathology of meningiomas. *Pathol Annu* 1990;25 Pt 2:159-192.
2. Sanson M, Cornu P. Biology of meningiomas. *Acta Neurochir (Wien)* 2000;142:493-505.
3. Maiuri F, Iaconetta G, de Divitiis O, Cirillo S, Di Salle F, De Caro ML. Intracranial meningiomas: correlations between MR imaging and histology. *Eur J Radiol* 1997;31:69-75.
4. Chen TC, Zee CS, Miller CA, Weiss MH, Tang G, Chin L, Levy ML, Apuzzo MLJ. Magnetic resonance imaging and pathological correlates of meningiomas. *Neurosurgery* 1992;31:1015-1021.
5. Engelhard HH. Progress in the diagnosis and treatment of patients with meningiomas. Part I: diagnostic imaging, preoperative embolization. *Surg Neurol* 2001;55:89-101.
6. Kokubo M, Shibamoto Y, Takahashi JA, Sasai K, Oya N, Hashimoto N, Hiraoka M. Efficacy of conventional radiotherapy for recurrent meningioma. *J Neurooncol* 2000;48:51-55.
7. Yamasaki F, Yoshioka H, Hama S, Sugiyama K, Arita K, Kurisu K. Recurrence of meningiomas. *Cancer* 2000;89:1102-1110.
8. Ojemann SG, Sneed PK, Larson DA, Gutin PH, Berger MS, Verhey L, Smith V, Petti P, Wara W, Park E, McDermott MW. Radiosurgery for malignant meningioma: results in 22 patients. *J Neurosurg* 2000;93Suppl3:62-67.
9. Roche PH, Regis J, Dufour H, Fournier HD, Delsanti C, Pellet W, Grisoli F, Peragut JC. Gamma knife radiosurgery in the management of cavernous sinus meningiomas. *J Neurosurg* 2000;93Suppl3:68-73
10. Hug EB, DeVries A, Thornton AF, Munzenride JE, Pardo FS, Hedley-Whyte ET, Bussiere MR, Ojemann R. Management of atypical and malignant meningiomas: role of high-dose, 3D-conformal radiation therapy. *J Neurooncol* 2000;48:151-160.
11. Gray, LH, Conger, AD, Ebert, Hornsey MS, Scott OCA. The concentration of oxygen dissolved in tissues at the time of irradiation as a factor in radiotherapy. *Br J Radiol* 1953;26:638-648.
12. Lartigau E, Lusinchi A, Weeger P, Wibault P, Luboinski B, Eschwege F, Guichard M. Variations in tumour oxygen tension (pO<sub>2</sub>) during accelerated radiotherapy of head and neck carcinoma. *Eur J Cancer* 1998;34:856-861.
13. Partridge SE, Aquino-Parsons C, Luo C, Green A, Olive PL. A pilot study comparing intratumoural oxygenation using the comet assay following 2.5% and 5% carbogen and 100% oxygen. *Int J Radiat Oncol Biol Phys* 2001;49:575-580.
14. Kaanders JHAM, Pop, LA, Marres HAM, Bruaset I, van den Hoogen FJA, Merckx MAW, van der Kogel AJ. ARCON: experience in 215 patients with advanced head-and-neck cancer. *Int J Radiat Oncol Biol Phys* 2002;52:769-778.
15. Schuurin J, Rijpkema M, Bernsen H, Bernsen P, van der Maazen R, Kaanders J, van der Kogel AJ, Heerschap A. Effect of breathing a hyperoxic hypercapnic gas mixture on the oxygenation of meningiomas; preliminary results. *J NeuroOncol* 2002;57:127-132.

16. Rijpkema M, Kaanders J, Joosten F, van der Kogel A, Heerschap A. Effects of breathing a hyperoxic hypercapnic gas mixture on blood oxygenation and vascularity of head and neck tumours as measured by MRI. *Int J Radiat Biol Phys* 2002;53:1185-1191.
17. Ogawa S, Lee TM, Nayak AS, Glynn P. Oxygenation-sensitive contrast in magnetic resonance image of rodent brain at high magnetic fields. *Magn Reson Med* 1990;14:68-78.
18. Neeman M, Dafni H, Bukhari O, Braun RD, Dewhirst MW. In vivo BOLD contrast MRI mapping of subcutaneous vascular function and maturation: validation by intravital microscopy. *Magn Reson Med* 2001;45:887-898.
19. Punwani S, Ordidge RJ, Cooper CE, Amess P, Clemence M. MRI measurements of cerebral deoxyhaemoglobin concentration [dHb]-- correlation with near infrared spectroscopy (NIRS). *NMR Biomed* 1998;11:281-289.
20. Vaupel P, Kallinowski F, Okunieff P. Blood flow, oxygen and nutrient supply, and metabolic microenvironment of human tumours: a review. *Cancer Res* 1989;49:6449-6465.
21. Rijpkema M, Kaanders JHAM, Joosten FBM, van der Kogel AJ, Heerschap A. Method for quantitative mapping of dynamic MRI contrast agent uptake in human tumours. *J Magn Res Imaging* 2001;14:457-463.
22. Tofts PS, Brix G, Buckley DL, Evelhoch JL, Henderson E, Knopp MV, Larsson HB, Lee TY, Mayr NA, Parker GJ, Port RE, Taylor J, Weisskoff RM. Estimating kinetic parameters from dynamic contrast-enhanced T(1)-weighted MRI of a diffusible tracer: standardized quantities and symbols. *J Magn Reson Imaging* 1999;10:223-232.
23. Thews O, Kelleher DK, Vaupel P. Dynamics of tumour oxygenation and red blood cell flux in response to inspiratory hyperoxia combined with different levels of inspiratory hypercapnia. *Radiother Oncol* 2002;62:77-85.
24. Dewhirst MW, Ong ET, Rosner GL, Rehmus SW, Shan S, Braun RD, Brizel DM, Secomb TW. Arteriolar oxygenation in tumour and subcutaneous arterioles: effects of inspired air oxygen content. *Br J Cancer Suppl* 1996;27:S241-S246.
25. Falk SJ, Ward R, Bleehen NM. The influence of carbogen breathing on tumour tissue oxygenation in man evaluated by computerised pO<sub>2</sub> histography. *Br J Cancer* 1992;66:919-924.
26. van der Sanden BP, Heerschap A, Hoofd L, Simonetti AW, Nicolay K, van der TA, Colier WN, van der Kogel AJ. Effect of carbogen breathing on the physiological profile of human glioma xenografts. *Magn Reson Med* 1999;42:490-499.
27. Al Hallaq HA, River JN, Zamora M, Oikawa H, Karczmar GS. Correlation of magnetic resonance and oxygen microelectrode measurements of carbogen-induced changes in tumour oxygenation. *Int J Radiat Oncol Biol Phys* 41: 151-159, 1998.
28. Howe FA, Robinson SP, McIntyre DJ, Stubbs M, Griffiths JR. Issues in flow and oxygenation dependent contrast (FLOOD) imaging of tumours. *NMR Biomed* 2001;14:497-506.
29. Griffiths JR, Taylor NJ, Howe FA, Saunders MI, Robinson SP, Hoskin PJ, Powell MEB, Thoumine M, Caine LA, Baddeley H. The response of human tumours to carbogen breathing, monitored by Gradient-Recalled Echo Magnetic Resonance Imaging. *Int J Radiat Oncol Biol Phys* 1997;39:697-701.



30. Robinson SP, Rodrigues LM, Howe FA, Stubbs M, Griffiths JR. Effects of different levels of hypercapnic hyperoxia on tumour  $R(2)^*$  and arterial blood gases. *Magn Reson Imaging* 2001;19:161-166
31. Mathura KR, Bouma GJ, Ince C. Abnormal microcirculation in brain tumours during surgery. *Lancet* 2001;358:1698-1699.
32. Nakatsuka M, Mizuno S. Investigation of blood flow in meningothelial and fibrous meningiomas by xenon-enhanced CT scanning. *Neurol Res* 2000;22:615-619.
33. Bruening R, Wu RH, Yousry TA, Berchtenbreiter C, Weber J, Peller M, Steiger HJ, Reiser M. Regional relative blood volume MR maps of meningiomas before and after partial embolization. *J Comput Assist Tomogr* 1998;22:104-110.
34. Kadota T, Kuriyama K, Inoue E, Fujita M, Nakagawa H, Kuroda C. MR angiography of meningioma. *Magn Reson Imaging* 1993;11:473-483.
35. Hawighorst H, Engenhardt R, Knopp MV, Brix G, Grandy M, Essig M, Miltner P, Zuna I, Fuss M, van Kaick G. Intracranial meningiomas: time- and dose-dependent effects of irradiation on tumour microcirculation monitored by dynamic MR imaging. *Magn Reson Imaging* 1997;15:423-432.
36. Fujii K, Fujita N, Hirabuki N, Hashimoto T, Miura T, Kozuka T. Neuromas and meningiomas: evaluation of early enhancement with dynamic MR imaging. *AJNR Am J Neuroradiol* 1992;13:1215-1220.
37. Steinberg F, Rohrborn HJ, Otto T, Scheufler KM, Streffer C. NIR reflection measurements of hemoglobin and cytochrome aa3 in healthy tissue and tumours. Correlations to oxygen consumption: preclinical and clinical data. *Adv Exp Med Biol* 1997;428:69-77.
38. Rostrup E, Larsson HB, Toft PB, Garde K, Ring PB, Henriksen O. Susceptibility contrast imaging of CO<sub>2</sub>-induced changes in the blood volume of the human brain. *Acta Radiol* 1996;37:813-822
39. Dunn TJ, Braun RD, Rhemus WE, Rosner GL, Secomb TW, Tozer GM, Chaplin DJ, Dewhirst MW. The effects of hyperoxic and hypercarbic gases on tumour blood flow. *Br J Cancer* 1999;80:117-126.
40. Jain RK. Determinants of tumour blood flow. *Cancer Res* 1988;48:2641-2658.

# 7

## CHARACTERISATION OF OLIGODENDROGLIOMAS USING SHORT ECHO TIME $^1\text{H}$ MR SPECTROSCOPIC IMAGING

Mark Rijpkema

Janneke Schuurin

Yvonne van der Meulen

Marinette van der Graaf

Hans Bernsen

Rudolf Boerman

Albert van der Kogel

Arend Heerschap

---

This chapter is based on:

Rijpkema M, Schuurin J, van der Meulen Y, van der Graaf M, Bernsen H, Boerman R, van der Kogel A, Heerschap A. Characterization of oligodendrogliomas using short echo time  $^1\text{H}$  MR Spectroscopic Imaging. NMR Biomed, in press.

**ABSTRACT**

Oligodendroglial tumours may not be distinguished easily from other brain tumours based on clinical presentation and MRI alone. Identification of these tumours however may have therapeutical consequences. The purpose of this study was to characterise and identify oligodendrogliomas by their metabolic profile as measured by  $^1\text{H}$  MR Spectroscopic Imaging (MRSI). Fifteen patients with oligodendroglial tumours (8 high grade oligodendrogliomas, 7 low grade oligodendrogliomas) underwent MRI and short echo time  $^1\text{H}$  MRSI examinations. Five main metabolites found in brain MR spectra were quantified and expressed as ratios of tumour to contralateral white matter tissue. The level of lipids plus lactate was also assessed in the tumour. For comparison also six patients with a low grade astrocytoma were included in the study. The metabolic profile of oligodendrogliomas showed a decreased level of N-acetylaspartate and increased levels of choline containing compounds and glutamine plus glutamate compared to white matter. The level of glutamine plus glutamate was significantly higher in low grade oligodendrogliomas than in low grade astrocytomas and may serve as a metabolic marker in diagnosis and treatment planning. In high grade oligodendrogliomas large resonances of lipids plus lactate were observed in contrast to low grade tumours.

## INTRODUCTION

Oligodendrogliomas represent 5-18% of all intracranial gliomas and arise preferentially in the cortex and white matter of the cerebral hemispheres (1). The majority of oligodendrogliomas are low grade tumours (1,2). Based on clinical presentation, oligodendroglial tumours may not be distinguished easily from other brain tumours, especially from astrocytomas. Until recently, the identification of oligodendrogliomas among brain tumours did not have therapeutical consequences. However, with the recognition that oligodendrogliomas are uniquely sensitive to chemotherapy, differential diagnosis of these tumours has become increasingly important. Since Cairncross and McDonald observed that recurrent anaplastic oligodendrogliomas respond to chemotherapy (3), several groups have reported on the chemosensitivity of both high and low grade oligodendrogliomas and mixed oligoastrocytomas (4-7). As a result oligodendrogliomas are increasingly being treated with chemotherapy, in contrast to e.g. astrocytomas, which are substantially more resistant to chemotherapeutic agents (4-7).

In general brain tumours are pathologically diagnosed by analysis of tumour tissue obtained (invasively) by biopsy. Both Magnetic Resonance Imaging (MRI) and <sup>1</sup>H Magnetic Resonance Spectroscopy (MRS) have proven to be powerful noninvasive tools for the characterisation of brain tumours (8). MRI is well-established in obtaining the anatomical localisation and extent of tumours. However, conventional MRI techniques are limited in the diagnosis of brain tumour type (9). Furthermore, MRI investigation of blood brain barrier damage using an extragenous contrast agent (e.g. Gadolinium-DTPA) cannot reliably differentiate oligodendroglial tumour grades. Low grade oligodendrogliomas may show contrast enhancement, while lack of contrast enhancement does not equate with low grade malignancy (10).

MR spectroscopy may provide additional information in cases in which the differential diagnosis of tumours by MRI is difficult (11). Metabolic information obtained by MRS has proven to be promising in the accurate diagnosis of human brain tumours (8,9,12) and the evaluation and monitoring of therapy (13,14). Most of these studies so far covered astrocytomas, the most common form of glial tumours. The aim of this study was to characterise oligodendrogliomas by their metabolic profile to enable specific identification of these tumours. For this purpose patients with high and low grade oligodendrogliomas were examined by short echo time <sup>1</sup>H MRSI.

## PATIENTS AND METHODS

Fifteen patients with histologically proven oligodendroglial tumours were included in this study. Four patients had mixed tumours (two low grade and two high grade

oligoastrocytomas) with a predominant component of oligodendroglioma, which were categorised as oligodendrogliomas in this study. Seven tumours were pathologically characterised as low grade (WHO grade II) and eight as high grade oligodendroglial tumours (WHO grade III). For comparison also six patients with a low grade astrocytoma (WHO grade II) were included in the study. The age and sex distribution was comparable in all groups: male/female 5/2, age  $39 \pm 9$ ; male/female 5/3, age  $45 \pm 12$ ; and male/female 5/1, age  $41 \pm 14$ , respectively. All patients were previously untreated and gave informed consent to participate in this study. Approval for the study was obtained from the local ethics committee.

MRI and MRS were carried out on a 1.5 T Siemens Vision system. After conventional T1 weighted, T2 weighted and PD weighted imaging, MR Spectroscopic Imaging (MRSI) was performed. MR spectra were recorded both with and without water suppression using a 16x16 2D STEAM MRSI sequence. Sequence parameters were TR 2500 ms, TE 20 ms, TM 30 ms, slice thickness 15 mm, FoV 200 mm. The measurement time to obtain all MRSI data was ~30 minutes. After MR spectroscopy a bolus injection of Gadolinium-DTPA (Gd-DTPA) was applied and conventional T1 weighted images were recorded. In five patients this Gd-DTPA contrast enhancement was measured before the MR spectroscopy.

Processing of the MRSI data consisted of the following. A Hamming filter of 50% was applied in k-space before spatial Fourier transform using the LUISE software package (Siemens, Erlangen, Germany). Tumour MRSI voxels were selected from areas that showed Gd-DTPA contrast enhancement. If no contrast enhancement was seen MRSI voxels were selected from the T1 weighted and T2 weighted MR images. To obtain an internal standard, spectra of up to three voxels located in contralateral white matter were used for each patient. All spectra were analysed by LCModel (15). The main metabolites NAA (N-acetylaspartate plus N-acetylaspartylglutamate), Cr (creatine plus phosphocreatine), Cho (choline containing compounds), Ino (myo-inositol), and Glx (glutamine plus glutamate) were quantified and expressed as ratio of tumour to contralateral white matter. In the spectral region around 1.3 ppm both lactate and lipids were assessed by LCModel. The lipid signal was quantitated as a single peak at 1.3 ppm. Since the use of a short echo time (20 ms) generally does not allow accurate differentiation between signal contributions from lipids and lactate in this spectral region, the metabolite levels of both compounds were summed. All statistical analyses were performed using Student's t-test (two-sided).

## RESULTS

All twenty-one patients included in this study successfully completed the MRI and MRSI protocol. In 8 patients (2 low grade oligodendrogliomas, 2 high grade

oligodendrogliomas, 4 astrocytomas) no Gd-DTPA contrast enhancement was observed in the tumour and the conventional T1 weighted and T2 weighted images were used to delineate the tumour. Sagittal and transversal MR images of a patient with a low grade oligodendroglioma are shown in figure 7.1. The grid indicating the position of the MRSI voxels is plotted on these images. To characterise the tumour by its metabolic profile a voxel in the tumour was selected on the Gd-DTPA enhanced image (figure 7.1c, marked square). The corresponding spectrum is shown in figure 7.2b. Contralaterally located white matter voxels were carefully selected to avoid contribution from white matter abnormalities that were observed on the MR images of some patients. In figure 7.2a the spectrum from white matter (figure 7.1b, marked square) is displayed. A spectrum from a high grade oligodendroglioma is shown in figure 7.2c.



Figure 7.1. MR images of a patient with a low grade oligodendroglioma in the right hemisphere. The grid indicates the position of the MRSI voxels. (a) Sagittal localiser image. (b) Transversal PD weighted image. (c) Transversal T1 weighted image after Gd-DTPA administration, displaying the tumour as a hypointense region with slight Gd-DTPA contrast enhancement (hyperintense). The marked square on the PD weighted image (b) indicates the location from which the white matter spectrum in figure 7.2a was obtained; the marked square on the T1 weighted contrast enhanced image (c) indicates the location from which the tumour spectrum in figure 7.2b was obtained.

	tumour / WM
NAA	0.45 ± 0.17 **
Cho	1.88 ± 0.99 **
Cr	0.82 ± 0.32
Ino	1.28 ± 0.69
Glx	1.38 ± 0.39 **

Table 7.1. Ratios of the five main metabolites found in all oligodendrogliomas (n=15) relative to white matter. Numbers are mean ± standard deviation. WM = white matter. \*\* Tumour versus white matter, p<0.01.

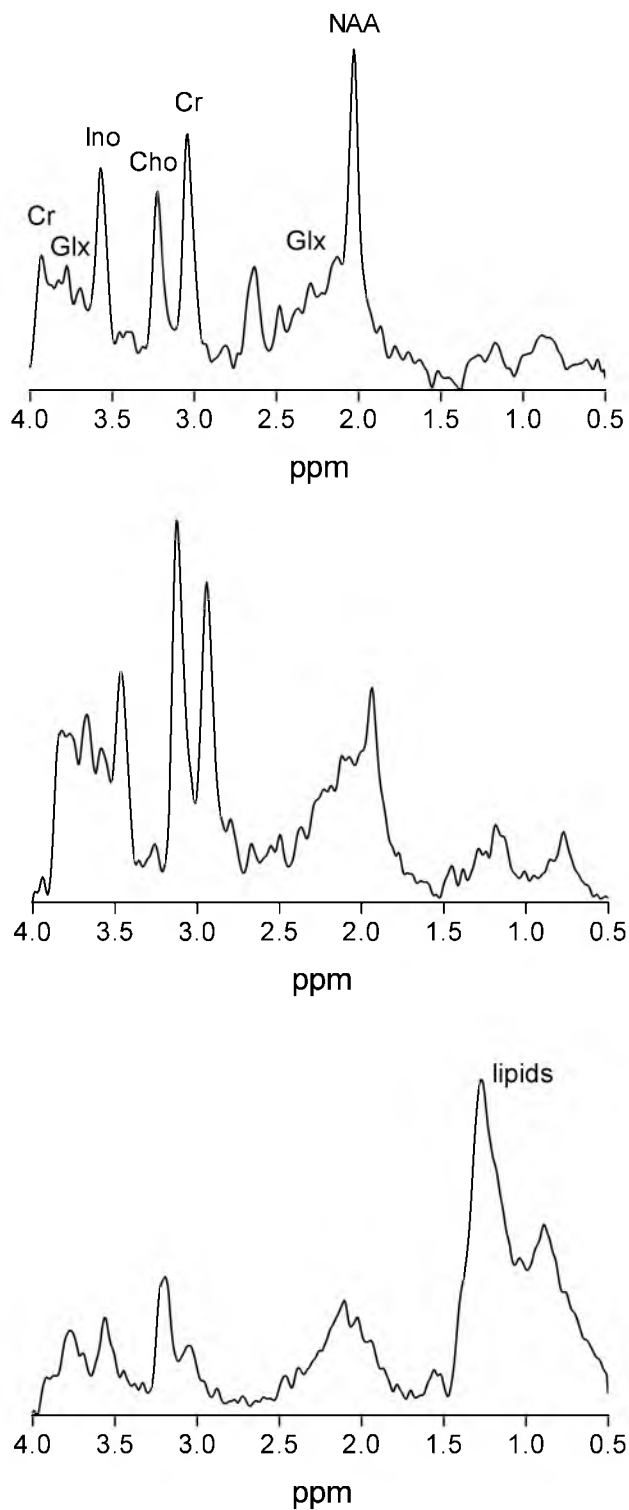


Figure 7.2.  $^1\text{H}$  MR spectra obtained from short echo time STEAM MRSI (TR 2500, TE 20 ms) data sets. (a) Spectrum from white matter with peak assignments to NAA, Cr, Cho, Ino and Glx. (b) Spectrum from a low grade oligodendroglioma featuring a decreased level of NAA and increased levels of Cho and Glx compared to white matter. (c) Spectrum from a high grade oligodendroglioma showing large lipid and lactate resonances.

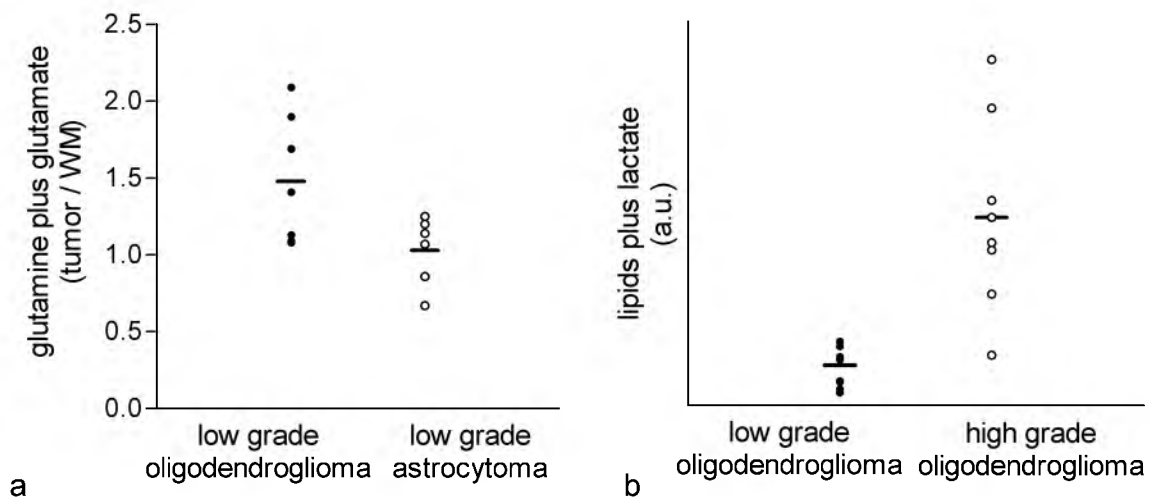


Figure 7.3. Scatter plots showing the distribution of metabolite levels for all patients. (a) Glutamine plus glutamate levels for low grade oligodendrogliomas and low grade astrocytomas. (b) Lipid plus lactate levels for low grade and high grade oligodendrogliomas. The mean of the corresponding metabolite levels is indicated in both figures.

All spectra were analysed and the tissue levels of the main metabolites NAA, Cr, Cho, Ino, and Glx were normalised to white matter levels for each patient. The results are shown in table 7.1 for all oligodendrogliomas. Besides a metabolic profile generally observed in brain tumours (decreased level of NAA and increased level of Cho) also a significant increase in Glx was found in oligodendroglial tumours.

Comparison of low grade oligodendrogliomas with low grade astrocytomas showed that Glx was significantly higher in oligodendrogliomas (table 7.2). The distribution of individual glutamine plus glutamate levels for low grade tumours is shown in figure 7.3a.

Within the group of oligodendrogliomas, no significant difference was found between low grade tumours and high grade tumours in any of the main metabolites (table 7.2). Interestingly, the relative level of all of these metabolites was lower in high grade tumours than in low grade tumours. The signal intensity of lipids plus lactate did differentiate low grade from high grade tumours significantly ( $p < 0.01$ , table 7.2). In figure 7.3b a plot is shown visualising the distribution of lipid plus lactate levels for both low grade and high grade oligodendrogliomas.

## DISCUSSION

A common observation in <sup>1</sup>H MR spectroscopy of glial tumours is a decreased level of NAA and an increased level of Cho. NAA is a major brain metabolite involved in cell signalling, regulation of interactions of brain cells, and the establishment and maintenance of the nervous system (16). The presence of NAA is used increasingly



in clinical MRS studies as a neuronal marker, although mature oligodendrocytes have also been shown to express NAA *in vitro* (17). Elevated Cho levels are consistent with an increased choline turnover in relation to membrane biosynthesis by proliferating cells (11). In this study both a decreased level of NAA and an increased level of Cho were found, in concordance with the general metabolic profile of glial tumours (8,18).

	low grade astrocytoma (tumour / WM)	low grade oligodendroglioma (tumour / WM)	high grade oligodendroglioma (tumour / WM)
NAA	0.47 ± 0.16	0.51 ± 0.17	0.40 ± 0.16
Cho	1.99 ± 0.88	2.20 ± 1.08	1.60 ± 0.87
Cr	0.92 ± 0.25	0.97 ± 0.33	0.70 ± 0.26
Ino	1.44 ± 0.64	1.59 ± 0.54	1.01 ± 0.72
Glx	1.03 ± 0.22	1.48 ± 0.41*	1.30 ± 0.38
Lipids + lactate <sup>§</sup>	3.9 ± 3.4	5.2 ± 2.4	24.7 ± 12.4 <sup>#</sup>

Table 7.2. Ratios of the five main metabolites found in low grade astrocytomas, low grade oligodendrogliomas, and high grade oligodendrogliomas relative to white matter. Numbers are mean ± standard deviation. WM = white matter. <sup>§</sup> The level of lipids plus lactate is expressed in arbitrary units, not as ratio to white matter. <sup>#</sup> High grade oligodendroglioma versus low grade oligodendroglioma,  $p < 0.01$ . \* Low grade oligodendroglioma versus low grade astrocytoma,  $p < 0.05$ .

More strikingly, in the present study an increased level of Glx compared to white matter was found in oligodendrogliomas, which may differentiate these tumours from other glial tumours. Glutamate is the major excitatory transmitter in the human brain and its complex metabolic coupling between neurons and glial cells and interconversion to glutamine have been recognised (19-21). Comparison among the low grade tumours in this study demonstrated that Glx was the only metabolite measured that showed a statistically significant difference between oligodendrogliomas and astrocytomas (table 7.2). Although there is some overlap in the Glx levels of these tumours (see figure 7.3a), information on Glx levels can be used to assist in distinguishing low grade oligodendrogliomas from low grade astrocytomas. Distinction between these tumour types is important in diagnosis and treatment planning and usually cannot be made based on clinical presentation and MRI alone.

The potential role for elevated levels of Glx as a metabolic marker for oligodendrogliomas is supported further by *in vitro* NMR analyses of extracts of brain tumours. Tugnoli et al (22) described intense multiplets assigned to Glx as one of the main spectroscopic features in <sup>1</sup>H MR spectra of low grade oligodendrogliomas. In the oligodendroglioma studied by Peeling et al (23) up to two times more Glx was found compared to other brain tumours (e.g. astrocytomas). Also, studies using cultured cells derived from nervous tissue showed a high level of Glx in oligodendrocytes and oligodendrocyte type 2 astrocyte progenitor (O-2A

progenitor) cells compared to other neural cells such as astrocytes and neurons (24,25). Besides Glx, also alanine and glycine have been proposed by in vitro NMR studies and amino acid analyses to be useful as metabolic markers for oligodendrogliomas (24,26), but this could not be demonstrated in this study.

To the best of our knowledge, this study reports on the largest population of patients with oligodendroglial tumours assessed by <sup>1</sup>H MRS, and is the first that used short echo time MRSI of these tumours. So far, in vivo MRS studies of oligodendrogliomas have used long echo times and focused mainly on NAA, Cho, and Cr. The metabolite concentrations in the tumour expressed as ratio to normal brain tissue were found to be 0.1-0.4 for NAA, 0.5-0.9 for Cr, and 1.4-1.9 for Cho (27,28), which is in agreement with the results of the present study (table 7.1). Tissue level ratios of Cho/Cr in oligodendrogliomas have been reported in the range of 0.3-1.6 (18,27,28). In this study a Cho(tumour)/Cr(tumour) ratio of  $0.7 \pm 0.3$  was found (data not shown). Immunohistochemical studies demonstrated that this metabolite ratio parallels with the cell proliferation index for Ki-67 (MIB-1) positive cells (28); a parameter that was shown to be of prognostic relevance for patients with oligodendrogliomas (28,29).

In line with in vivo MRS, in vitro NMR analyses of surgically obtained tumour specimens of oligodendrogliomas show decreased levels of NAA and Cr, and an increased level of Cho compared to normal brain (22,23,27,30,31). Other metabolic features that have been described include an elevated level of Ino (22-24,32). In the present study an increase in Ino was found in oligodendrogliomas compared to white matter, but statistical significance could only be demonstrated in low grade tumours ( $p=0.03$ ), not in the total group of oligodendrogliomas ( $p=0.14$ , table 7.1). In vivo MRS at 1.5 T usually lacks sensitivity to distinguish myo-inositol from glycine, both resonating at  $\sim 3.55$  ppm (33), although the use of different echo times may enable distinction between these metabolites (34). Different levels of both myo-inositol and glycine have been observed in glial tumours in vivo and in vitro (22,23,34,35). Interpretation of this data however is complicated because of the lower spectral resolution of MRS in vivo than in vitro. One has to consider also that biopsies and tumour extracts are not necessarily representative for a whole tumour as measured by in vivo MRS, and the tumour volume measured in vivo may partially contain normal brain tissue as well.

In the WHO tumour grading system oligodendrogliomas are divided into grade II (low grade) and grade III (high grade) tumours (1). In PET studies metabolic differences have been demonstrated between low grade and high grade oligodendrogliomas (36,37). In vivo MRS already showed to be useful in distinguishing the grades of other brain tumours (e.g. astrocytomas, 11,14,38-40). In the present study, none of the main metabolites analysed showed a statistically significant difference between low grade and high grade oligodendrogliomas,

although borderline significance was reached for Ino (table 7.2,  $p < 0.10$ ). However, in tumours with high lipid resonances the levels of NAA and Glx might be overestimated, because contribution from lipid protons in unsaturated fatty acid chains (which resonate in the 2.0-2.6 ppm region) was not corrected for in the analysis. The lipids plus lactate signal did show a significant difference between high grade tumours and low grade oligodendrogliomas (table 7.2,  $p < 0.01$ ). This positive correlation between tumour grade and lipids plus lactate signal is also commonly found in other glial tumours. In high grade tumours mobile lipids accumulate in necrotic tissue, as was demonstrated by ex vivo MRS and histological investigations (41). The amount of mobile lipid signal was shown to correlate directly with histopathological grade (39). Both apoptosis, microscopic cellular necrosis and cell proliferation may contribute to the signal of mobile lipids (41-44). However, the observation that the relative level of all of the main metabolites was lower in high grade tumours than in low grade tumours (table 7.2) suggests a decreased cellularity in high grade tumours. In gliomas the Cho signal intensity has already been shown to correlate with local cellularity as measured by diffusion MRI (45).

Lipids plus lactate signal intensity as a marker for malignancy of oligodendrogliomas is relevant in both diagnosis and treatment planning. Grading of oligodendroglial tumours according to the WHO criteria has been shown to be of prognostic relevance and a significant predictor of survival (29,46). Furthermore, treatment of oligodendrogliomas may be deferred until there is clinical or radiological evidence of progression, unless patients have disabling symptoms or signs at presentation (2). In this respect, MRS could be used as a noninvasive tool for low grade oligodendrogliomas to monitor a development into higher malignancy of these tumours.

#### ACKNOWLEDGEMENTS

Funding from INTERPRET (EC-project IST-1999-10310 INTERPRET International Network for Pattern Recognition of Tumors Using Magnetic Resonance) is kindly acknowledged. The neurosurgeons from the Nijmegen Neurosurgical Centre are gratefully acknowledged for their assistance in patient recruitment. Also, the authors thank the MRI technicians of the department of radiology for their assistance.

## REFERENCES

1. Kleihues P, Cavenee K. Oligodendroglial tumours. In: Pathology and genetics of tumours of the nervous system. IARC Press, Lyon, France, 55-69, 2000.
2. DeAngelis LM. Brain tumors. *N Engl J Med* 344:114-123, 2001.
3. Cairncross JG, MacDonald DR. Successful chemotherapy for recurrent malignant oligodendroglioma. *Ann Neurol* 23:360-364, 1988.
4. Pech IV, Peterson K, Cairncross JG. Chemotherapy for brain tumors. *Oncology (Huntingt)* 12:537-543, 547, 1998.
5. Friedman HS, Lovell S, Rasheed K, Friedman AH. Treatment of adults with progressive oligodendroglioma with carboplatin (CBDCA): preliminary results. Writing Committee for The Brain Tumor Center at Duke. *Med Pediatr Oncol* 31:16-18, 1998.
6. Soffietti R, Ruda R, Bradac GB, Schiffer D. PCV chemotherapy for recurrent oligodendrogliomas and oligoastrocytomas. *Neurosurgery* 43:1066-1073, 1998.
7. Chinot O. Chemotherapy for the treatment of oligodendroglial tumors. *Semin Oncol* 28:13-18, 2001.
8. Nelson SJ, Vigneron DB, Dillon WP. Serial evaluation of patients with brain tumors using volume MRI and 3D <sup>1</sup>H MRSI. *NMR Biomed* 12:123-138, 1999.
9. Preul MC, Caramanos Z, Collins DL, Villemure JG, Leblanc R, Olivier A, Pokrupa R, Arnold D. Accurate, noninvasive diagnosis of human brain tumors by using proton magnetic resonance spectroscopy. *Nat Med* 2:323-325, 1996.
10. Ginsberg LE, Fuller GN, Hashmi M, Leeds NE, Schomer DF. The significance of lack of MR contrast enhancement of supratentorial brain tumors in adults: histopathological evaluation of a series. *Surg Neurol* 49:436-440, 1998.
11. Lee PL, Gonzalez RG. Magnetic resonance spectroscopy of brain tumors. *Curr Opin Oncol* 12:199-204, 2000.
12. Norfray JF, Tomita T, Byrd SE, Ross BD, Berger PA, Miller RS. Clinical impact of MR spectroscopy when MR imaging is indeterminate for pediatric brain tumors. *Am J Roentgenol* 173:119-125, 1999.
13. Gill SS, Thomas DG, Van Bruggen N, Gadian GD, Peden CJ, Bell JD, Cox IJ, Menon DK, Iles RA, Bryant, DJ, Coutts G. Proton MR spectroscopy of intracranial tumours: in vivo and in vitro studies. *J Comput Assist Tomogr* 14:497-504, 1990.
14. Kaibara T, Tyson RL, Sutherland GR. Human cerebral neoplasms studied using MR spectroscopy: a review. *Biochem. Cell Biol* 76:477-86, 1998.
15. Provencher SW. Estimation of metabolite concentrations from localized in vivo proton NMR spectra. *Magn Reson Med* 30:672-679, 1993.
16. Baslow MH. Functions of N-acetyl-L-aspartate and N-acetyl-L-aspartylglutamate in the vertebrate brain: role in glial cell-specific signaling. *J Neurochem* 75:453-459, 2000.

17. Bhakoo KK, Pearce D. In vitro expression of N-acetyl aspartate by oligodendrocytes: implications for proton magnetic resonance spectroscopy signal in vivo. *J Neurochem* 74:254-262, 2000.
18. Negendank WG, Sauter R, Brown TR, et al. Proton magnetic resonance spectroscopy in patients with glial tumors: a multicenter study. *J Neurosurg* 84:449-458, 1996.
19. Dagani F, D'Angelo E. Glutamate metabolism, release, and quantal transmission at central excitatory synapses: implications for neural plasticity. *Funct Neurol* 7:315-336, 1992.
20. Peng L, Hertz L, Huang R, Sonnewald U, Petersen SB, Westergaard N, Larsson O, Schousboe A. Utilization of glutamine and of TCA cycle constituents as precursors for transmitter glutamate and GABA. *Dev Neurosci* 15:367-377, 1993.
21. Tsacopoulos M, Magistretti PJ. Metabolic coupling between glia and neurons. *J Neurosci* 16:877-885, 1996.
22. Tugnoli V, Tosi MR, Barbarella G, Ricci R, Leonardi M, Calbucci F, Bertoluzza A. Magnetic resonance spectroscopy study of low grade extra and intracerebral human neoplasms. *Oncol Rep* 5:1199-1203, 1998.
23. Peeling J, Sutherland G. High-resolution  $^1\text{H}$  NMR spectroscopy studies of extracts of human cerebral neoplasms. *Magn Reson Med* 24:123-136, 1992.
24. Urenjak J, Williams SR, Gadian DG, Noble M. Proton nuclear magnetic resonance spectroscopy unambiguously identifies different neural cell types. *J Neurosci* 13:981-989, 1993.
25. Bhakoo KK, Williams IT, Williams SR, Gadian DG, Noble MD. Proton nuclear magnetic resonance spectroscopy of primary cells derived from nervous tissue. *J Neurochem* 66:1254-1263, 1996.
26. Roda JM, Pascual JM, Carceller F, Gonzalez-Llanos F, Perez-Higueras A, Solivera J, Barrios L, Cerdan S. Nonhistological diagnosis of human cerebral tumors by  $^1\text{H}$  magnetic resonance spectroscopy and amino acid analysis. *Clin Cancer Res* 6:3983-3993, 2000.
27. Usenius JP, Kauppinen RA, Vainio PA, Hernesniemi JA, Vapalahti MP, Paljarvi LA, Soimakallio S. Quantitative metabolite patterns of human brain tumors: detection by  $^1\text{H}$  NMR spectroscopy in vivo and in vitro. *J Comput Assist Tomogr* 18:705-713, 1994.
28. Barbarella G, Ricci R, Pirini G, Tugnoli V, Tosi MR, Bertoluzza A, Calbucci F, Leonardi M, Trevisan C, Eusebi V. In vivo single voxel  $^1\text{H}$  MRS of glial brain tumors: correlation with tissue histology and in vitro MRS. *Int J Oncol* 12:461-468, 1998.
29. Deghani F, Schachenmayr W, Laun A, Korf HW. Prognostic implication of histopathological, immunohistochemical and clinical features of oligodendrogliomas: a study of 89 cases. *Acta Neuropathol (Berl)* 95:493-504, 1998.
30. Carpinelli G, Carapella CM, Palombi L, Raus L, Caroli F, Podo F. Differentiation of glioblastoma multiforme from astrocytomas by in vitro  $^1\text{H}$  MRS analysis of human brain tumors. *Anticancer Res* 16:1559-1563, 1996.

31. Carapella CM, Carpinelli G, Knijn A, Raus L, Caroli F, Podo F. Potential role of in vitro <sup>1</sup>H magnetic resonance spectroscopy in the definition of malignancy grading of human neuroepithelial brain tumours. *Acta Neurochir Suppl (Wien)* 68:127-132, 1997.
32. Kotitschke K, Jung H, Nekolla S, Haase A. High-resolution one- and two-dimensional <sup>1</sup>H MRS of human brain tumor and normal glial cells. *NMR Biomed* 7:111-120, 1994.
33. Govindaraju V, Young K, Maudsley AA. Proton NMR chemical shifts and coupling constants for brain metabolites. *NMR Biomed* 13:129-153, 2000.
34. Mader I, Roser W, Hagberg G, Schneider M, Sauter R, Seelig J, Radue EW, Steinbrich W. Proton chemical shift imaging, metabolic maps, and single voxel spectroscopy of glial brain tumors. *MAGMA* 4:139-150, 1996.
35. Castillo M, Smith JK, Kwock L. Correlation of myo-inositol levels and grading of cerebral astrocytomas. *Am J Neuroradiol* 21:1645-1649, 2000.
36. Derlon JM, Petit-Taboue MC, Chapon F, Beaudouin V, Noel MH, Creveuil C, Courtheoux P, Houtteville JP. The in vivo metabolic pattern of low-grade brain gliomas: a positron emission tomographic study using <sup>18</sup>F-fluorodeoxyglucose and <sup>11</sup>C-L- methylmethionine. *Neurosurgery* 40:276-287, 1997.
37. Derlon JM, Chapon F, Noel MH, Khouri S, Benali K, Petit-Taboue MC, Houtteville JP, Chajari MH, Bouvard G. Non-invasive grading of oligodendrogliomas: correlation between in vivo metabolic pattern and histopathology. *Eur J Nucl Med* 27:778-787, 2000.
38. Gotsis ED, Fountas K, Kapsalaki E, Toulas P, Peristeris G, Papadakis N. In vivo proton MR spectroscopy: the diagnostic possibilities of lipid resonances in brain tumors. *Anticancer Res* 16:1565-1567, 1996.
39. Negendank W, Sauter R. Intratumoral lipids in <sup>1</sup>H MRS in vivo in brain tumors: experience of the Siemens cooperative clinical trial. *Anticancer Res* 16:1533-1538, 1996.
40. Tedeschi G, Lundblom N, Raman R, Bonavita S, Duyn J, Alger J, DiChiro G. Increased choline signal coinciding with malignant degeneration of cerebral gliomas: a serial proton magnetic resonance spectroscopy imaging study. *J Neurosurg* 87:516-524, 1997.
41. Kuesel AC, Sutherland GR, Halliday W, Smith IC. <sup>1</sup>H MRS of high grade astrocytomas: mobile lipid accumulation in necrotic tissue. *NMR Biomed* 7:149-155, 1994.
42. Remy C, Fouilhe N, Barba I, Sam-Lai E, Lahrech H, Cucurella MG, Izquierdo M, Moreno A, Ziegler A, Massarelli R, Decorps M, Arus C. Evidence that mobile lipids detected in rat brain glioma by <sup>1</sup>H nuclear magnetic resonance correspond to lipid droplets. *Cancer Res* 57:407-414, 1997.
43. Cheng LL, Anthony DC, Comite AR, Black PM, Tzika AA, Gonzalez RG. Quantification of microheterogeneity in glioblastoma multiforme with ex vivo high-resolution magic-angle spinning (HRMAS) proton magnetic resonance spectroscopy. *Neuro-oncol* 2:87-95, 2000.
44. Hakumaki JM, Kauppinen RA. <sup>1</sup>H NMR visible lipids in the life and death of cells. *Trends Biochem Sci* 25:357-362, 2000.

45. Gupta RK, Sinha U, Cloughesy TF, Alger JR. Inverse correlation between choline magnetic resonance spectroscopy signal intensity and the apparent diffusion coefficient in human glioma. *Magn Reson Med* 41:2-7, 1999.
46. Wharton SB, Hamilton FA, Chan WK, Chan KK, Anderson JR. Proliferation and cell death in oligodendrogliomas. *Neuropathol Appl Neurobiol* 24:21-28, 1998.

# 8

## SUMMARY



Magnetic Resonance Imaging (MRI) and Magnetic Resonance Spectroscopy (MRS) techniques allow us to investigate patients with tumours in a noninvasive way. These techniques can be used not only for tumour identification, but also for tumour characterisation. In this thesis, MRI and MRS have been applied to investigate tumour physiology and metabolism in patients with tumours in the head-neck region, patients with oligodendrogliomas, and patients with meningiomas. Identification and characterisation of these tumours could assist in prediction of treatment response and selection of the best therapeutical option for these patients.

The biological and clinical background of the tumours studied in this thesis is described in chapter 1. Tumours often feature a more chaotic vascular architecture than normal tissue and a heterogeneous blood supply. This may result in local hypoxia and necrosis. Information on tumour physiology may aid not only to the characterisation of tumours, but also to treatment planning. Tumour blood flow for example is of fundamental importance to the efficacy of chemotherapy (drug delivery) and radiotherapy (oxygen supply).

The general principles of MR imaging and MR spectroscopy and their main applications as used in this thesis are summarised in chapter 2. Two of the central MR approaches to monitor physiological processes in tumours are dynamic contrast enhanced MRI and blood oxygen level dependent (BOLD) MRI. Dynamic contrast enhanced MRI can be applied to assess vascular parameters including tumour blood flow, vascular permeability, and blood volume. BOLD MRI can be used to assess changes in the blood oxygenation status. In chapter 3 these techniques are applied to study the physiology of squamous cell carcinomas of the larynx. The clinical application of BOLD MRI for the assessment of tumours was illustrated by showing the potential to predict treatment response to radiotherapy with hyperoxygenation.

A detailed description of the acquisition and analysis of dynamic contrast enhanced MRI data is presented in chapter 4. The MRI contrast agent Gadolinium-DTPA was administered by bolus injection and its effect was monitored in time by fast MR imaging. A simple algorithm was developed for automatic extraction of the arterial input function from the dynamic contrast enhanced MRI data. This arterial input function was used in the pixelwise pharmacokinetic determination of physiological vascular parameters in normal and tumour tissue. Maps were reconstructed to show the spatial distribution of parameter values. To test the reproducibility of the method eleven patients with different types of tumours were each measured twice, and the rate of contrast agent uptake in the tumour was calculated. The results show that normalising the dynamic contrast enhanced MRI data using individual coregistered arterial input functions, instead of one common arterial input function for all patients, substantially reduces the variation between successive measurements. It was

concluded that the proposed method enables the reproducible assessment of contrast agent uptake rates in human tumours.

Both dynamic contrast enhanced MRI and BOLD MRI were used to assess the effects of breathing a hyperoxic hypercapnic gas mixture on blood oxygenation and vascularity of head and neck tumours, as described in chapter 5. For tumours in the head-neck region breathing carbogen and administration of nicotinamide has been shown to result in a significantly improved tumour response to accelerated radiotherapy (ARCON). This may be caused by improved tumour oxygenation, possibly intermediated by vascular effects. For this reason, both blood oxygenation and vascular effects of breathing a hyperoxic hypercapnic gas mixture (98% O<sub>2</sub> + 2% CO<sub>2</sub>) were assessed in patients with tumours in the head-neck region. Tumour vascularity and oxygenation were investigated by dynamic Gadolinium-DTPA contrast enhanced MRI and BOLD MRI respectively. Eleven patients with primary head and neck tumours were each measured twice; with and without breathing the hyperoxic hypercapnic gas mixture. BOLD MR imaging revealed a significant increase of the MRI time constant of transverse magnetisation decay (T<sub>2</sub><sup>\*</sup>) in the tumour during hypercapnic hyperoxygenation, which correlates to a decrease of the deoxyhaemoglobin concentration. No changes in overall tumour vascularity were observed, as measured by the Gadolinium-DTPA contrast agent uptake rate in the tumour. It was concluded that breathing a hyperoxic hypercapnic gas mixture improves tumour blood oxygenation in patients with head and neck tumours, which may contribute to the success of the ARCON therapy.

A similar MRI study investigating the effects of hyperoxygenation is described in chapter 6 for meningiomas. Because meningiomas tend to recur after (partial) surgical resection, radiotherapy is increasingly being applied for the treatment of these tumours. Radiation dose levels are limited however to avoid radiation damage to the surrounding normal tissue. The radiosensitivity of tumours can be improved by increasing tumour oxygen levels. In this study BOLD MRI was applied to investigate if breathing a hyperoxic hypercapnic gas mixture could improve the oxygenation of meningiomas. In addition, dynamic Gadolinium-DTPA contrast enhanced MRI was used to assess changes in tumour vascularity under hyperoxic hypercapnic conditions. Ten meningioma patients were each studied without and with breathing a gas mixture consisting of 2% CO<sub>2</sub> and 98% O<sub>2</sub>. Values of T<sub>2</sub><sup>\*</sup> and the Gadolinium-DTPA uptake rate were calculated under both conditions. In six tumours a significant increase in the value of T<sub>2</sub><sup>\*</sup> in the tumour was found, suggesting an improved tumour blood oxygenation, which exceeded the effect in normal brain tissue. Contrarily, two tumours showed a significant T<sub>2</sub><sup>\*</sup> decrease. The change in T<sub>2</sub><sup>\*</sup> was found to correlate with both the Gadolinium-DTPA uptake rate and with the change in the Gadolinium-DTPA uptake rate. The overall effect of hypercapnic hyperoxia on meningiomas was suggested to be a balance between oxygenation and vascular effects. Improved oxygenation of blood entering the

tumour may be counteracted by a reduction in tumour blood volume and flow. It was concluded that the proposed MRI protocol may assist in radiation treatment selection in patients with meningiomas.

In chapter 7 an MR spectroscopy study is described characterising brain tumours, in particular oligodendrogliomas. These tumours may not be distinguished easily from other brain tumours based on clinical presentation and MRI alone. Identification of oligodendrogliomas however may have therapeutical consequences, as they show a unique chemosensitivity. In this study oligodendrogliomas were characterised and identified by their metabolic profile as measured by  $^1\text{H}$  MR spectroscopy. Fifteen patients with oligodendroglial tumours (8 high grade oligodendrogliomas, 7 low grade oligodendrogliomas) underwent MRI and short echo time  $^1\text{H}$  MRS examinations. Five main metabolites found in brain MR spectra were quantified and expressed as ratios of tumour to contralateral white matter tissue. The level of lipids plus lactate was also assessed in the tumour. For comparison also six patients with a low grade astrocytoma were included in the study. In high grade oligodendrogliomas large resonances of lipids plus lactate were observed in contrast to low grade tumours. Thus, MRS could be used as a noninvasive tool for low grade oligodendrogliomas to monitor a development into higher malignancy of these tumours. Compared to white matter, the metabolic profile of oligodendrogliomas showed a decreased level of N-acetylaspartate and increased levels of choline containing compounds and glutamine plus glutamate. The level of glutamine plus glutamate was significantly higher in low grade oligodendrogliomas than in low grade astrocytomas and may serve as a metabolic marker in diagnosis and treatment planning.

# 9

## NEDERLANDSE SAMENVATTING

Met behulp van Magnetic Resonance Imaging (MRI) en Magnetic Resonance Spectroscopy (MRS) kunnen patiënten met tumoren op een niet-invasieve wijze bestudeerd worden. Deze technieken kunnen niet alleen gebruikt worden om tumoren te identificeren, maar ook om een tumor te karakteriseren. In dit proefschrift zijn MRI en MRS toegepast om de fysiologie en het metabolisme te onderzoeken van tumoren in het hoofd-hals gebied, meningiomen en oligodendrogliomen. Identificatie en karakterisering van deze tumoren kunnen bijdragen aan het voorspellen van de respons op een behandeling en de selectie van de beste behandelingsstrategie voor deze patiënten.

In hoofdstuk 1 staan de biologische en klinische achtergronden beschreven van de tumoren die bestudeerd zijn in dit proefschrift. In vergelijking met normaal weefsel hebben tumoren vaak een heterogene bloedvoorziening en is het bloedvatenstelsel minder goed geordend. Dit kan tot gevolg hebben dat er plaatselijk een tekort komt aan zuurstof (hypoxie) of dat cellen doodgaan (necrose). Dit soort informatie over een tumor kan belangrijk zijn voor de planning van therapie. Zo is de doorbloeding van een tumor van groot belang voor chemotherapie (toevoer van geneesmiddelen) en radiotherapie (toevoer van zuurstof).

Het algemene principe van MRI en MRS en de voor dit proefschrift belangrijkste toepassingen zijn samengevat in hoofdstuk 2. Om fysiologische processen in kaart te brengen zijn twee MRI methoden met name van belang: MRI waarbij de opname van contrastmiddel gemeten wordt in een tumor (dynamische contrast MRI) en MRI die gevoelig is voor deoxyhemoglobine in het bloed (blood oxygen level dependent, BOLD MRI). Met dynamische contrast MRI kunnen vasculaire- en weefsel-eigenschappen bestudeerd worden, zoals permeabiliteit van bloedvaten, bloedvolume en doorbloeding. BOLD MRI kan gebruikt worden om veranderingen in de oxygenatie van het bloed te onderzoeken. In hoofdstuk 3 worden deze technieken toegepast op plaveiselcelcarcinomen van de larynx. Ook wordt de potentie van BOLD MRI om de respons op radiotherapie te voorspellen toegelicht.

De methode van het opnemen en analyseren van gegevens bij dynamische contrast MRI is beschreven in hoofdstuk 4. Na intraveneuze toediening van het MRI contrastmiddel Gadolinium-DTPA werd de opname in tumoren anderhalve minuut lang gemeten. Het verloop van de concentratie Gadolinium-DTPA in de tijd in grote arteriën werd met behulp van een algoritme bepaald. Deze zogenaamde arteriële input functie was nodig om met een farmacokinetisch model de fysiologische parameters van normaal- en tumorweefsel te berekenen. Door dit voor elk pixel te doen konden er van deze parameters ook afbeeldingen gemaakt worden. Om de reproduceerbaarheid van de methode te testen werd van elf patiënten de opnamesnelheid van het contrastmiddel twee keer gemeten. De resultaten lieten zien dat de variatie tussen de twee metingen verminderde als de dynamische contrast MRI gegevens genormaliseerd werden met een individueel opgenomen

arteriële input functie. De conclusie was dat de voorgestelde methode het mogelijk maakt om opname van contrastmiddel in tumoren op een reproduceerbare wijze te meten.

BOLD MRI en dynamische contrast MRI werden beide toegepast om de oxygenatie van het bloed en de vasculaire eigenschappen van tumoren in het hoofd-hals gebied te bestuderen. Hierbij ademen de patiënten een gasmengsel van 98% O<sub>2</sub> en 2% CO<sub>2</sub> (hyperoxygenatie). Dit onderzoek staat beschreven in hoofdstuk 5. Er was al aangetoond dat de respons van tumoren in het hoofd-hals gebied op radiotherapie verbeterde als deze behandeling gecombineerd werd met toediening van nicotinamide en het ademen van carbogeen (ARCON). Dit zou verklaard kunnen worden door een toegenomen hoeveelheid zuurstof in de tumor. Daarom werden de vasculaire eigenschappen en de oxygenatie van het bloed in de tumor gemeten voor en tijdens hyperoxygenatie. Elf patiënten met tumoren in het hoofd-hals gebied werden op deze wijze bestudeerd. BOLD MRI resultaten lieten een sterke toename van de MRI parameter T2\* zien tijdens hyperoxygenatie, wat duidt op een afname van de hoeveelheid deoxyhemoglobine. Er werden geen veranderingen waargenomen in de snelheid van opname van het contrastmiddel. De conclusie was dat het ademen van het gasmengsel de oxygenatie van het bloed in de tumor verbetert bij patiënten met tumoren in het hoofd-hals gebied en dat dit mogelijk bijdraagt aan het succes van de ARCON therapie.

Een soortgelijke studie voor meningiomen staat beschreven in hoofdstuk 6. Omdat meningiomen vaak hernieuwde groei vertonen na (gedeeltelijke) operatieve verwijdering, wordt radiotherapie in toenemende mate toegepast. De hoeveelheid straling die gegeven kan worden is echter gelimiteerd om schade in het omliggende hersenweefsel te voorkomen. De gevoeligheid voor radiotherapie kan wel verbeterd worden door de hoeveelheid zuurstof in de tumor te vergroten. In deze studie werd BOLD MRI toegepast om de oxygenatie van het bloed in de tumor te meten voor en tijdens het ademen van een gasmengsel van 98% O<sub>2</sub> en 2% CO<sub>2</sub>. Ook werd een dynamische contrast MRI uitgevoerd om veranderingen in de vasculaire eigenschappen van de tumor onder deze condities in kaart te brengen. Tien patiënten met meningiomen werden op deze wijze bestudeerd. In zes tumoren werd een sterke toename in T2\* gevonden, wat duidt op een verbeterde oxygenatie van het bloed in de tumor. In twee tumoren werd echter een tegengesteld effect waargenomen. De verandering in T2\* bleek te correleren met de verandering in de opnamesnelheid van het contrastmiddel. De conclusie was dat het effect van hyperoxygenatie op meningiomen een samenspel is van oxygenatie- en vasculaire effecten. Hoewel het bloed dat een tumor binnenstroomt meer zuurstof zal bevatten tijdens hyperoxygenatie, kan deze verbeterde oxygenatie weer tegengewerkt worden door een afname in het bloedvolume of de doorbloeding van de tumor. Het voorgestelde MRI protocol kan in individuele gevallen bijdragen tot de keuze wel of

niet hyperoxygenatie toe te passen bij radiotherapeutische behandeling van deze tumoren.

In hoofdstuk 7 staat een MRS studie beschreven om hersentumoren te karakteriseren, in het bijzonder oligodendrogliomen. Deze tumoren kunnen niet gemakkelijk van andere hersentumoren onderscheiden worden op basis van de klinische symptomen en MRI beelden. De identificatie van oligodendrogliomen is echter belangrijk, omdat deze tumoren wel positief op chemotherapie reageren, terwijl andere gliale tumoren dat doorgaans niet doen. In deze studie werd het metabole profiel van vijftien patienten met oligodendrogliomen (8 hooggradige en 7 laaggradige tumoren) gemeten met behulp van  $^1\text{H}$  MR spectroscopie. De vijf belangrijkste metabolieten die gewoonlijk gevonden worden in MR spectra van de hersenen werden geanalyseerd, evenals de hoeveelheid lipiden en lactaat. Om te kunnen vergelijken met andere tumoren werden ook zes patiënten met laaggradige astrocytomen opgenomen in de studie. In hooggradige oligodendrogliomen werd een hoge concentratie aan lipiden en lactaat waargenomen in tegenstelling tot laaggradige tumoren. Vergeleken met normaal hersenweefsel (witte stof) liet het metabole profiel van oligodendrogliomen een afname zien van N-acetylaspartaat en een toename van choline-verbindingen en glutamine plus glutamaat. De concentratie glutamine plus glutamaat was ook significant hoger in laaggradige oligodendrogliomen dan in laaggradige astrocytomen en zou zodoende gebruikt kunnen worden als metabole marker voor tumor diagnose en het plannen van therapie.

# DANKWOORD

In de afgelopen jaren heb ik van veel mensen bijzonder waardevolle ondersteuning gehad in het hele proces van het opzetten en uitvoeren van onderzoek, het verwerken en interpreteren van gegevens en het presenteren en publiceren van de resultaten. Een aantal mensen wil ik in het bijzonder noemen.

Allereerst mijn promotores, Arend Heerschap en Bert van der Kogel, bedankt voor jullie vertrouwen, voor de wetenschappelijke vrijheid die jullie mij gegeven hebben en de begeleiding daarbij. Jullie hebben op inspirerende wijze in het hele proces klaargestaan met goede raad welke kant op te sturen. Daarnaast wil ik ook zeker Hans Kaanders en Janneke Schuuring noemen, die beiden onmisbaar waren bij de opzet en uitvoering van de hoofdhal- en hersentumoronderzoeken en ook met groot enthousiasme betrokken zijn gebleven bij de studies.

Bij het uitvoeren van de metingen had ik de zeer gewaardeerde hulp van de MRI laboranten, waarvan ik in het bijzonder Denise, Jolanda en Yvonne wil noemen. Voor de studies waarbij in de magneet carbogeen geademd werd kon ik rekenen op de ARCON laboranten Anke, Janine en Sylvia; bedankt voor jullie inzet. Verder wil ik alle patiënten bedanken voor het deelnemen aan mijn onderzoek.

Dataverwerking! Voor de klinische interpretatie van MR beelden had ik de hulp van Frank. Computerprogramma's van HenkJan en Sjaak hebben menig gigabyte verslonden en voor de adviezen bij het opstellen van farmacokinetische modellen wil ik ook Boudewijn noemen. Van Hein kreeg ik regelmatig nuttige en niet zo nuttige tips over statistische methoden.

Het opschrijven van de resultaten van het onderzoek doe je vooral alleen. Maar bij het kritisch doorlezen en corrigeren van abstracts, artikelen en dit boekje zijn naast de mede-auteurs veel mensen betrokken geweest, voornamelijk uit de spectroscopiegroep. Ook bedank ik Simone en Susan van het secretariaat voor ondersteuning op het hele traject.

Naast publiceren heb ik ook mijn onderzoek mogen presenteren op verschillende bijeenkomsten en conferenties. Vooral in het buitenland werd dat regelmatig gecombineerd met een paar daagjes vakantie, waarvoor ik alle reisgenoten wil bedanken en in het bijzonder Hanneke wil noemen.

En dit alles heeft plaatsgevonden in een niet alleen stimulerende maar ook gezellige werksfeer. Hiervoor bedank ik de hele spectroscopiegroep - met name ook Janneke, mijn ex-kamergenoten Yvonne, Erik, Sjaak en Claudia, en mijn huidige



kamergenoten Hanneke, KlaasJan en Yvonne, die de diepere psychologische betekenis van uitroep 'taart!' niet snel zullen vergeten.

Tenslotte gaat mijn dank uit naar mijn ouders, mijn zus, familie en vrienden, die geprobeerd hebben te begrijpen wat ik nou eigenlijk precies gedaan heb de afgelopen jaren, maar die er toch ook vooral voor gezorgd hebben dat ik het werk even kon vergeten.

MR

## CURRICULUM VITAE

Mark Rijkema werd op 22 februari 1972 in Zutphen geboren. Na het VWO afgerond te hebben besloot hij na enig afwegen scheikunde te gaan studeren. In 1996 studeerde hij af aan de Katholieke Universiteit Nijmegen met als afstudeer-richtingen toxicologie/farmacologie en microbiologie. In 1997 werd hij aangesteld als junior onderzoeker op de afdeling Radiologie van het Universitair Medisch Centrum Nijmegen, waar hij van 1998 tot 2002 als AiO promotie onderzoek deed en tot op heden werkzaam is.



## LIST OF PUBLICATIONS

- Schwarz AJ, Rijpkema M, Collins DJ, Payne GS, Prock T, Woodward AC, Heerschap A, Leach MO. SAR and tissue heating with a clinical  $^{31}\text{P}$  MRS protocol using surface coils, adiabatic pulses and proton-decoupling. *Magnetic Resonance in Medicine* 44:692-700, 2000.
- Klomp DWJ, Collins DJ, van den Boogert HJ, Schwarz A, Rijpkema M, Prock T, Payne GS, Leach MO, Heerschap A. Radio-frequency probe for  $^1\text{H}$  decoupled  $^{31}\text{P}$  MRS of the head and neck region. *Magnetic Resonance Imaging* 19:755-759, 2001.
- Rijpkema M, Kaanders JHAM, Joosten FBM, van der Kogel AJ, Heerschap A. Method for quantitative mapping of dynamic MRI contrast agent uptake in human tumors. *Journal of Magnetic Resonance Imaging* 14(4):457-463, 2001.
- Rijpkema M, Kaanders J. Functional MR imaging of laryngeal cancer. In: *Imaging of the larynx*. Hermans R (Ed.), Springer, Berlin, 175-184, 2002.
- Schuurung J, Rijpkema M, Bernsen H, Bernsen P, van der Maazen R, Kaanders J, van der Kogel A, Heerschap A. Effect of breathing a hyperoxic hypercapnic gas mixture on the oxygenation of meningiomas; preliminary results. *Journal of NeuroOncology* 57(2):127-132, 2002.
- Shukla-Dave A, Poptani H, Loevner LA, Mancuso A, Serrai H, Rosenthal DI, Kilger AM, Nelson DS, Zakian KL, Arias-Mendoza F, Rijpkema M, Koutcher JA, Brown TR, Heerschap A, Glickson JD. Prediction of treatment response of head and neck cancers with P-31 MR spectroscopy from pretreatment relative phosphomonoester levels. *Academic Radiology* 9(6):688-694, 2002.
- Rijpkema M, Kaanders J, Joosten F, van der Kogel A, Heerschap A. Effects of breathing a hyperoxic hypercapnic gas mixture on blood oxygenation and vascularity of head and neck tumors as measured by MRI. *International Journal of Radiation Oncology Biology Physics* 53(5):1185-1191, 2002.

- Rijpkema M, Schuurin J, van der Meulen Y, van der Graaf M, Bernsen H, Boerman R, van der Kogel A, Heerschap A. Characterization of oligodendrogliomas using short echo time  $^1\text{H}$  MR Spectroscopic Imaging. NMR in Biomedicine, in press.
- Witjes H, Rijpkema M, van der Graaf M, Melssen WJ, Heerschap A, Buydens LMC. Recognition of brain tumors in multispectral magnetic resonance images using principal component and linear discriminant analysis. Journal of Magnetic Resonance Imaging, accepted for publication.

#### SCIENTIFIC ABSTRACTS & PRESENTATIONS

Rijpkema M, Heerschap A. Characterization of tumors by  $^{31}\text{P}$  MRS and dynamic Gadolinium contrast enhanced MRI: Research perspectives. Biomed Concerted Action, Nuclear Magnetic Resonance Assessment of Tumour Oxygenation, annual scientific meeting, Gatwick, UK, February 6-7, 1999. *(lecture)*

Schwarz AJ, Rijpkema M, Collins DJ, Payne GS, Woodward AC, van den Boogert H, Heerschap A, Leach MO. Local SAR and surface heating issues in a  $^{31}\text{P}$  MRS clinical trial using adiabatic pulses and proton decoupling with surface coils. ISMRM, 7th scientific meeting and exhibition, Philadelphia, USA, 22-28 May 1999. *(poster)*

van Cappellen van Walsum AM, Rijpkema M, Heerschap A, Nijhuis JG, Jongsma HW. Cerebral metabolite levels, energy status and intracellular pH during hypoxia in fetal lambs, as monitored by  $^1\text{H}$  and  $^{31}\text{P}$  MR spectroscopy. ISMRM, 7th scientific meeting and exhibition, Philadelphia, USA, 22-28 May 1999. *(poster)*

Arias-Mendoza F, Brown TR, Charles HC, Zakian K, Schwarz A, Doyle VL, Nelson SJ, Rijpkema M, Glickson JD, Evelhoch JL. Methodological standardization for a multi-institutional in vivo trial of localized  $^{31}\text{P}$  MR spectroscopy in human cancer research. ISMRM, 7th scientific meeting and exhibition, Philadelphia, USA, 22-28 May 1999. *(poster)*

Rijkema M, Witjes H, Schuurin J, Melssen W, Buydens L, Heerschap A. Characterization of oligodendrogliomas using MR imaging and 2D CSI  $^1\text{H}$  MR spectroscopy.

ESMRMB, 16th annual meeting, Sevilla, Spain, September 16-19, 1999.

*(lecture)*

van Cappellen van Walsum AM, Rijkema M, Heerschap A, Nijhuis JG, Jongsma HW.  $^1\text{H}$  and  $^{31}\text{P}$  MR spectroscopy of fetal lamb brain during hypoxia.

Fetal and Neonatal Physiological Society, 26th annual meeting, Vlieland, The Netherlands, September 1999.

*(lecture)*

Simonetti AW, Melssen WJ, Rijkema M, Heerschap A, Buydens LMC. Magnetic Resonance Spectroscopy and chemometrics for differentiation between tumorous and healthy brain tissue.

NWO/CW study group Analytical Chemistry, annual meeting, Lunteren, The Netherlands, November 8-9, 1999.

*(poster)*

van Cappellen van Walsum AM, Rijkema M, Heerschap A, Oeseburg B, Nijhuis JG, Jongsma HW. Cerebral  $^1\text{H}$  and  $^{31}\text{P}$  spectroscopy parameters related to systemic acidosis in hypoxic fetal lambs.

European Society of Magnetic Resonance in Neuropediatrics, 6th Congress, Marseille, France, January 19-22, 2000.

*(lecture)*

Rijkema M, Kaanders J, Joosten F, van der Sanden B, van der Kogel A, Heerschap A. Effects of carbogen breathing on tissue oxygenation and perfusion in head and neck tumors as measured by MRI.

ISMRM, 8th scientific meeting and exhibition, Denver, USA, April 1-7, 2000.

*(poster)*

Simonetti AW, Melssen WJ, Rijkema M, Heerschap A, Buydens LMC. Unsupervised chemometric methods to automatically discriminate between  $^1\text{H}$ -MRSI spectra in patients with a brain tumor.

ISMRM, 8th scientific meeting and exhibition, Denver, USA, April 1-7, 2000.

*(poster)*

Klomp D, Collins D, van den Boogert H, Schwarz A, Rijkema M, Prock T, Leach M, Heerschap A. Probe for  $^1\text{H}$  decoupled  $^{31}\text{P}$  MRS of the head and neck region.

ISMRM, 8th scientific meeting and exhibition, Denver, USA, April 1-7, 2000.

*(poster)*

Serrai H, Loevner LA, Zakian K, Arias-Mendoza F, Rijpkema M, Koutcher JA, Brown TR, Charles HC, Leach MO, Griffiths JR, Nelson SJ, Evelhoch JL, Heerschap A, Glickson JD. Monitoring response of head & neck tumors to therapy using in vivo localized  $^{31}\text{P}$  decoupled MR Spectroscopy: a preliminary study.

ISMRM, 8th scientific meeting and exhibition, Denver, USA, April 1-7, 2000.

*(poster)*

Rijpkema M, Kaanders J, Joosten F, van der Sanden B, van der Kogel A, Heerschap A. Effects of carbogen breathing on tissue oxygenation and perfusion in head and neck tumors as measured by MRI.

Biomed Concerted Action, Development of methods for rapid analysis of tumour oxygenation to allow treatment stratification, annual scientific meeting, Pisa, Italy, June 2-5, 2000.

*(lecture)*

Rijpkema M, Kaanders J, Joosten F, van der Sanden B, van der Kogel A, Heerschap A. Method to investigate heterogeneity in human tumors by mapping of  $\text{T2}^*$  and Gadolinium uptake.

ISMRM, workshop on MR in experimental and clinical cancer research in the new millennium, Geiranger, Norway, August 10-13, 2000.

*(poster)*

Rijpkema M, Kaanders J, Joosten F, van der Kogel A, Heerschap A. Effecten van carbogeen ademen op weefsel oxygenatie en perfusie in hoofd-hals tumoren: een MRI studie.

Nederlandse Werkgroep Hoofd-HalsTumoren, najaarsvergadering, Berg en Dal, The Netherlands, November 17, 2000.

*(lecture)*

Heerschap A, van der Sanden B, Rijpkema M. MR methods for the non-invasive assessment of the physiology of tumours related to oxygenation.

Biomed Concerted Action, development of methods for rapid analysis of tumour oxygenation to allow treatment stratification, final scientific meeting, Amsterdam, The Netherlands, February 17-19, 2001.

*(lecture)*

Rijpkema M, Schuurin J, Heerschap A. Characterization of oligodendrogliomas using short echo time 2D  $^1\text{H}$  MRSI.

ISMRM, 9th scientific meeting and exhibition, and ESMRMB, 18th annual meeting and exhibition, joint annual meeting, Glasgow, UK, April 21-27, 2001.

*(poster)*

Rijkema M, Kaanders J, Joosten F, van der Kogel A, Heerschap A. Effects of carbogen breathing on tissue oxygenation and perfusion in head and neck tumors as measured by MRI.

ISMRM, 9th scientific meeting and exhibition, and ESMRMB, 18th annual meeting and exhibition, joint annual meeting, Glasgow, UK, April 21-27, 2001.

*(lecture)*

Rijkema M, Schuurin J, Heerschap A. Characterization of Oligodendrogliomas using Short Echo Time 2D  $^1\text{H}$  MRSI.

International network for pattern recognition of tumours using Magnetic Resonance (INTERPRET) meeting, Barcelona, Spain, April 5-7, 2001.

*(lecture)*

van Laarhoven H, de Geus-Oei L, Rijkema M, Oyen W, Punt C, Wagener D, Ruers T, Barentsz J, Heerschap A. Correlation between Gadolinium-DTPA and  $^{18}\text{F}$ -Fluoro-2-Deoxy-Glucose uptake in colorectal liver metastases as measured by MRI and PET. 14e Nederlandse Internistendagen, Veldhoven, The Netherlands, April 24-26, 2002.

*(publication in The Netherlands Journal of Medicine)*

de Geus-Oei L, van Laarhoven H, Rijkema M, Punt C, Ruers T, Barentsz J, Heerschap A, Corstens F, Oyen W. Correlation between  $^{18}\text{F}$ FDG-uptake and dynamic Gadolinium uptake in colorectal liver metastases.

49th Annual Meeting of the Society of Nuclear Medicine, Los Angeles, USA, June 15-19, 2002.

*(poster)*

van der Meulen Y, van der Graaf M, Rijkema M, Schuurin J, Heerschap A. Short and long echo time in  $^1\text{H}$  MR Spectroscopy.

ISMRM Section for Magnetic Resonance Technologists, 11th annual meeting, Honolulu, USA, May 17-19, 2002.

*(poster)*

Rijkema M, Schuurin J, Kaanders J, van der Kogel A, Heerschap A. Effects of breathing a hyperoxic hypercapnic gas mixture on the oxygenation and vascularity of meningiomas as measured by MRI.

ISMRM, 10th scientific meeting and exhibition, Honolulu, USA, May 18-24, 2002.

*(lecture)*

Rijkema M, van der Meulen Y, Schuurin J, Mooyaart E, van der Graaf M, Heerschap A. Characterization of an intracranial neoplasm of lipoid origin by  $^1\text{H}$  MR Spectroscopy.

ISMRM, 10th scientific meeting and exhibition, Honolulu, USA, May 18-24, 2002.

*(poster)*



van der Graaf M, Rijpkema M, van der Meulen Y, Majos C, Moreno A, Ziegler A, Howe F, Opstad K, Heerschap A. System quality assurance in a multicenter study on brain tumor MR Spectroscopy (INTERPRET).

ISMRM, 10th scientific meeting and exhibition, Honolulu, USA, May 18-24, 2002.

*(poster)*

van Laarhoven H, de Geus-Oei L, Rijpkema M, Oyen W, Punt C, Wagener D, Ruers T, Barentsz J, Heerschap A. Correlation between dynamic Gadolinium uptake and <sup>18</sup>Fluoro-2-Deoxy-Glucose uptake in colorectal liver metastases.

ISMRM, 10th scientific meeting and exhibition, Honolulu, USA, May 18-24, 2002.

*(lecture)*

Simonetti A, Melssen W, Rijpkema M, Heerschap A, Postma G, Schuurin J, Buydens L. Identification of brain tumors by segmentation and classification of MRI and MRSI data.

ISMRM, 10th scientific meeting and exhibition, Honolulu, USA, May 18-24, 2002.

*(poster)*

van Dorsten F, Klomp D, Fütterer J, Rijpkema M, de La Rosette J, Barentsz J, Heerschap A. Towards an advanced protocol for tumour detection in the prostate gland using 3D <sup>1</sup>H MR Spectroscopic Imaging and dynamic contrast enhanced MRI.

ISMRM, 10th scientific meeting and exhibition, Honolulu, USA, May 18-24, 2002.

*(lecture)*

van der Graaf, Rijpkema M, van der Meulen YM, Majós C, Moreno A, Ziegler A, Howe FA, Opstad K, Heerschap A. System quality assurance in INTERPRET, a multicenter study on brain tumor MR Spectroscopy.

ESMRMB, 19th annual meeting, Cannes, France, August 22-25, 2002.

*(poster)*

van Laarhoven H, de Geus-Oei L, Rijpkema M, Ruers T, Oyen W, Punt C, Heerschap A, Barentsz J. Relation between Gadolinium-DTPA and <sup>18</sup>Fluoro-2-Deoxy-Glucose uptake in liver metastases of colorectal cancer as measured by MRI and PET.

Radiologendagen, Noordwijkerhout, The Netherlands, September 19-20, 2002.

*(lecture)*

Rijpkema M, Schuurin J, Bernsen P, Bernsen H, Kaanders J, van der Kogel A, Heerschap A. BOLD MRI response to hypercapnic hyperoxia in patients with meningiomas: correlation with Gadolinium-DTPA uptake rate.

ISMRM, workshop on In vivo functional and molecular assessment of cancer, Santa Cruz, USA, October 19-21, 2002.

*(poster discussion)*

van Laarhoven H, Rijpkema M, Punt C, Ruers TJ, Barentsz JO, Heerschap A. Reproducibility of dynamic contrast enhanced MRI in liver metastasis of colorectal cancer.

ISMRM, workshop on In vivo functional and molecular assessment of cancer, Santa Cruz, USA, October 19-21, 2002.

*(lecture)*

Rijpkema M, Schuurin J, van der Meulen Y, van der Graaf M, Bernsen H, Boerman R, van der Kogel A, Heerschap A. Characterization of oligodendrogliomas using short echo time  $^1\text{H}$  MR Spectroscopic Imaging.

RSNA, 88th Scientific Assembly and Annual Meeting, Chicago, USA, December 1-6, 2002.

*(lecture)*

---

ISMRM: International Society for Magnetic Resonance in Medicine  
ESMRMB: European Society for Magnetic Resonance in Medicine and Biology  
RSNA: Radiological Society of North America



EEN VREEMDE AVOND -  
DE BOMEN LIJKEN BOMEN  
EN HET GRAS IS GROEN

(W.J. van der Molen)